






<p>Final Report</p>	<p align="center">ESA Project SMARTCARB</p> <p align="center">Study on use of satellite measurements of auxiliary reactive trace gases for fossil fuel carbon dioxide emission estimation contract no 4000119599/16/NL/FF/mg</p>	  
----------------------------	---	---




SMARTCARB – Use of satellite measurements of auxiliary reactive trace gases for fossil fuel carbon dioxide emission estimation

Final Report of ESA study contract n° 4000119599/16/NL/FF/mg
Final Version: 31 January 2019



For the attention of: Dr. Yasjka MEIJER – ESA / ESTEC
 Dr. Armin LÖSCHER – ESA / ESTEC

	Function	Name	Signature	Date
Written by	Project Scientist	Consortium		31 Jan 2019
Approved by	Project Manager / Scientific manager	Dominik BRUNNER (Empa)		31 Jan 2019
Written by: Gerrit KUHLMANN, Valentin CLÉMENT, Julia MARSHALL, Oliver FUHRER, Grégoire BROQUET, Christina SCHNADT-POBERAJ, Dominik BRUNNER				
Cite as: G. Kuhlmann, V. Clément, J. Marshall, O. Fuhrer, G. Broquet, C. Schnadt-Poberaj, A. Löscher, Y. Meijer, and D. Brunner (2018): SMARTCARB – Use of Satellite Measurements of Auxiliary Reactive Trace Gases for Fossil Fuel Carbon Dioxide Emission Estimation, Final report of ESA study contract n°4000119599/16/NL/FF/mg, project led by Empa (Switzerland).				

<p>Final Report</p>	<p>ESA Project SMARTCARB Study on use of satellite measurements of auxiliary reactive trace gases for fossil fuel carbon dioxide emission estimation contract no 4000119599/16/NL/FF/mg</p>	  Max Planck Institute for Biogeochemistry 
----------------------------	--	--

Document status




Version	Date	Reason for the revision
0.1	5 Dec 2018	First draft compiled from deliverables
1.0	31 Jan 2019	Suggestions by Y. Meijer from 19 Dec incorporated, chapter 6 updated based on final version of D5

Study consortium

Name	Organization
Dominik Brunner	Empa, Switzerland
Gerrit Kuhlmann	Empa, Switzerland
Valentin Clément	C2SM, Switzerland
Christina Schnadt-Poberaj	C2SM, Switzerland
Julia Marshall	MPI Jena, Germany




External experts

Name	Organization
Grégoire Broquet	LSCE, France
Oliver Fuhrer	MeteoSwiss, Switzerland

Final Report	ESA Project SMARTCARB Study on use of satellite measurements of auxiliary reactive trace gases for fossil fuel carbon dioxide emission estimation contract no 4000119599/16/NL/FF/mg	  
---------------------	---	---




Applicable documents

	Reference	Title
(RD-1)	Ciais et al. (2015)	Towards a European Operational Observing System to Monitor Fossil CO ₂ Emission.
(RD-2)	NOV-7090-NT-2516	Final report of CarbonSat Earth Explorer 8 Candidate Mission "LOGOFLUX 1 – Inverse Modelling and Mission Performance Statement", NOVELTIS, Version 1.1, 23 July 2014
(RD-3)	NOV-7248-NT-5330	Final report of CarbonSat Earth Explorer 8 Candidate Mission "LOGOFLUX 2 - Flux Inversion Performance Study", NOVELTIS, Version 1.1, 12 October 2015
(RD-4)		Technical proposal: SMARTCARB – Use of satellite measurements of auxiliary reactive trace gases for fossil fuel carbon dioxide emission estimation
(RD-5)	EOP-SM/3063/YM-ym	Statement of Work, Study on use of CO and NO ₂ observations for estimating fossil CO ₂ emissions, ESA, EOP-SM/3063/YM-ym, v1.0, 04 Nov 2016
(RD-6)		Technical note: Project sketch "Assessing the synergy of satellite CO ₂ combined with CO and NO ₂ measurements for the quantification of anthropogenic point source emissions on simulating emissions", Empa, v2, 02 August 2016
(RD-7)	SP-1330/1	Report for Mission Selection: CarbonSat, ESA SP-1330/1 (2 volume series), European Space Agency, Noordwijk, The Netherlands, 2015.
(D1)	4000119599/16/NL/FF/mg	Deliverable 1 of ESA study contract n° 4000119599/16/NL/FF/mg: Requirements for Model Simulations Covering a Large City and Power Plant
(D2)	4000119599/16/NL/FF/mg	Deliverable 2 of ESA study contract n° 4000119599/16/NL/FF/mg: Specifications for satellite observations.
(D3)	4000119599/16/NL/FF/mg	Deliverable 3 of ESA study contract n° 4000119599/16/NL/FF/mg: Description of model setup and simulated satellite data.
(D4)	4000119599/16/NL/FF/mg	Deliverable 4 of ESA study contract n° 4000119599/16/NL/FF/mg: Estimating CO ₂ emission through flux inversion

Final Report	ESA Project SMARTCARB Study on use of satellite measurements of auxiliary reactive trace gases for fossil fuel carbon dioxide emission estimation contract no 4000119599/16/NL/FF/mg	  Max Planck Institute for Biogeochemistry 
---------------------	---	---

Acronyms

AK	Averaging kernels
AMF	Air mass factors
AOD	Aerosol optical depth
BG	Background
CAMS	Copernicus Atmospheric Monitoring Service
CARMA	Carbon Monitoring for Action
CO	Carbon monoxide
CO ₂	Carbon dioxide
COD	Cirrus optical depth
COSMO	Consortium for Small-Scale Modelling
CSCS	Swiss National Supercomputing Centre (Italian: Centro Svizzero di Calcolo Scientifico)
CTH	Cirrus top height
C2SM	Center for Climate System Modelling, ETH Zürich
EC	European Commission
ECMWF	European Centre for Medium-Range Weather Forecasts
EPF	Error parametrization formula
E-PRTR	European Pollutant Transfer and Release Register
ESA	European Space Agency
EVI	Enhanced Vegetation Index
FLEXPART	Flexible Particle Dispersion Model
GOSAT	Greenhouse Gases Observing Satellite
GHG	Greenhouse Gases
GPU	Graphics Processing Unit
GPP	Gross Primary Production
IFS	Integrated Forecast System
IC/BC	Initial Conditions / Boundary Condition
LSCE	Laboratoire des Science du Climat et de l'Environnement
LOGOFLUX	Local to global scale CO ₂ and CH ₄ fluxes from CarbonSat
LSWI	Land Surface Water Index
MACC	Monitoring Atmospheric Composition and Climate project
MARS	Meteorological Archival and Retrieval System
MODIS	Moderate Resolution Imaging Spectrometer

Final Report	ESA Project SMARTCARB Study on use of satellite measurements of auxiliary reactive trace gases for fossil fuel carbon dioxide emission estimation contract no 4000119599/16/NL/FF/mg	  Max Planck Institute for Biogeochemistry 
---------------------	---	---

MPI	Max Planck Institute
MRD	Mission requirements document
Mt	Megatons (10^9 kg)
NFR	Nomenclature For Reporting
NIR	Near infrared
NO ₂	Nitrogen dioxide
NO _x	Nitrogen oxides (NO + NO ₂)
NWP	Numerical Weather Prediction
OCO-2	Orbiting Carbon Observatory 2
OSSE	Observing System Simulation Experiment
ppm	Parts per million (10^{-6})
PPV	Positive predictive value
RMSD	Root mean square deviation
SMARTCARB	Satellite Measurements of Auxiliary Reactive Trace gases for fossil fuel CARBOn dioxide emission estimation
SNAP	Standardized Nomenclature for Air Pollutants
SNR	Signal to noise ratio
SSO	Sun-synchronous orbit
SRON	Netherlands Institute for Space Research
SWIR	Short-wave infrared
SYNMAP	Synergetic Land Cover Product
SZA	Solar zenith angle
TNO	Netherlands Organization for Applied Scientific Research (Dutch: Nederlandse Organisatie voor Toegepast Natuurwetenschappelijk Onderzoek)
TPR	True positive rate
UTC	Universal Time Coordinated
UVNS	Ultraviolet, visible, near- and shortwave infrared
VEG50	Vegetation 50 scenario for which indicated noise level holds
VCD	Vertical Column Density
VDI	Association of German Engineers (German: Verein Deutscher Ingenieure)
VPRM	Vegetation Photosynthesis and Respiration Model
XCO ₂	Column averaged dry air mole fraction of CO ₂







Final Report	ESA Project SMARTCARB Study on use of satellite measurements of auxiliary reactive trace gases for fossil fuel carbon dioxide emission estimation contract no 4000119599/16/NL/FF/mg	  Max Planck Institute for Biogeochemistry 
---------------------	---	---

Table of content

1. INTRODUCTION.....	7
1.1 OBJECTIVES OF THE PRESENT DOCUMENT	9
2. REQUIREMENTS FOR MODEL SIMULATIONS.....	10
2.1 MODEL REQUIREMENTS	10
2.2 MODEL SETUP	13
2.3 COSMO-GHG MODEL	22
3. SPECIFICATIONS FOR SATELLITE OBSERVATIONS	24
3.1 INSTRUMENT SCENARIOS.....	24
3.2 INSTRUMENT ERROR CHARACTERISTICS	27
4. MODEL SETUP AND SIMULATED SATELLITE OBSERVATIONS	31
4.1 GENERATION OF SYNTHETIC SATELLITE OBSERVATIONS	31
4.2 RESULTS.....	35
5. ESTIMATING CO₂ EMISSIONS	50
5.1 EMISSIONS FROM BERLIN AND POWER PLANTS IN A GLOBAL CONTEXT	50
5.2 COVERAGE AND POTENTIAL FOR PLUME DETECTION	52
5.3 PLUME DETECTION FROM SATELLITE IMAGES.....	59
5.4 ESTIMATING THE EMISSIONS OF THE CITY OF BERLIN	77
5.5 ESTIMATING THE EMISSIONS OF POWER PLANTS	89
6. SUMMARY AND RECOMMENDATIONS.....	94
6.1 SUMMARY	94
6.2 RECOMMENDATIONS	99
7. REFERENCES	105

<p>Final Report</p>	<p align="center">ESA Project SMARTCARB</p> <p align="center">Study on use of satellite measurements of auxiliary reactive trace gases for fossil fuel carbon dioxide emission estimation</p> <p align="center">contract no 4000119599/16/NL/FF/mg</p>	  
----------------------------	---	---

1. Introduction




The combustion of fossil fuels is the main source of today's increase in atmospheric carbon dioxide (CO₂), the most important greenhouse gas (GHG) driving climate change. In order to limit the risks and impact of climate change, 195 countries agreed at the Paris climate conference in 2015 a long-term goal of keeping the global average temperature increase to well below 2°C above pre-industrial levels. Reaching this goal will require dramatic cuts to the emissions of CO₂ and other greenhouse gases in the coming decades. The parties to the Paris Agreement communicated their emission reduction targets in the form of Nationally Determined Contributions. In order to control the progress towards these targets, the countries have to regularly summarize their emissions, estimated from socioeconomic activity data and emission factors, in the form of National Inventory Reports (NIR). The collective progress of all parties will then be assessed every five years in so-called Global Stocktakes.

To build confidence in this process, it will be critical to evaluate the "bottom-up" emissions reported by the countries against the actual increase of GHG concentrations in the atmosphere. The atmospheric science community therefore proposed the application of "top-down" methods, which quantify emissions from GHG measurements in combination with atmospheric transport models, as an independent source of information to support the verification of the data reported by the countries.

Due to the ongoing urbanization worldwide and the fact that cities account for approximately 70% of global GHG emissions, cities will play a key role in the design of future climate policies. There is, therefore, a growing interest of city governments in quantifying their GHG emissions in order to evaluate the effectiveness of different mitigation policies. Similar to the country level, top-down estimation of emissions from atmospheric concentration measurements has a large potential to support the cities in this process.

Due to the key role of CO₂, the European Commission asked the scientific community to outline the necessary components of a global CO₂ emission monitoring system and the steps towards its implementation. A first report was published by Ciais et al. (2015), which identified as a key component a constellation of CO₂ satellites with imaging capability complemented by ground-based observations and atmospheric transport and inverse modeling. A second report refining the overall concept and proposing a timeline for its implementation in the framework of the European Earth observation program Copernicus was published by Pinty et al. (2018).

The satellites (referred to as Sentinel CO₂ satellites in the following) should observe in the near infrared range of the spectrum where CO₂ can be measured with almost constant sensitivity between the Earth's surface and the top of the atmosphere. The corresponding products are column mean dry air mole fractions of CO₂, termed XCO₂ in the following. Furthermore, they should combine a wide swath of at least 200 km with a small pixel size of about 2 km x 2 km to be able to image the plumes of individual point sources such as large cities and power plants (Bovensmann et al., 2010; Pillai et al., 2016; Velazco et al., 2011). These measurements would also contribute to the monitoring of atmospheric CO₂ and of its natural sources and sinks and of its anthropogenic emissions at country and global scale.

<p>Final Report</p>	<p align="center">ESA Project SMARTCARB</p> <p align="center">Study on use of satellite measurements of auxiliary reactive trace gases for fossil fuel carbon dioxide emission estimation</p> <p align="center">contract no 4000119599/16/NL/FF/mg</p>	  
----------------------------	---	---

However, the local enhancements in XCO₂ generated even by strong point sources are very small (typically <1%) compared to the large-scale atmospheric background. This puts extremely high demands on precision and accuracy of the measurements. A further challenge is to discriminate the local plumes against variations in background XCO₂ caused by biospheric CO₂ fluxes and other anthropogenic emissions upstream of the source. Measurements of auxiliary trace gases such as carbon monoxide (CO) or nitrogen dioxide (NO₂) co-emitted with CO₂ but not measurably influenced by biospheric fluxes were therefore proposed to support such a CO₂ mission.




This idea formed the basis of the SMARTCARB project, which should develop the requirements for the Sentinel CO₂ satellites in combination with NO₂ or CO instruments with respect to observing and quantifying CO₂ emissions from large point sources. The project had the following specific objectives:

- Assess the potential for detecting CO₂ emission plumes from cities and power plants from Sentinel CO₂ satellites using their imaging capability
- Analyze and compare the performance of flux inversion and mass balance methods to quantify the CO₂ emissions of these sources based on the detected plumes
- Assess how additional satellite measurements of CO and NO₂ can assist in the detection of plumes and quantification of CO₂ emissions
- Assess the impact of different noise levels of the CO₂, CO and NO₂ instruments on the performance of the emission estimates
- Compare the performance when data is available of co-emitted CO and NO₂ either measured at the same time, i.e. from the same satellite, or with a delay on the same day, i.e. from a different satellite (Sentinel-5)

In order to address these questions, SMARTCARB conducted Observing System Simulation Experiments (OSSEs) with the following elements:




- High-resolution realistic simulations ("nature runs") of CO₂, CO, and NO₂ for the complete year 2015 over a domain covering the city of Berlin and several power plants
- Separation of CO₂, CO and NO₂ into a total of 50 tracers representing different types of emissions, natural fluxes, and background concentrations, allowing to isolate the plumes from Berlin and individual power plants from other sources
- Development of high-resolution datasets of anthropogenic emissions and biospheric CO₂ fluxes with realistic temporal variability and vertical distribution of emissions including plume rise for power plant emissions
- Generation of synthetic satellite observations of CO₂, CO and NO₂ for constellations of up to six satellites as well as for observations from Sentinel-5 (only NO₂ and CO) using orbit simulations and simple parameterizations of instrument noise
- Estimation of the emissions from Berlin and power plants from the synthetic observations using inverse modeling or mass balance methods

With this setup, a direct link between the satellite observations and the final products, i.e. emission estimates, could be established, which allowed assessing and comparing the overall performance of different satellite and instrument scenarios.

<p>Final Report</p>	<p>ESA Project SMARTCARB</p> <p>Study on use of satellite measurements of auxiliary reactive trace gases for fossil fuel carbon dioxide emission estimation</p> <p>contract no 4000119599/16/NL/FF/mg</p>	  
----------------------------	--	---

1.1 Objectives of the present document

This report summarizes the results of the study. The report was compiled from the project deliverables written during the study. Section 2 describes requirements for model simulations covering a large city and a larger power plant. Section 3 specifies the range of considered observation characteristics for creating the synthetic datasets of CO₂, CO and NO₂ satellite observations. Section 4 describes the generation of synthetic satellite observations from the “nature runs” and shows examples of resulting two-dimensional fields and satellite observations. Section 5 describes the estimation of the CO₂ emissions from Berlin and Jänschwalde power stations. Finally, Section 6 summarizes the study and gives recommendations.

Final Report	ESA Project SMARTCARB Study on use of satellite measurements of auxiliary reactive trace gases for fossil fuel carbon dioxide emission estimation contract no 4000119599/16/NL/FF/mg	  
---------------------	---	---

2. Requirements for model simulations

This chapter describes model requirements and the final model settings used for the simulations including domain size, spatial resolution, tracer setup, emission inventories and initial and boundary conditions (IC/BC). Furthermore, the GPU accelerated version of the COSMO-GHG model is described and benchmarked.

2.1 Model requirements




In SMARTCARB, synthetic datasets of CO₂, CO and NO₂ satellite observations will be created from high-resolution model simulations. The dataset will consist of column averaged dry air mole fractions of CO₂ (XCO₂) and vertical column densities (VCD) of CO and NO₂ extracted for each instrument pixel from the three-dimensional simulated fields. The model fields will also be used for estimating random and systematic uncertainties in the observations and for masking cloudy pixels. To conduct the simulations, we need to define model requirements in terms of domain size, horizontal and vertical resolution, CO₂, CO and NO₂ tracers, input and output data, and simulation time period.

2.1.1 Model domain and resolution

The domain size needs to be large enough to cover the plumes of two different anthropogenic sources, a large city and a large power plant, downwind over a distance where the plume is still detectable by the satellite. Furthermore, the model should be setup in such a way that variations in the CO₂ background into which the investigated plume is embedded are realistically captured at all relevant spatial scales down to the satellite pixel resolution. These variations can be caused by changes in the large-scale background, by synoptic transport from remote sources and sinks, and by more regional contributions from biospheric and anthropogenic fluxes upstream of the source.

A simple approach for specifying the domain size would be to take the sum of plume extent plus swath width around each point source. The plume can be defined as the area where the enhancement in XCO₂ above background exceeds the detection limit of the satellite instrument. The detection limit is generally defined as three standard deviations of the random uncertainty. However, since the plume will be detected by a collection of neighboring pixels, a better measure for the detection limit may be the detection limit for a single pixel divided by the square root of the number of pixels in the entire or in a portion of the plume.

Since the model resolution needs to be appropriate to resolve the atmospheric variability at all scales detectable by the satellite, the horizontal resolution of the model should be comparable or better than the resolution of the satellite observations. In this context the model grid resolution is not the only criterion, since the effective resolution of an Eulerian model is always lower due to numerical diffusion, the magnitude of this diffusion being largely depending on the chosen advection scheme (e.g. Rood, 1987). The combination of model resolution and advection scheme should be able to preserve the sharp concentration

<p>Final Report</p>	<p>ESA Project SMARTCARB</p> <p>Study on use of satellite measurements of auxiliary reactive trace gases for fossil fuel carbon dioxide emission estimation</p> <p>contract no 4000119599/16/NL/FF/mg</p>	  
----------------------------	--	---

gradients in the vicinity of point sources, at least at the scales resolved by the satellite observations.

The vertical resolution needs to be appropriate for resolving planetary boundary layer processes and wind shear profile, which strongly affect the dispersion of air pollutants released at the surface. It should also be appropriate to resolve the vertical concentration gradients that affect the satellite observations. Furthermore, the resolution needs to be high enough for correctly assigning vertically confined and elevated emission plumes such as those from power plants.

2.1.2 CO₂, CO and NO₂ tracers

The model needs to simulate the transport of different CO₂, CO and NO₂ tracers that will provide the quantitative link between emission sources and concentrations required by the inversion framework. The tracers should allow us to discriminate between:

- a) background concentrations transported from outside the model domain,
- b) emissions from the two points sources (city and power plant) and other emissions in the model domain,
- c) emissions from different source categories (e.g. power plants and traffic emissions),
- d) CO₂ from biospheric gross primary production (GPP) and biospheric respiration.




For addressing more specific questions related to the objectives of the study, the tracers should also allow us to distinguish between

- a) emissions released at different hours of the day to study the influence of overpass times and temporal separation between satellite orbits,
- b) emissions released at different emission heights to study the impact of plume rise at stacks,
- c) total mass of each species for checking if the model preserves the total mass,
- d) time-varying and constant emissions to study the impact of uncertainties in the emission time profiles,
- e) chemical conversion of the tracers, mostly relevant for NO₂, considering, for example, different NO_x decay times.

2.1.3 Input data

Key inputs are realistic fields of CO₂, CO and NO₂ emissions and of biospheric CO₂ fluxes, especially in the surroundings of the investigated sources. Since simulations at the high resolution required in this study can only be conducted with a limited area model, another important input are initial and boundary conditions for both the trace gases and the meteorology. These inputs need to be provided in a form that allows assigning concentrations to all individual tracers as outlined above. NO₂ tracers are simulated as nitrogen oxide (NO_x = NO + NO₂) and then split into NO and NO₂ based on an empirical formula.

The spatial resolution of the anthropogenic emissions and biospheric fluxes should be similar to the model resolution in order to resolve the atmospheric variability at all scales detectable by the satellite. In particular, major point sources, i.e. power plants and industry, should be

<p>Final Report</p>	<p>ESA Project SMARTCARB</p> <p>Study on use of satellite measurements of auxiliary reactive trace gases for fossil fuel carbon dioxide emission estimation</p> <p>contract no 4000119599/16/NL/FF/mg</p>	  
----------------------------	--	---

located as exactly as possible. The resolution of the boundary conditions should be high enough that the variability in the CO₂ background is not underestimated. Without a dedicated investigation, it is difficult to specify an appropriate resolution. As a general rule, the influence of the boundary conditions decreases with increasing size of the model domain. This is another argument for not choosing only a small domain surrounding the sources.

Emissions and boundary conditions also need to be resolved in time, ideally with a resolution of 1-3 hours. Emissions need realistic diurnal, weekly and seasonal cycles.

For stack emissions, the emission height needs to be increased by an additional plume rise that depends on the flue gas properties (temperature and flow) and the actual meteorology (wind speed and temperature profile). If the plume rise is not considered, tracer concentrations downstream can be biased (Guevara et al., 2014). Therefore, a plume rise model should be used to account for the effective emission heights.

2.1.4 Output data

The output data need to be specified in terms of output variables, resolution and output frequency. The resolution should correspond to the native resolution of the model in order to preserve the full information. 3-D output should include all tracer fields as well as the meteorological variables required for calculating XCO₂ and VCDs of CO and NO₂. Furthermore, the output data needs to include all parameters required for the inversion (e.g. wind fields) and cloud information for masking cloudy pixels. The output data need to be frequent enough to calculate the satellite data at the correct overpass time, which requires output with at least hourly resolution to reduce the uncertainty due to temporal interpolation.


The model also needs to be able to simulate realistic spatial and temporal distribution of clouds, because the model fields will be used to filter cloudy observations in the synthetic dataset. To correctly simulate the temporal development of convective clouds it is essential to use a convection-resolving model since convection-parameterizations still fail to reproduce the diurnal cycle of convective clouds (Ban et al., 2014).

2.1.5 Simulation period

The simulation period needs to cover a representative set of seasonally varying meteorological situations and illumination conditions. It should provide enough satellite overpasses to build representative statistics. The simulation period is ultimately limited by the high computational cost for such simulations.

In the SMARTCARB proposal, we suggested that at least two months each in summer and winter should be simulated and additional months will be added if computational resources permit (RD-4). Therefore, suitable time periods need to be selected to represent typical weather conditions (and hence cloud cover) in the respective seasons.

The temporal coverage of the satellite instrument depends on the satellite specifications (swath width and resolution) and cloud coverage. The cloud coverage depends on type of climate prevailing over the model domain. For high latitudes, the number of observations is also limited, especially in winter, because observations under large solar zenith angles need

<p>Final Report</p>	<p>ESA Project SMARTCARB</p> <p>Study on use of satellite measurements of auxiliary reactive trace gases for fossil fuel carbon dioxide emission estimation</p> <p>contract no 4000119599/16/NL/FF/mg</p>	
----------------------------	--	---

to be discarded. The number of observations can be artificially increased by sampling each day of the simulation.

2.2 Model setup

In this section, model settings are chosen based on the model requirements described in the previous section and the benchmark simulation in Section 2.3.2.

2.2.1 Specification of satellite observations

The model requirements depend on the specifications of the satellites that are described in Section 3. The main specifications that drive the model requirements are the satellite swath, pixel size, and coverage.

In this section, the reference scenario will be a CO₂ satellite based on the concepts developed for the Earth Explorer 8 candidate mission with an equator crossing time at 11:30 hrs. local time, a spatial resolution of 2 × 2 km² and swath widths of 180 km or 240 km (ESA, 2015). The temporal coverage would be 12 days or better poleward of 40° latitude and 30 days at the equator for a single satellite. For a constellation of CO₂ satellites the temporal coverage would be accordingly smaller, up to every three days poleward of 40° for four satellites.

For the co-emitted trace gases CO and NO₂, the following three scenarios will be covered:




- 1) Sentinel-5 flying at 9:30 hrs. local time,
- 2) an instrument like Sentinel-5 flying at the same local time and orbit as the CO₂ satellite,
- 3) an instrument flying at the same time and orbit as the CO₂ satellite with the same spatial resolution and swath width.

Sentinel-5 has a planned ground pixel size smaller than 8 km at nadir, a swath width of 2600 km and would provide daily global coverage.

2.2.2 Model domain and resolution

A well-suited domain covers the city of Berlin and the nearby power plant Jänschwalde as shown in Figure 1. These two sources produce distinct CO₂ plumes as previously demonstrated in the LOGOFLUX studies (RD-2, RD-3).

The typical lengths of CO₂ plumes of these two sources were estimated from COSMO-7 simulations with lower spatial resolution (7 × 7 km²) conducted for the CarboCount-CH project (Liu et al., 2017). For the CO₂ satellite, we assumed a random uncertainty of 1 ppm which is slightly smaller than the uncertainty estimated for CarbonSat (1.5 ppm) (ESA, 2015). Furthermore, we assume that the plume may be detectable in a sample of 10 × 10 pixels (20 km × 20 km). With these assumptions, the detection limit would be about 0.3 ppm. A typical length of CO₂ plumes from Berlin and Jänschwalde corresponding to this threshold was estimated to be about 200 to 300 km downstream for strong wind speeds.

Final Report	<p>ESA Project SMARTCARB</p> <p>Study on use of satellite measurements of auxiliary reactive trace gases for fossil fuel carbon dioxide emission estimation</p> <p>contract no 4000119599/16/NL/FF/mg</p>	  
---------------------	--	---

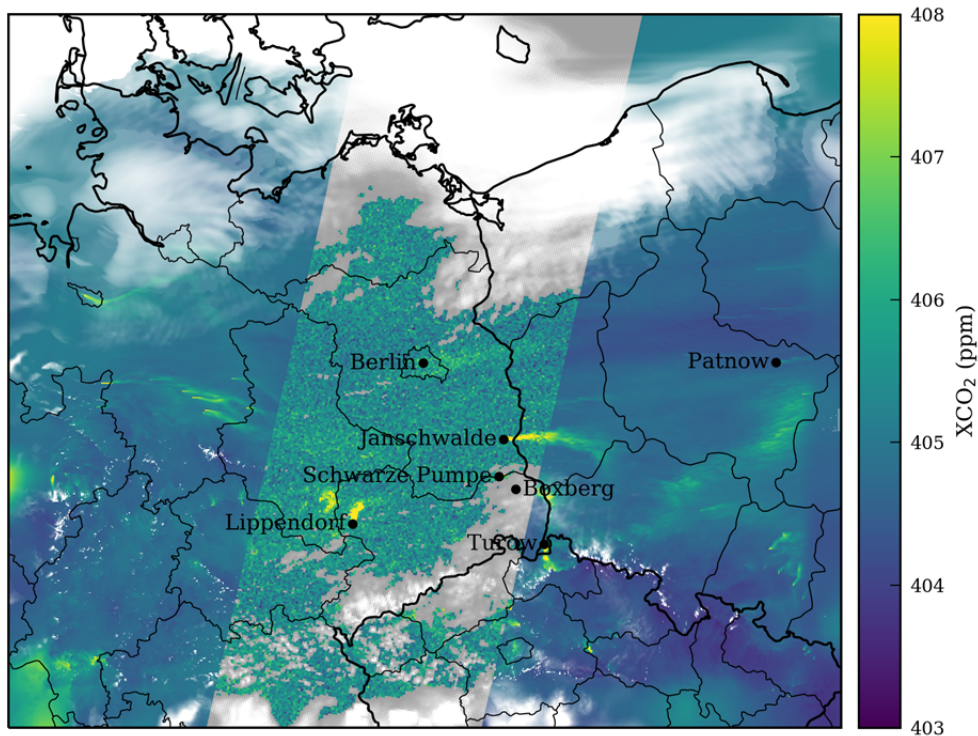


Figure 1: The SMARTCARB model domain ($700 \times 600 \times 60$ grid cells) with approximately $1.1 \text{ km} \times 1.1 \text{ km}$ spatial resolution and the swath of a CO_2 satellite (250 km).

Considering the satellite specification and expected plume lengths, the size of the COSMO model domain was specified as 700×600 grid cells with a resolution of 0.01° ($\sim 1.1 \text{ km}$) and 60 vertical levels. The size of the domain is thus $780 \text{ km} \times 670 \text{ km}$ (Figure 1). The model domain is nested in the northeastern corner of the COSMO-7 domain using the same rotated pole coordinate system as used for COSMO-7 (north pole: 43°N , -170°E). This spatial resolution is high enough to resolve the pixels of the CO_2 satellite and the domain is large enough to fully cover most of the plumes expected from Berlin and Janschwalde. The vertical resolution is identical to the one used by MeteoSwiss for their $1 \text{ km} \times 1 \text{ km}$ weather forecast simulations and is sufficient for resolving the dynamics of the planetary boundary layer and clearly sufficient for simulating realistic vertical profiles of the investigated trace gases. The lowest model layer has a depth of 20 m. The highest model level is located in the stratosphere at approximately 24 km. The swath width of Sentinel-5 is too wide for simulating the whole swath with this high spatial resolution. However, for inverse modelling mainly the overlap between the CO_2 and NO_2 measuring instruments is important.

2.2.3 Tracer setup

A possible setup with a total of more than 40 tracers was presented in RD-4. This setup was critically reviewed based on the model requirements. A set of conditions has been defined which shall be used as reference scenario in the study. The reference simulation can be considered to represent the most realistic configuration with time-varying emissions, a plume rise for the major sources and a NO_x decay e-folding time of four hours. In total, 50 tracers will be transported in the simulation (Table 1).







Final Report	ESA Project SMARTCARB Study on use of satellite measurements of auxiliary reactive trace gases for fossil fuel carbon dioxide emission estimation contract no 4000119599/16/NL/FF/mg	  Max Planck Institute for Biogeochemistry 
---------------------	---	--

Table 1: Overview of tracers used with the COSMO model.

Tracer name ¹	Description	Number of tracers
	Carbon dioxide	
CO2_BG	time-varying CO ₂ mass fraction at lateral boundary	1
CO2_GPP	time-varying CO ₂ surface flux from gross primary production	1
CO2_RA	time-varying CO ₂ surface flux from respiration	1
CO2_TOT	time-varying CO ₂ emissions for all sources in domain	1
CO2_SURF	time-varying CO ₂ emissions for all sources in domain but emitted at surface	1
CO2_A	time-varying CO ₂ emissions for all sources in domain excl. Berlin and power plants	1
CO2_BV	time-varying CO ₂ emissions for all sources in Berlin	1
CO2_BC	time-constant CO ₂ emissions for all sources in Berlin	1
CO2_Bx	time-varying CO ₂ emissions for industry (0), heating (1) and traffic (2) in Berlin	3
CO2_Txx	time-varying CO ₂ emissions in Berlin for eight 3-hourly time intervals	8
CO2_JV	time-varying CO ₂ emissions for six major power plants (incl. Jänschwalde)	1
CO2_JC	time-constant CO ₂ emissions for six major power plants (incl. Jänschwalde)	1
CO2_NPR	time-varying CO ₂ emissions for six major power plants (incl. Jänschwalde) without plume rise	1
		Σ 22
	Carbon monoxide	
CO_BG	time-varying CO mass fraction at lateral boundary	1
CO_TOT	time-varying CO emissions for all sources in domain	1
CO_SURF	time-varying CO emissions for all sources in domain but emitted at surface	1
CO_A	time-varying CO emissions for all sources in domain excl. Berlin and power plants	1
CO_BV	time-varying CO emissions for all sources in Berlin	1
CO_BC	time-constant CO emissions for all sources in Berlin	1
CO_Bx	time-varying CO emissions for industry (0), heating (1) and traffic (2) in Berlin	3
CO_JV	time-varying CO emissions for six major power plants (incl. Jänschwalde)	1
CO_JC	time-varying CO emissions for six major power plants (incl. Jänschwalde)	1
CO_NPR	time-varying CO emissions for six major power plants (incl. Jänschwalde) without plume rise	1
		Σ 12
	Nitrogen oxides	
NOX_BG	time-varying NO _x mass fraction at lateral boundary	1
NOX_TOT	time-varying NO _x emissions for all sources in domain	1
NOX_SURF	time-varying NO _x emissions for all sources in domain but emitted at surface	1
NOX_A	time-varying NO _x emissions for all sources in domain excl. Berlin and power plants	1
NOX_BV	time-varying NO _x emissions for all sources in Berlin	1
NOX_BC	time-constant NO _x emissions for all sources in Berlin	1
NOX_Bx	time-varying NO _x emissions for industry (0), heating (1) and traffic (2) in Berlin	3
NOX_Rxx	time-varying NO _x emissions in Berlin for inert and decaying NO _x (e-folding times: 2, 12, and 24 hours)	4

Final Report	ESA Project SMARTCARB Study on use of satellite measurements of auxiliary reactive trace gases for fossil fuel carbon dioxide emission estimation contract no 4000119599/16/NL/FF/mg	  Max Planck Institute for Biogeochemistry 
---------------------	---	--

NOX_JV	time-varying NO _x emissions for Jänschwalde	1
NOX_JC	time-constant NO _x emissions for Jänschwalde	1
NOX_NPR	time-varying NO _x emissions for six major power plants (incl. Jänschwalde) without plume rise	1
		Σ 16
	Total number of tracers:	Σ 50

¹ tracer short name used in the COSMO-GHG model

2.2.4 Input data

Initial and boundary conditions

For meteorology, the IC/BC will be obtained from the operational COSMO-7 analysis system of MeteoSwiss (available as hourly fields at a resolution of $7 \times 7 \text{ km}^2$), which itself is driven at its boundaries by operational ECMWF IFS analyses.

The most suitable input datasets for trace gases were identified in collaboration with Richard Engelen from ECMWF. For CO₂ and CO, we will use output from a simulation without data assimilation but indirectly constrained by in-situ data at a very high resolution of $0.15^\circ \times 0.15^\circ$ (T1279, ~15 km, levels 37-137). The simulation can be retrieved from ECMWF's MARS archive as experiment "gf39" under class "RD". For NO and NO₂, we will use the CAMS operational product (daily forecast) constrained by satellite observations at $0.5^\circ \times 0.5^\circ$ spatial resolution (T255, ~60 km). The experiment code is "0001" under class "MC".




CO₂, CO and NO_x emissions

Different emission inventories were considered for providing emissions of CO₂, CO and NO_x. Since a high spatial resolution is required, we decided on the TNO/MACC-III inventory that has a spatial resolution of about $7 \times 7 \text{ km}^2$ and provides information on strong point sources at their exact location (Kuenen et al., 2014).

Emissions of major point sources will be cross-checked with emissions from the European Pollutant Release and Transfer Register (E-PRTR, <http://prtr.ec.europa.eu>). The largest point sources, incl. Jänschwalde and the entire city of Berlin, will be removed from TNO/MACC-III and will be treated separately.

For the city of Berlin, an inventory with very high spatial resolution was obtained from the "Senatsverwaltung für Stadtentwicklung und Umwelt" for 2012 (Senatsverwaltung für Stadtentwicklung und Umwelt, Juni 2016). The inventory includes emissions of over 30 pollutants including CO, CO₂ and NO_x for seven major source categories.

The emissions for Berlin were provided as shape files, a geospatial vector data format, storing emissions as point, line and area sources. The vector data were re-projected to the rotated pole coordinate system used in COSMO and then rasterized by computing for each grid cell of the COSMO model domain the intersecting length and area of the line and area sources, respectively, thus preserving the total emissions.

Final Report	ESA Project SMARTCARB Study on use of satellite measurements of auxiliary reactive trace gases for fossil fuel carbon dioxide emission estimation contract no 4000119599/16/NL/FF/mg	  Max Planck Institute for Biogeochemistry 
---------------------	---	--

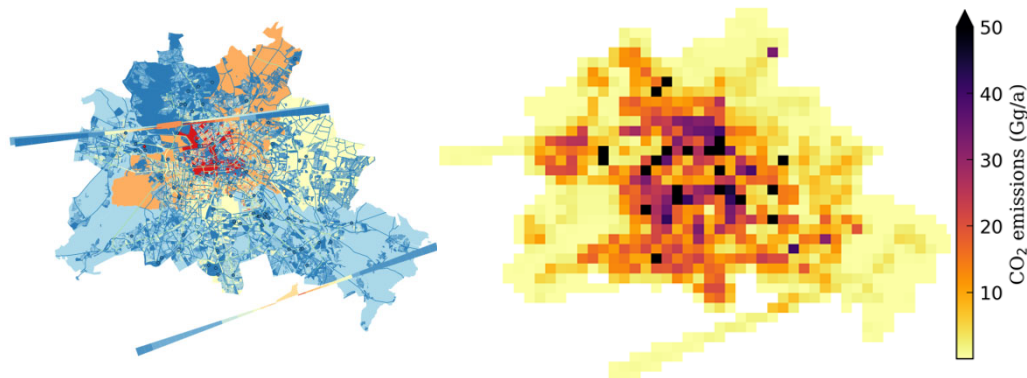


Figure 2: (left): Sketch of CO₂ emission in the Berlin inventory showing point, line and area sources from different emission categories. (right): Total CO₂ emissions re-projected and rasterized on the COSMO model grid.




Table 2: Allocation of source categories from the Berlin inventory and TNO/MACC-III in three source categories used in SMARTCARB simulations (traffic, industry and heating) based on NFR09 sector codes.

Emission category	Berlin emission inventory (code)	TNO/MACC-III (SNAP category)
(A) Traffic	Other traffic (3) Offroad (4) Construction sites (5) Road transport ¹ (9)	Road transport (7) Non-road transport (8)
(B) Industry	Industry and commerce (1) Additional sources ² (6) Biogenic sources ³ (7)	Energy industry (1) Industry (34) Extraction and distribution of fossil fuels (5) Product use (6) Waste treatment (9) Agriculture (10)
(C) Heating	Building heating (2)	Non-industrial combustion (2)

¹emissions from road transport were estimated from an inventory from 2009; ²source category without CO, CO₂ or NO_x emissions; ³only NO_x emissions will be used

The major emission categories differ in the TNO/MACC-III and Berlin inventory, but are ultimately based on NFR09 sector codes. The sector codes were used to cluster these categories into the three major emission categories that will be used in the simulations: (A) traffic, (B) industry and (C) domestic heating (Table 2).

The most recent version of the Berlin inventory does not yet include emissions from minor roads. For minor roads, only emissions for the year 2009 and only for NO_x are available. Thus, CO and CO₂ emission will be estimated using emission ratios of CO₂/NO_x and CO/NO_x calculated from the road emissions for major roads. For simplicity a constant ratio is assumed. The CO₂/NO_x factor is (355.5 ± 45.4) kg CO₂ / kg NO_x and the CO/NO_x factor is (5.7 ± 2.7) kg CO / kg NO_x. The uncertainty of this method is expected to be quite large, in particular for CO where the standard deviation of the conversion factor is quite large. On the

<p>Final Report</p>	<p>ESA Project SMARTCARB</p> <p>Study on use of satellite measurements of auxiliary reactive trace gases for fossil fuel carbon dioxide emission estimation</p> <p>contract no 4000119599/16/NL/FF/mg</p>	  
----------------------------	--	---

other hand, minor roads account only for 22% of NO_x emission suggesting that the error for total emissions remains small.

Temporal profiles

The emission inventories provide only total annual emissions. In order to calculate hourly emissions, emission scaling factors are applied to compute diurnal, weekly and annual cycles. We will use scaling factors based on factors critically reviewed in the TROTREP project (Bultjes et al., 2003).

Vertical profiles

Emission heights need to be calculated for all emissions that are not emitted at the surface. These are emissions from point sources such as power plants or industrial facilities and emissions from heating that are typically emitted at the roof top and stored as area source in both the TNO/MACC-III and Berlin inventory. The Berlin inventory also includes aircraft emissions during climb and descent at the two airports in the city.

Emissions are vertically distributed using distribution probability tables based on tables created during COST 728 actions (http://www.cost.eu/COST_Actions/essem/728, accessed Apr. 2017) that have been used also in the EMEP unified modelling system (<http://ies-webarchive.jrc.ec.europa.eu/citydelta/>, accessed Apr. 2017). For this study, the tables were critically reviewed and updated for the model requirements. The number of layers was increased from seven to 16 with top of the highest layer at 3330 m instead of 990 m. The additional layers allow for finer vertical distribution of the emissions and higher emission heights from plume rise calculations of the major point sources. Table 3 and Table 4 shows the vertical distributions used for point, line and area sources.

For the aircraft emissions in Berlin, we calculate the emission height along the flight track assuming a climb and descent rate of 3 degrees. While the descent rate is constant for instrument descent, climb rates differ largely based on aircraft type, loading and weather conditions.

Plume rise

For point sources, the emission height can be much higher than the geometric height of a stack because of the buoyancy of the flue gas. The plume rise depends on the stack geometry (height and diameter), flue gas properties (temperature, humidity, and exit velocity) and meteorological conditions (wind speed, stability classes).

The Association of German Engineers (VDI: Verein Deutscher Ingenieure) provides guidelines for calculating the plume rise for stacks (VDI guideline 3782(3), (VDI, 1985)) and cooling towers (VDI guideline 3784(2), (VDI, 1990)). The guideline for stacks uses empirical equations for estimating the plume raise based on a modified Briggs equation (Briggs, 1982) and the guideline for cooling towers recommends using the numerical model of Schatzmann and Policastro (1984).




Final Report	ESA Project SMARTCARB Study on use of satellite measurements of auxiliary reactive trace gases for fossil fuel carbon dioxide emission estimation contract no 4000119599/16/NL/FF/mg	  Max Planck Institute for Biogeochemistry 
---------------------	---	--




Table 3: Emission heights based on SNAP categories for point sources.

SNAP Category		0 - 4 m	4 - 30 m	30 - 60 m	60 - 90 m	90 - 125	125 - 170	170 - 310	310 - 470	470 - 710	710 - 990
1	Energy industry	0.00	0.00	0.00	0.00	0.00	0.00	0.08	0.46	0.29	0.17
2	Non-industrial combustion	0.05	0.25	0.30	0.20	0.15	0.05	0.00	0.00	0.00	0.00
3	Combustion in manufacturing industry	0.00	0.04	0.08	0.12	0.16	0.20	0.20	0.15	0.05	0.00
4	Production processes	0.00	0.20	0.30	0.30	0.15	0.05	0.00	0.00	0.00	0.00
5	Extraction & distribution of fossil fuels	0.00	0.20	0.30	0.30	0.15	0.05	0.00	0.00	0.00	0.00
6	Product use	0.50	0.50	0.00	0.00	0.00	0.00	0.00	0.00	0.00	0.00
7	Road transport	1.00	0.00	0.00	0.00	0.00	0.00	0.00	0.00	0.00	0.00
8	Non-road transport	1.00	0.00	0.00	0.00	0.00	0.00	0.00	0.00	0.00	0.00
9	Waste treatment (for CH ₄)	0.50	0.50	0.00	0.00	0.00	0.00	0.00	0.00	0.00	0.00
	Waste treatment (other species)	0.10	0.00	0.10	0.15	0.20	0.20	0.15	0.07	0.03	0.00
10	Agriculture	1.00	0.00	0.00	0.00	0.00	0.00	0.00	0.00	0.00	0.00

Table 4: Emission heights based on SNAP categories for line and area sources.

SNAP Category		0-4m	4-30m	30-60m	60-90m	90-125	125-170	170-310	310-470	470-710	710-990
1	Energy industry	0.00	0.25	0.25	0.25	0.25	0.00	0.00	0.00	0.00	0.00
2	Non-industrial combustion	0.00	0.75	0.25	0.00	0.00	0.00	0.00	0.00	0.00	0.00
3	Combustion in manufacturing ind.	0.00	0.25	0.25	0.25	0.25	0.00	0.00	0.00	0.00	0.00
4-10	Other categories	1.00	0.00	0.00	0.00	0.00	0.00	0.00	0.00	0.00	0.00

Plume rise calculations for larger model domains are challenging. First, the number of point sources is quite large. E-PRTR lists about 4000 point sources in the model domain emitting CO₂, CO or NO_x. Second, the input data required for the calculations are often confidential and not available in a central database. Third, plume rise calculations for cooling towers have high computational costs and are not feasible for longer simulations. However, nowadays the flue gas of (large) power plants is often released through the cooling towers, since after the mandatory desulfurization it is too cold and hence not sufficiently buoyant for being released over a classical stack (Busch et al., 2002). A further complication is that in the case of

<p>Final Report</p>	<p align="center">ESA Project SMARTCARB</p> <p align="center">Study on use of satellite measurements of auxiliary reactive trace gases for fossil fuel carbon dioxide emission estimation</p> <p align="center">contract no 4000119599/16/NL/FF/mg</p>	  
----------------------------	---	---

multiple stacks or cooling towers located next to each other, the plumes start to interact and to further enhance the plume rise.

Because of these challenges, we will implement a simplified approach for simulating the plume rise for the major point sources in the model domain. Despite its simplicity, it is a major step forward compared to previous CO₂ studies, which neglected this effect. The plume rise will be calculated using the empirical equations for stacks (VDI 3782(3)) with meteorological data from the COSMO-7 model extracted at the location of the major stacks in the domain. Since auxiliary parameters are not always available for each point source, reasonable parameters are estimated from a published statistics (Pregger and Friedrich, 2009). As an example, Figure 3 shows the emission height calculated for the Jänschwalde power plant emitted via one of its cooling towers (H = 120) using parameters from Pregger and Friedrich (2009). From the figures it is quite clear that the emission height is often much higher than the stack height and also has a clear diurnal cycle.

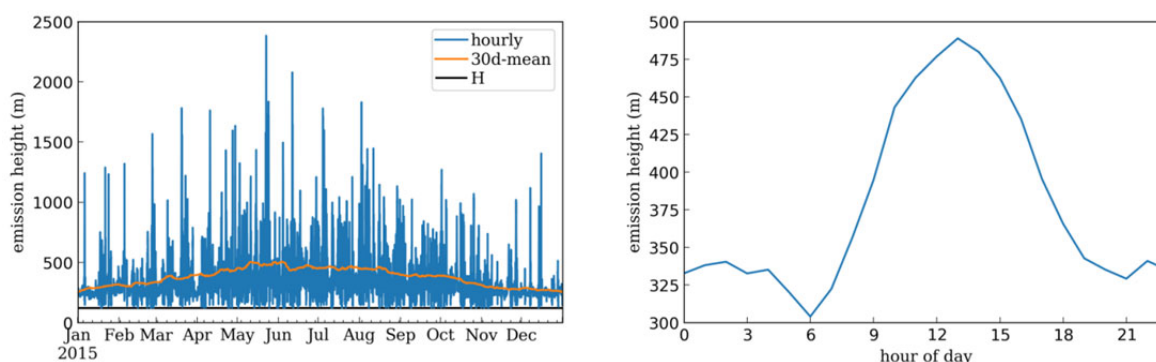





Figure 3: (left): Mean emission heights of CO₂ emitted by the power plant in Jänschwalde for 2015. The plume rise was calculated according to VDI 3782(3) using COSMO-7 profiles of temperature and wind speed. (right): Average diurnal cycle of plume rise.

Biospheric fluxes

MPI-BGC will use VPRM (Vegetation Photosynthesis and Respiration Model (Mahadevan et al., 2008) to produce hourly biosphere fluxes, both photosynthesis and respiration, on the grid of the COSMO model. This diagnostic model is based on meteorological input along with the Enhanced Vegetation Index (EVI) and Land Surface Water Index (LSWI) calculated from MODIS reflectances. These are available as an 8-day product (MOD09A1) at 500 m spatial resolution. These indices will be smoothed via loess filtering and interpolated onto the COSMO grid. Vegetation classes at the grid resolution are determined from the 1-km SYNMAP land cover map (Jung et al., 2006). Further parameters required for VPRM are based on fits to flux tower measurements representative of these vegetation classes. The model will be run offline in point mode, driven by the highest resolution ECMWF meteorological data available. It is also possible to run VPRM online within a mesoscale model, driven with the higher-resolution meteorological parameters (temperature and photosynthetically-active radiation), but this is not implemented in COSMO.

Final Report	ESA Project SMARTCARB Study on use of satellite measurements of auxiliary reactive trace gases for fossil fuel carbon dioxide emission estimation contract no 4000119599/16/NL/FF/mg	  Max Planck Institute for Biogeochemistry 
---------------------	---	---

2.2.5 Output data

Output data will be hourly fields of tracers (see Table 1 for complete list) and meteorological parameters including cloud information that are computed by the convection-resolving COSMO model. The meteorological output will include all fields that are needed to run offline FLEXPART-COSMO simulations. A complete list of the meteorological output is provided in Table 5.




Table 5: Meteorological output fields.

Variable	dim	Units COSMO	COSMO GRIB code ¹ / table (name) / levtype
Temperature	3	K	11 / 2 (T)
Wind east-west	3	m s ⁻¹	33 / 2 (U)
Wind north-south	3	m s ⁻¹	34 / 2 (V)
Wind vertical	3	m s ⁻¹	40 / 2 (W)
Specific humidity	3	kg kg ⁻¹	51 / 2 (QV)
Surface pressure	2	Pa	1 / 2 (PS) / 1
Total cloud cover	2	0-1	71 / 2 (CLCT)
10-m wind U	2	m s ⁻¹	33 / 2 (U_10M) / 105
10-m wind V	2	m s ⁻¹	34 / 2 (V_10M) / 105
2-m temperature	2	K	11 / 2 (T_2M) / 105
2-m dew point temperature	2	K	17 / 2 (TD_2M) / 105
Acc. large scale precipitation	2	kg m ⁻²	102 / 201 (RAIN_GSP) + 79 / 2 (SNOW_GSP)
Acc. convective precipitation	2	kg m ⁻²	113 / 201 (RAIN_CON) + 78 / 2 (SNOW_CON)
Acc. surface sensible heat flux	2	W m ⁻²	122 / 2 (ASHFL_S)
Acc. surface solar radiation	2	W m ⁻²	111 / 2 (ASOB_S)
Acc. E-W surface stress	2	N m ⁻²	124 / 2 (AUMFL_S)
Acc. N-S surface stress	2	N m ⁻²	125 / 2 (AVMFL_S)
Surface geopotential (orography)	2	m	8 / 2 (HSURF)
Land-sea mask	2	0-1	81 / 2 (FR_LAND)
Surface roughness	2	m	83 / 2 (Z0)
Soil temperature level 1	2	K	85 / 2 (T_SOIL)
Snow depth	2	kg m ⁻²	65 / 2 (W_SNOW)
Cloud ice water content	3	kg kg ⁻¹	33 / 201 (QI)
Cloud liquid water content	3	kg kg ⁻¹	31 / 201 (QC)
Cloud cover	3	0-1	29 / 201 (CLC)

¹see DWD tables at: https://www.ncl.ucar.edu/Document/Manuals/Ref_Manual/NclFormatSupport.shtml#GRIB1-built-in-parameter-tables, accessed Apr. 2017.

2.2.6 Simulation period

The computational demand of the simulations was analyzed for the model setup using a simulation benchmark with the GPU accelerated version of COSMO (see Section 2.3.2). The benchmark showed that a complete year could be simulated in only about 21 days. Since this is a realistic target for the present project, we will attempt to simulate a complete year

<p>Final Report</p>	<p>ESA Project SMARTCARB</p> <p>Study on use of satellite measurements of auxiliary reactive trace gases for fossil fuel carbon dioxide emission estimation</p> <p>contract no 4000119599/16/NL/FF/mg</p>	  
----------------------------	--	---

instead of only two months as suggested in the SMARTCARB proposal. The estimates for the proposal were too conservative since the significant performance gain that can be achieved with the GPU version was underestimated.

A CO₂ satellite with a 200 km swath and 2×2 km² pixel size will provide about 10 observations per year under favorable conditions (Bovensmann et al., 2010; ESA, 2015). A simulation period of one year should thus be suitable and generate a sufficiently large number of study cases. We will simulate the year 2015 as this will allow us validating the simulations against CO₂ observations from GOSAT and OCO-2.

2.3 COSMO-GHG model

2.3.1 COSMO-GHG model

The Consortium for Small-Scale Modelling (COSMO) is a consortium of seven European national weather services formed in October 1998 which aims to develop, improve and maintain a non-hydrostatic limited area atmospheric model. The COSMO model is used for both operational and research applications by the members of the consortium, universities and research institutes.




COSMO is the first NWP model worldwide that has been fully and successfully ported to GPUs (Führer et al., 2014). MeteoSwiss is already using this GPU accelerated version of the model, called COSMO-POMPA and based on version 5.01 of the official model releases, for its operational weather forecasts.

The COSMO-GHG model is an extension of COSMO with modules for the passive transport of greenhouse gases (GHG). The extension builds on the tracer module, which was developed for COSMO to provide a flexible mechanism for incorporating passively transported tracers (Roches and Führer, 2012). The tracer module has been fully integrated in COSMO version 5.0 and also in COSMO-POMPA. COSMO-GHG includes additional routines for simulating a set of tracers which are not only passively transported but also experience the influence of three-dimensional emissions or surface fluxes read in from external datasets.

In the framework of SMARTCARB, the GHG extension is currently ported to the GPU version and will be used for conducting the simulations in this project.

2.3.2 Simulation benchmark

In order to estimate the computational demand, a benchmark was conducted for the model domain defined in Section 2.2 with the GPU-accelerated version of COSMO. The performance and scaling of COSMO-POMPA has been benchmarked on two systems at the Swiss National Supercomputing Centre (CSCS), the old Piz Daint (CPU E5-2670 and GPU K20x) and the new more powerful Piz Daint, for different domain sizes and resolutions and for different node configurations. If sufficient work is allocated to each GPU (per-GPU sub-domain size of at least 100 × 100 grid points), it has been shown that performance results can be scaled simply via the total number of time steps and grid points required to execute the simulation. Furthermore, it has been shown that the performance gain when moving from old Piz Daint to new Piz Daint is 2.0x. For the estimation of our requirements, we use benchmarks from




Final Report	ESA Project SMARTCARB Study on use of satellite measurements of auxiliary reactive trace gases for fossil fuel carbon dioxide emission estimation contract no 4000119599/16/NL/FF/mg	  Max Planck Institute for Biogeochemistry 
---------------------	---	--

MeteoSwiss' COSMO-1 configuration as a baseline. Benchmarks conducted for the CarboCount-CH project indicate that the additional computation cost for each additional tracer is of the order of 2.5%. Here, we make the conservative assumption of an extra cost of 3% per tracer. Based on these benchmarks, we estimated the total node hours for one day and for one year of simulation, respectively, for two different domain sizes (Table 6). For one year of simulation with 55 tracers for the domain proposed for SMARTCARB (700 x 600 x 60 grid cells, time step 10 s), we estimate a total of 7532 node hours. Due to increased I/O demands and accounting for a safety margin due to job failure, we estimate the cost of a full year of simulation for our setup of 8000 node hours.

Table 6: Estimated node hours for one day/one year of simulation with 55 tracers for the model domain proposed for SMARTCARB as well as the COSMO-1 domain for reference. The horizontal model dimensions are i_e and j_e , the model time step (s) is dt , and the number.

Scenario	Target					Node hours		
	i_e	j_e	dt	tracer	time	CPU old Daint	GPU old Daint	GPU new Daint
SMARTCARB, 1 day	700	600	10	55	24	151.7	41.3	20.6
COSMO-1, 1 day	1158	774	10	55	24	323.7	88.1	44.0
SMARTCARB, 1 year	700	600	10	55	8760	55361	15064	7532
COSMO-1, 1 year	1158	774	10	55	8760	118141	32148	16074

If the simulations would be conducted on 16 GPUs, the total computation time for one year is about 21 days. Therefore, a simulation period of one year appears feasible with this model version. This is a much longer simulation period than the two months suggested in the SMARTCARB proposal, because the performance gain on GPU was underestimated.

<p>Final Report</p>	<p>ESA Project SMARTCARB</p> <p>Study on use of satellite measurements of auxiliary reactive trace gases for fossil fuel carbon dioxide emission estimation</p> <p>contract no 4000119599/16/NL/FF/mg</p>	  
----------------------------	--	---

3. Specifications for satellite observations

The section describes platform and instrument scenarios and instrument and error characteristics for these scenarios.

3.1 Instrument scenarios

The instrument scenarios define the parameters of the CO₂, CO and NO₂ satellite observations in terms of orbit, spatial resolution and spatial and temporal coverage. These scenarios have been defined in collaboration with ESA considering the above objectives.




3.1.1 Platforms

For the scenarios, two platforms are considered: MetOp-SG-A (Meteorological Operational Satellite – Second Generation - A) and Sentinel CO₂ mission. MetOp-SG-A is a series of meteorological satellites in low earth orbit that will carry the Sentinel-5 instrument measuring NO₂ and CO vertical column densities (VCD). Sentinel CO₂ mission is a new proposed platform with a CO₂ instrument as the main payload as well as potentially an instrument for NO₂ and CO observations. Both satellites will be on sun-synchronous orbits (SSO) but with different equator crossing times and repeat cycles.

For the computation of orbits we adopted the orbit simulator of the Netherlands Institute for Space Research (SRON) kindly provided by Joost aan de Brugh and Jochen Landgraf. The SRON orbit simulator is a collection of Python modules that could easily be integrated into our model output processing chain. The simulator makes a few simplifying assumptions such as perfect circular orbits and tiled ground pixels. Table 7 summarizes the key orbit parameters for both platforms. Orbit periods were calculated to match a given cycle duration and length. The orbit period then determines the altitude of the circular orbits and the inclination of a sun-synchronous orbit. The altitude of the circular orbits is slightly larger than the typically used mean altitude for elliptic orbits.

Table 7: Satellite platforms considered in the study

Parameter	Sentinel CO ₂ mission	MetOp-SG-A
Orbit type	Sun-synchronous orbit	Sun-synchronous orbit
Inclination	97.77°	98.7°
Orbits per day	14+10/11days	14+6/29 days
Cycle duration	11 days	29 days
Cycle length	164 Orbits	412 orbits
Altitude	602.24 km	830.16 km
Orbit Period	96.58 minutes	101.36 minutes
Local Time in Descending Node (Equator Crossing Time)	11:30 hrs	9:30 hrs

Final Report	ESA Project SMARTCARB Study on use of satellite measurements of auxiliary reactive trace gases for fossil fuel carbon dioxide emission estimation contract no 4000119599/16/NL/FF/mg	  Max Planck Institute for Biogeochemistry 
---------------------	---	--

In addition to a single satellite, the potential of a constellation of multiple satellites will also be studied in the SMARTCARB project. The basic assumption for a constellation is that the individual satellites would be spaced equally in orbit within their repeat cycle (360° is a full repeat cycle) as illustrated in Figure 1.

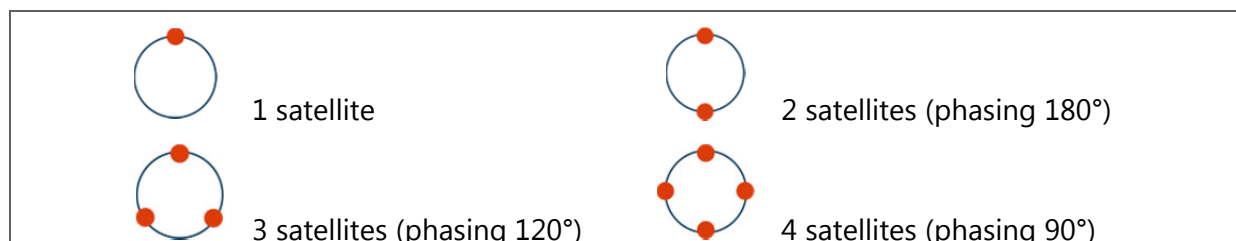


Figure 4: Satellite configuration of an orbit with multiple satellites.

3.1.2 Sentinel CO₂ mission

The Sentinel CO₂ satellite will carry an instrument for measuring CO₂ as well as an instrument for measuring NO₂ and CO VCDs. As reference scenario, we assume a CO₂ instrument with a 250 km wide swath and a ground pixel size of 4 km². The reference scenario for the NO₂/CO instruments assumes a wider swath of 350 km that encloses the CO₂ instrument with a 50 km context on each side. For the spatial resolution, three different scenarios have been included with pixel sizes at the sub-satellite point of 1 km², 4 km² or 16 km², respectively. Table 8 summarizes the key parameters for these instruments.

Table 8: Instrument scenarios on Sentinel CO₂ mission for CO₂, and NO₂/CO observations

Parameter	CO ₂ instrument	NO ₂ / CO instrument
Number of across-track pixels	125	340 / 170 / 85
Swath	250 km	350 km
Field of view	23.22 degree	32.1 degree
Pixel size at sub-satellite point	2×2 km ²	1×1 / 2×2 / 4×4 km ²
Along-track sampling time	0.286 seconds	0.143 / 0.286 / 0.572 seconds

Figure 5 shows the swath of the satellite computed with the SRON orbit simulator for a single orbit overlaid on the COSMO-GHG model simulation domain. The right-hand figure shows a zoom on the city of Berlin. In favorable cases, the city of Berlin and the power plant Jänschwalde can be covered by a single orbit. The zoom on Berlin shows that the satellite will have the potential to not only observe a city plume as a whole but also to resolve small-scale concentration gradients within the city and downwind.

Figure 6 shows the spatial coverage of the CO₂ and the CO/NO₂ instruments over Europe after a full orbit cycle of 11 days. Within this time period, each location within Europe will be seen by a single satellite once or twice for CO₂ and two to three times for NO₂ and CO due to the larger swath of these instruments. For a constellation of satellites, the numbers can be multiplied by the number of satellites. With a constellation of 3 satellites, for example, CO₂ observations over the city of Berlin could be obtained approximately every second day.

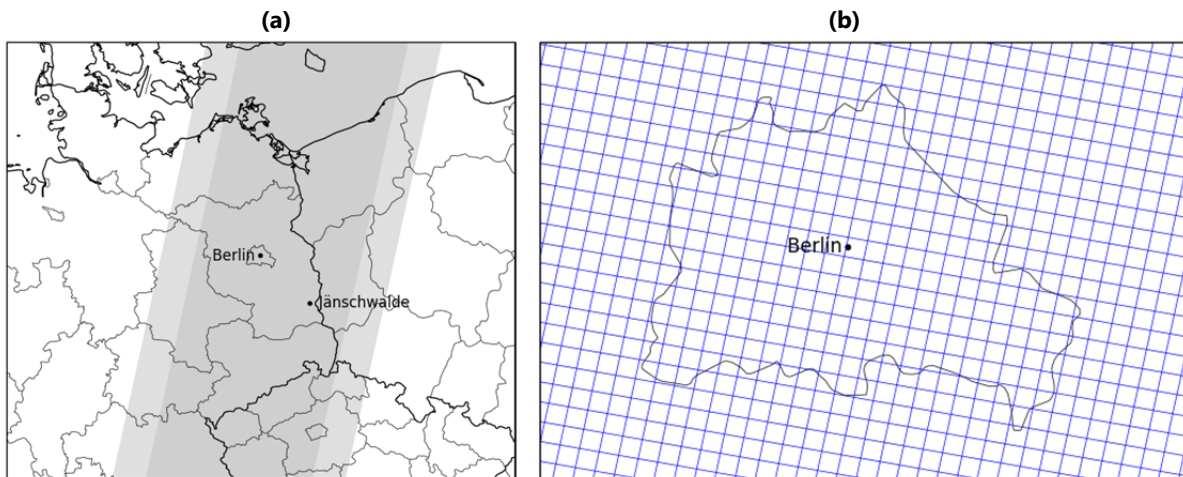


Figure 5: (a) Example swaths from Sentinel’s CO₂ and NO₂/CO instrument. The CO₂ instrument has a smaller swath (250 km) that is enclosed the by the NO₂/CO swath (350 km). (b) Zoom-in over Berlin showing Sentinel’s ground pixel with 2×2 km² resolution.

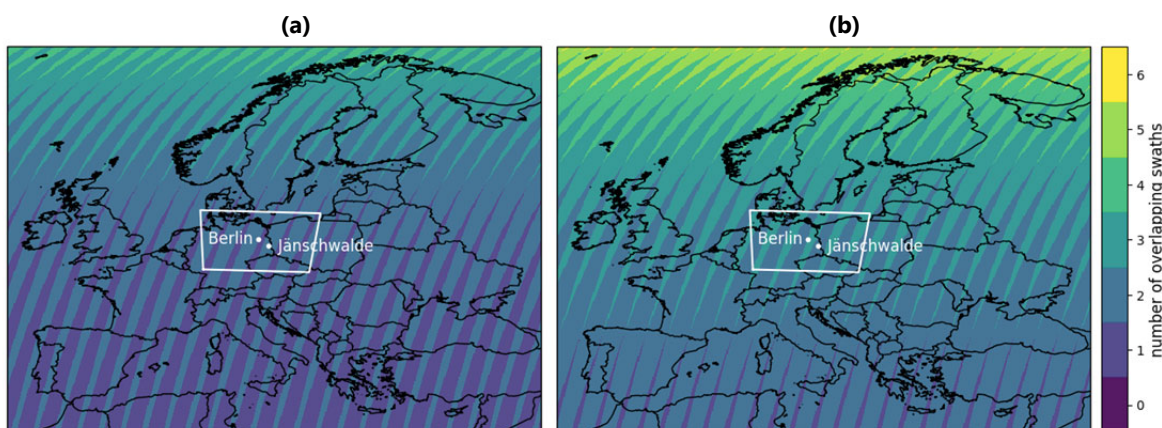


Figure 6: Spatial coverage of accumulated orbits for Sentinel CO₂ mission for the (a) CO₂ and (b) NO₂/CO instrument after 11 days (164 orbits).

3.1.3 MetOp SG A / Sentinel-5

MetOp SG A will carry the UVNS instrument. The instrument will measure NO₂ and CO columns within a swath of 2670 km and with a spatial resolution of 7.5 x 7.5 km² at the sub-satellite point. Table 9 summarizes the key instrument parameters. Note that the number of across-track pixels is only 208 in our calculations instead of 210 as officially assumed for Sentinel-5.

The pixel size of Sentinel-5 increases strongly in across-track direction due to the wide swath (Figure 7). In along-track direction the pixel size is approximately constant and directly determined by the sampling time (assuming tiled pixels). Figure 8 shows the coverage of Sentinel-5 within a single day. Global coverage is nearly achieved after a single day. In the model domain over Europe, the number of swaths per day will be 1 or 2.

Table 9: Instrument scenarios Sentinel-5

Parameter	Sentinel-5 / UVNS instrument
Number of across-track pixels	208
Swath	2670 km
Field of view	107.1 degree
Pixel size	7.5×7.5 km ² at sub-satellite point and 35×7.5 km ² at the edge
Sampling time	1.13 seconds

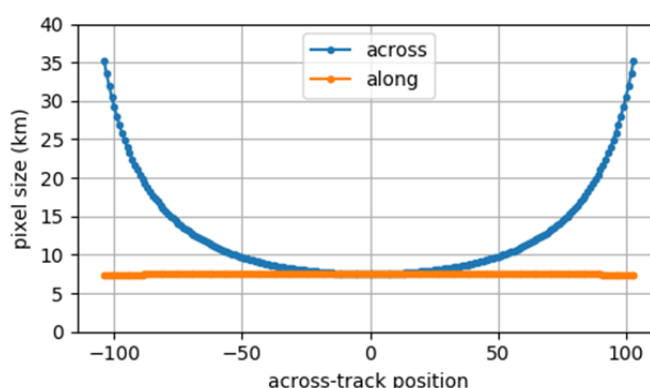


Figure 7: Sentinel-5 pixel size in across-track direction.

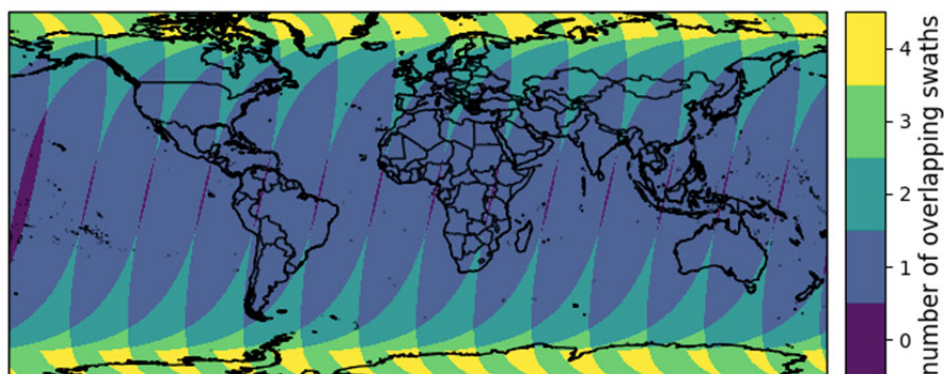





Figure 8: Spatial coverage of accumulated orbits for Sentinel-5 after 1 day (14 orbits)

3.2 Instrument error characteristics

Leveraging on previous studies for CarbonSat and on performance requirements for Sentinel-5, the error characteristics of the CO₂ instrument and of the CO and NO₂ instruments have been specified in collaboration with ESA.

In general, measurement errors have both random and systematic components. Systematic errors are particularly critical as they do not cancel out by averaging. At the same time, systematic errors are difficult to characterize.

In the following, the assumptions for the random components of the single sounding uncertainty of the different instruments are presented. For most instruments two or three

<p>Final Report</p>	<p align="center">ESA Project SMARTCARB</p> <p align="center">Study on use of satellite measurements of auxiliary reactive trace gases for fossil fuel carbon dioxide emission estimation</p> <p align="center">contract no 4000119599/16/NL/FF/mg</p>	  
----------------------------	---	---

scenarios are included in order to cover a realistic range between more or less demanding instruments.

3.2.1 CO₂ instrument

For XCO₂, three different uncertainty scenarios are assumed which relate back to the performance estimates derived for the Carbonsat mission concept (see Table 10). A detailed error budget for Carbonsat was presented in the Carbonsat Report for Mission Selection (ESA, 2015). In the LOGOFLUX study (RD-2, RD-3), error parametrization formula (EPF) for systematic errors have been developed which account for errors introduced by the following parameters (Buchwitz et al., 2013):

1. solar zenith angle (SZA)
2. albedo in the NIR band (760 nm)
3. albedo in the SWIR-1 band (1600 nm)
4. cirrus optical depth (COD)
5. cirrus top height (CTH)
6. aerosol optical depth (AOD) at 550 nm

The systematic errors introduced in this way are spatially and temporally correlated with the underlying aerosol, cirrus and surface reflectance fields. The errors are computed with the following regression formula

$$Q = \sum_i C_i X_i$$

where Q is the error. C_i are coefficients and X_i are the input parameters whose values are summarised in Table 10 and Table 11.

In SMARTCARB, we will calculate random and systematic errors based on SZA and albedos in the NIR and SWIR-1 band. Albedos will be taken from the MODIS albedo product at 1 km spatial resolution. A detailed consideration of COD, CTH and AOD are outside the scope of the study as they would require the collection and processing of a large amount of additional data. Thus, these parameters will not be included in the error calculations, which is less critical for the random component.

After computation of Q some further steps are needed to compute the final values:

- Systematic errors: A SZA bias correction needs to be applied by subtracting the term SZA/70.0 – 0.2.
- Random errors: If the computed random errors are smaller than the minimum value (here: 0.7 ppm) the value is set to the minimum value.

The random error calculated with the regression formula is about 1.5 ppm over vegetation with a SZA of 50 degrees (VEG50 scenario). To obtain random errors for the three scenarios (Table 10), the computed errors will be divided by 3.0, 2.0 and 1.5, respectively.




Final Report	ESA Project SMARTCARB Study on use of satellite measurements of auxiliary reactive trace gases for fossil fuel carbon dioxide emission estimation contract no 4000119599/16/NL/FF/mg	  Max Planck Institute for Biogeochemistry 
---------------------	---	---

Table 10: Uncertainty scenarios

Scenario name	Species	Satellite(s)	Reference noise
CO ₂ low noise	CO ₂	CO ₂ Sentinel	$\sigma_{\text{VEG50}} = 0.5$ ppm
CO ₂ medium noise	CO ₂	CO ₂ Sentinel	$\sigma_{\text{VEG50}} = 0.7$ ppm
CO ₂ high noise	CO ₂	CO ₂ Sentinel	$\sigma_{\text{VEG50}} = 1.0$ ppm
NO ₂ low noise	NO ₂	CO ₂ Sentinel	$\sigma_{\text{ref}} = 1 \times 10^{15}$ molecules cm ⁻² or 15%, whichever is larger
NO ₂ high noise	NO ₂	CO ₂ Sentinel	$\sigma_{\text{ref}} = 2 \times 10^{15}$ molecules cm ⁻² or 15%, whichever is larger
NO ₂ Sentinel-5	NO ₂	Sentinel-5	$\sigma_{\text{ref}} = 1.3 \times 10^{15}$ molecules cm ⁻² or 20%, whichever is larger
CO low noise	CO	Sentinel-5 / CO ₂ mission	$\sigma_{\text{ref}} = 4 \times 10^{17}$ molecules cm ⁻² or 10%, whichever is larger
CO high noise	CO	Sentinel-5 / CO ₂ mission	$\sigma_{\text{ref}} = 4 \times 10^{17}$ molecules cm ⁻² or 20%, whichever is larger

Table 11: Nadir error parametrization regression functions X₀ - X₇ (Buchwitz et al., 2013).




Function	Definition	Explanation	Valid Range
X ₀	1.0	Constant offset	-
X ₁	SZA - 50.0	Solar zenith angle (in degree)	0 - 80 degree
X ₂	ALB_NIR - 0.1	NIR albedo	0.03 - 0.7
X ₃	ALB_SWIR - 0.1	SWIR albedo	0.03 - 0.7
X ₄	AOD - 0.2	Aerosol optical depth at 550 nm	0 - 0.6
X ₅	COD - 0.05	Cirrus optical depth (NIR)	0 - 0.6
X ₆	CTH - 10.0	Cirrus top height (in km)	2 - 20 km
X ₇	AOD · INC_SZA · INC_ALB	where: AOD as in X ₄ $\text{INC_SZA} = \cos(84^\circ) / \cos(\text{SZA} + 9^\circ) \cdot \text{SZA} / 75$ $\text{INC_ALB} = 0.01 \cdot (1.01 / (\text{ALB_SWIR} + 0.01) - 1.0)$	

Table 12: CO₂ error parametrization regression coefficients C₀ - C₇ (Buchwitz et al., 2013).

Q	C ₀	C ₁	C ₂	C ₃	C ₄	C ₅	C ₆	C ₇
Rel. error	1.29121	-0.00220	-0.07275	-1.97335	-1.00620	0.34586	-0.00150	38.86071
Sys. error	0.30786	0.01191	1.97716	-1.55154	-1.40282	0.70400	-0.03020	-73.46152

3.2.2 NO₂ and CO instrument

The overall uncertainty of the NO₂ VCDs are due to (a) measurement noise and spectral fitting affecting the slant column densities, (b) uncertainties related to the separation of stratospheric and tropospheric column and (c) uncertainties in the auxiliary parameters used for air mass factor calculations such as clouds, surface reflectance, a priori profile shapes and aerosols (Boersma et al., 2004). The total uncertainties are dominated by uncertainties from spectral fitting for background pixels and by uncertainties in AMF calculations for polluted

Final Report	<p>ESA Project SMARTCARB</p> <p>Study on use of satellite measurements of auxiliary reactive trace gases for fossil fuel carbon dioxide emission estimation</p> <p>contract no 4000119599/16/NL/FF/mg</p>	  
---------------------	--	---

pixels, respectively. The spectral fitting uncertainty of previous instruments such as OMI was of the order of $1\text{-}2 \times 10^{15}$ molecules cm^{-2} and AMF uncertainties were about 15-20%. These ranges were used to define two different scenarios for a possible Sentinel-7 NO_2 instrument (see Table 4). Since the random error depends on the pixel size, we define additional scenarios where the errors for $2 \times 2 \text{ km}^2$ pixels is doubled for $1 \times 1 \text{ km}^2$ pixels and halved for $4 \times 4 \text{ km}^2$ pixels.




For the Sentinel-5 UVNIS instrument we assume a relative uncertainty of 20% and a minimum uncertainty of 1.3×10^{15} molecules per cm^2 .

Surface reflectance and clouds are two major sources of uncertainty for NO_2 observations. In case of clouds, the random noise can be estimated empirically from the cloud fraction as

$$\sigma_{VCD} = (1 + 3f) \cdot 1.5 \times 10^{15}$$

where f is the cloud radiance fraction (Wenig et al., 2008). Cloud fractions will be taken from the COSMO model.

The total uncertainty of CO VCDs depends on the (a) fitting noise and (b) a priori CO and CH_4 profiles and (c) surface reflectance, aerosols and clouds. We assume a single sounding precision of CO of about $4.0 \cdot 10^{17}$ and 10-20% for both platforms.

<p>Final Report</p>	<p>ESA Project SMARTCARB</p> <p>Study on use of satellite measurements of auxiliary reactive trace gases for fossil fuel carbon dioxide emission estimation</p> <p>contract no 4000119599/16/NL/FF/mg</p>	  
----------------------------	--	---

4. Model setup and simulated satellite observations

4.1 Generation of synthetic satellite observations

4.1.1 Model version and updates




The COSMO-GHG model system (Liu et al., 2017) and its setup for the SMARTCARB simulations was described in Section 2.2. Here, we briefly summarize the versions of COSMO-GHG and its pre-processor INT2LM that have been used and a few modifications that simplified their configuration with a large number of tracers.

INT2LM was branched from Version 2.4.1 on the Github repository of the Centre for Climate Systems Modelling (C2SM) at ETH Zurich. For SMARTCARB, we added the option to write out files in netCDF4 format, which allowed us to compress the hourly three-dimensional emission fields required as input for the COSMO-GHG simulations and thereby reduced their size significantly. Furthermore, a bug in the interpolation routines was identified and fixed, which was due to a rounding error and resulted in double counting or omission of some emissions (issue #7 on bug tracker). Finally, an option for reading tracer definitions from a `namelist` file (`INPUT_ART`) was implemented making it possible to change the tracer definitions without re-compiling the code.

COSMO-GHG was originally branched from Version 5.0_2017.5 on the C2SM repository. For SMARTCARB, the main upgrade was the porting of the GHG module to GPU as briefly described in Section 2.3. In addition, we added support for reading tracer definitions from the `INPUT_BGC` namelist file, similar to INT2LM. Furthermore, the option of exponential decay of tracers was implemented for simulating NO_x tracers with a fixed e-folding decay time. Finally, we added support for compressed netCDF4 output and extended the restart option of COSMO (dumping of current state to a binary file and restarting from this file with bit-identical results to a continuous simulation) to the GHG module.

4.1.2 Model setup

The modelling system was set up on the “Piz Daint” supercomputer at the Swiss National Supercomputing Centre (CSCS). The system is controlled by a collection of Bash and Python scripts (processing chain) and consists of a pre-processor for emissions, the INT2LM pre-processor for interpolating input data to the model grid, the GPU-accelerated COSMO-GHG model and the SMARTCARB post-processor. The post-processor uses orbits from the SRON orbit simulator, kindly provided by Jochen Landgraf and Joost aan de Brugh, for computing the synthetic satellite observations. Figure 9 shows a flow chart of the model simulation and data processing chain. Simulations over extended time periods are divided into smaller chunks (typically 72 hours) each being initialized from a restart file written at the end of the previous run.

<p>Final Report</p>	<p align="center">ESA Project SMARTCARB</p> <p align="center">Study on use of satellite measurements of auxiliary reactive trace gases for fossil fuel carbon dioxide emission estimation</p> <p align="center">contract no 4000119599/16/NL/FF/mg</p>	  
----------------------------	---	---

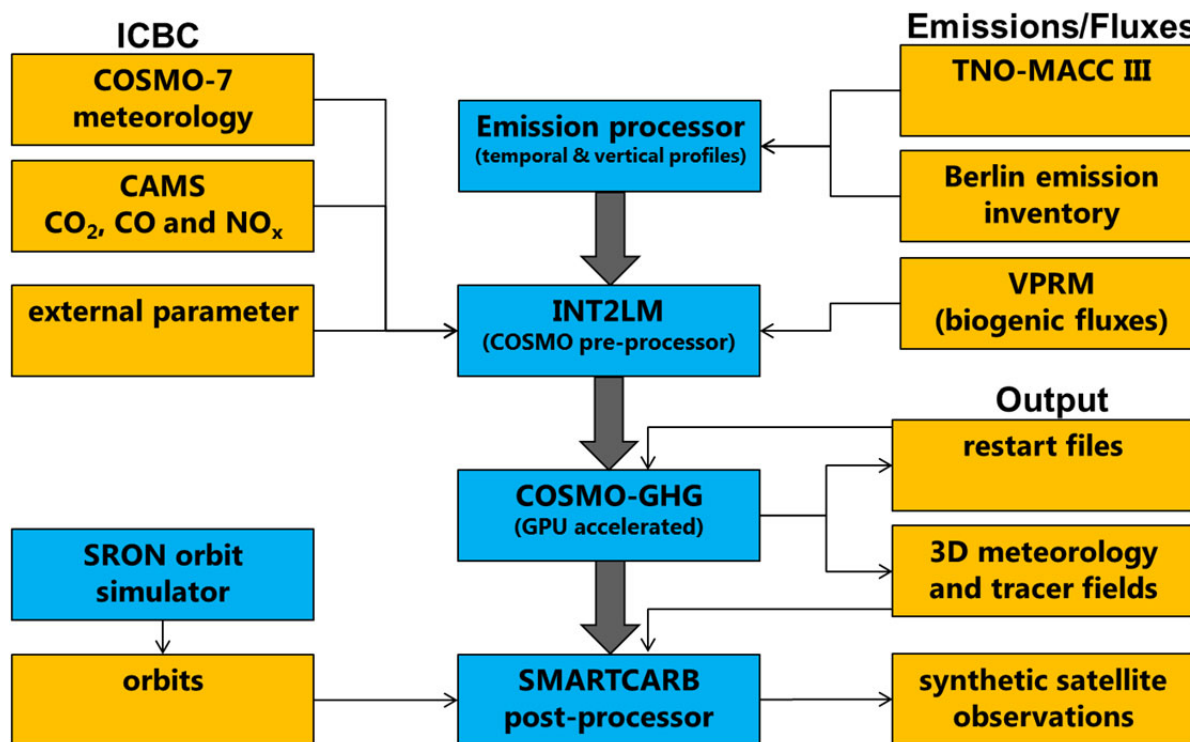





Figure 9: Processing chain with data (orange) and programs (blue).

4.1.3 Nature runs

The model was set up for the model domain described in Section 2.2 for two simulation periods starting in winter (1 January 2015) and summer (1 July 2015), respectively, in order to speed-up the computation.

The required input data for emissions and boundary conditions were collected and pre-processed with a dedicated emission processor written in IDL and finally processed with INT2LM to the format required by COSMO. The emission data processing included the merging of the Berlin and TNO/MACC-III inventory and the application of time profiles (diurnal, weekly and seasonal cycles) as described in Liu et al. (2017). Different from Liu et al. (2017), however, we also distributed the emissions in the vertical dimension according to pre-defined vertical profiles and considering meteorology-dependent plume rise for a subset of point sources. Hourly biospheric fluxes were generated by the VPRM model on the COSMO grid.

The simulations were conducted on 21 nodes (20 computation nodes for 5 x 4 subdomains and one I/O node) instead of the 16 nodes used in the benchmark, because memory requirements were too high for 16 nodes. Both simulations have been integrated over 6 months to cover the complete year 2015. A numerical instability producing unrealistic negative concentrations in the CO₂_GPP tracer occurred in the month of October which required a modification in the advection routine and made it necessary to restart the simulations from October onwards.

Final Report	ESA Project SMARTCARB Study on use of satellite measurements of auxiliary reactive trace gases for fossil fuel carbon dioxide emission estimation contract no 4000119599/16/NL/FF/mg	  Max Planck Institute for Biogeochemistry 
---------------------	---	--

Model output consists of hourly fields of the tracers and meteorological variables). All fields (except accumulated variables like rainfall) are instantaneous fields at the indicated time rather than hourly means. This section only covers the two periods 1 January to 19 May and 1 July to 22 November because the simulations for the remainder of the year have been completed only after writing this section.

4.1.4 Computational demand

The computational demand of COSMO-GHG for the “nature runs” in terms of node hours (NH) for one day of simulation were initially estimated to about 150 NH for the CPU version and 20 NH for the GPU version (see Deliverable D1). This speed-up was also found for our development version with a smaller domain and only a few tracers. However, the computational demand of the “nature runs” was larger than expected due to an underestimation of the computation time for data input and output (I/O).

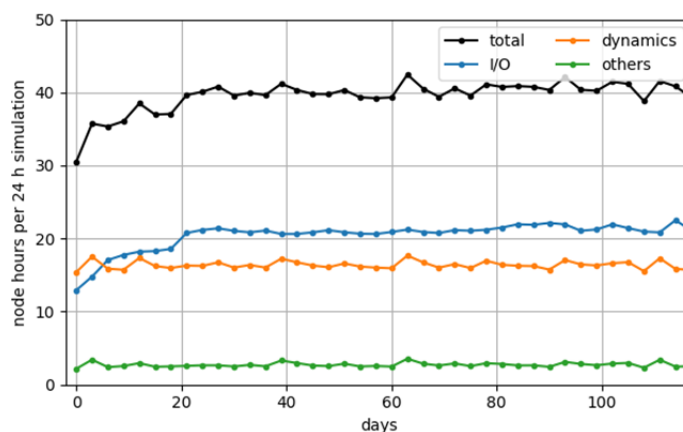





Figure 10: COSMO-GHG computation times for 3-day chunks of simulation #1 (1 Jan. 2015 – 1 May 2015) for “dynamics”, “I/O” and other computations.

Figure 10 shows the node hours required for the simulations from 1 Jan to 1 May 2015 divided into “dynamics” computations, “input and output (I/O)” and “others” (about 50% physics, i.e. radiation, cloud microphysics, soil processes, and turbulence). The computations of physics and dynamics use up about 20 NH per day of simulation similar to the originally estimated demand. However, “I/O” makes up about half of the demand and is thus not negligible. The “I/O” demand is mainly due to output which includes writing the model fields to the file system but also transferring the output data from the GPU to the CPU and from the computation nodes to the I/O node. The increase of the I/O demand with simulation time is due to increased file size which is initially about 1.5 GB but increases to 3.5 GB after about 20 days. The output file size is smaller in the beginning because compression of the output files is more effective when the tracers do not yet fill the entire model grid. The NH increase from 11 NH to 19 NH for output, but remain at about 2 NH for input.

Final Report	ESA Project SMARTCARB Study on use of satellite measurements of auxiliary reactive trace gases for fossil fuel carbon dioxide emission estimation contract no 4000119599/16/NL/FF/mg	  Max Planck Institute for Biogeochemistry 
---------------------	---	---

In conclusion, the GPU version is about 3-4 times faster than the CPU version. The performance gain is smaller than the initially estimated speedup due to the heavy computational demand for data output of the fifty tracer fields.

4.1.5 Generation of synthetic satellite observations

The generation of synthetic satellite observations involved the following four steps: First, the 3-D COSMO tracer fields (specific mass in units of kg tracer per kg moist air) were vertically integrated and converted to column mean dry air mole fractions. Second, instrument ground pixels were computed for different satellite scenarios using an orbit simulator. Third, the vertically integrated tracer fields were averaged over each ground pixel. Finally, instrument error fields were computed for each orbit.

Computation of column mean dry air mole fractions XCO_2

Assuming hydrostatic equilibrium, the weight of moist air in a vertical model layer k per m^2 (i.e. the partial column of moist air), is obtained from the pressure difference at the bottom and top of the volume as

$$M_k^{\text{air}} = \frac{p_{k+\frac{1}{2}} - p_{k-\frac{1}{2}}}{g}$$

with g the constant of gravity and p the pressure (Pa) at half levels (layer interfaces) of the model. The partial column of dry air is obtained by subtracting the mass of water vapour, i.e.

$$M_k^{\text{dry}} = M_k^{\text{air}} - M_k^{\text{air}} Q_k = M_k^{\text{air}} [1 - Q_k]$$

with specific humidity Q_k . The partial column of CO_2 is obtained as

$$M_k^{CO_2} = M_k^{\text{air}} \cdot sCO_{2k}$$

where sCO_{2k} is the specific mass of CO_2 (kg CO_2 / kg moist air) at model level k .

Finally, the column mean dry air mole fraction is obtained as the ratio of the sums of the masses of dry air and CO_2 over all levels k scaled by the respective molar weights:




$$XCO_2 = \frac{\sum_k M_k^{CO_2}}{\sum_k M_k^{\text{dry}}} \cdot \frac{m_{\text{dry}}}{m_{CO_2}} = \frac{\sum_k [p_{k+\frac{1}{2}} - p_{k-\frac{1}{2}}] sCO_{2k}}{\sum_k [p_{k+\frac{1}{2}} - p_{k-\frac{1}{2}}] [1 - Q_k]} \cdot \frac{m_{\text{dry}}}{m_{CO_2}}$$

with molar weights of dry air ($m_{\text{dry}} = 28.97$ g/mol) and CO_2 ($m_{CO_2} = 44.01$ g/mol).

NO_x and CO fields were converted from mass mixing ratios to mass concentrations (c_m) using pressure and temperature from the model. Furthermore, NO_x concentrations were converted to NO_2 concentration using the following empirical formula (Düring et al., 2011):

$$c_m[NO_2] = \frac{A \cdot c_m[NO_x]}{B + c_m[NO_x]} + C \cdot c_m[NO_x]$$

with $A = 29.0$, $B = 35.0$ and $C = 0.217$. Finally, both NO_2 and CO concentrations were vertically integrated to tropospheric vertical column densities (VCDs) in units of molecules per cm^2 of surface area. Hourly fields of vertically integrated tracers are part of the data1 package.

Final Report	ESA Project SMARTCARB Study on use of satellite measurements of auxiliary reactive trace gases for fossil fuel carbon dioxide emission estimation contract no 4000119599/16/NL/FF/mg	  Max Planck Institute for Biogeochemistry 
---------------------	---	---

Synthetic Level-2 satellite observations

The two-dimensional model fields were sampled along the satellite orbits computed with the SRON orbit simulator for the satellite scenarios defined in Section 3. Level-2 observations were created for a CO₂ instrument as well as for NO₂ and CO instruments on a constellation of up to six Sentinel CO₂ satellites. A constellation of six satellites would provide nearly daily coverage at the latitude of Berlin. In addition, Level-2 data of NO₂ and CO were computed for Sentinel-5. The XCO₂ (random) uncertainties were computed using the error parametrization formulas from Buchwitz et al. (2013) as described in Deliverable D2. The uncertainties depend on solar zenith angle and surface albedo. The effect of aerosols and cirrus clouds was not included in the computations. White-sky albedos were derived from the MODIS MCD43A3.006 product. Gaps in this product were filled firstly by temporal smoothing and remaining data gaps were filled by spatial interpolation. Figure 11 shows annual means of MODIS white-sky albedo in the near-infrared (MODIS Band 2, 841-867 nm) and shortwave infrared (Band 6, 1623-1652). In the near-infrared, the albedos are highest over vegetated regions. The city of Berlin is, therefore, comparatively dark.

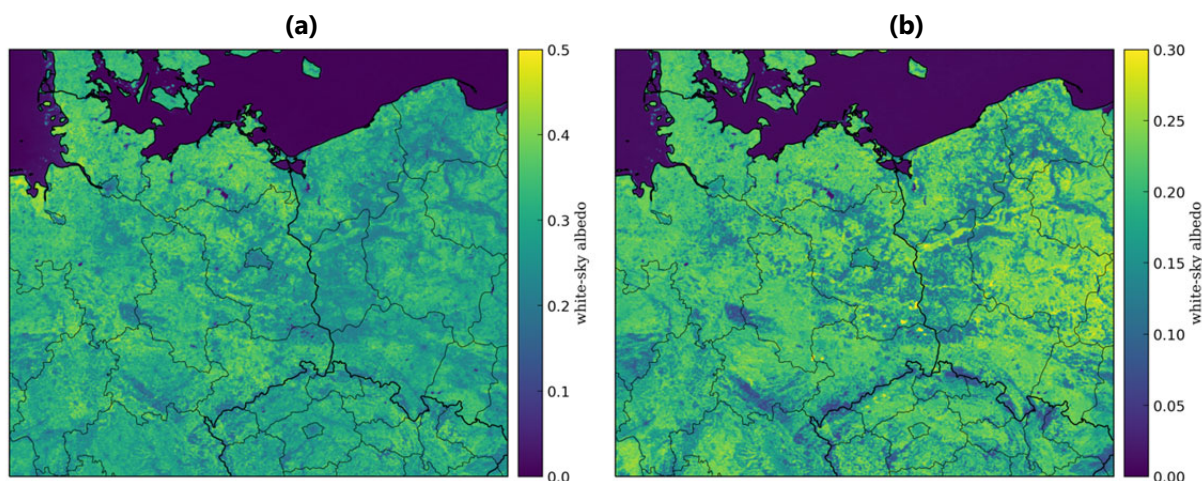


Figure 11: MODIS white-sky albedo averaged for 2015 (a) in the near infra-red (Band 2, 841-867 nm) and (b) in the short wave infra-red (Band 6, 1623-1652 nm).

4.2 Results

In this section, we present a selection of results from the nature runs and synthetic satellite observations in order to provide a flavor of the potential of the data for quantifying CO₂ emissions from point-sources that will be covered in Section 5. As mentioned above, the present analysis only covers the two periods 1 January till 19 May and 1 July till 22 November but could easily be extended to the full year.

4.2.1 Vertically integrated tracer fields

The vertically integrated tracer fields contain fifty CO₂, CO and NO₂ tracers as well as total cloud fractions for the simulation period (see Table 1).

Time series

To show the annual variability of XCO₂, CO and NO₂ columns over the city of Berlin, total columns were averaged over the area of Berlin over an area of approx. 30 km x 40 km.

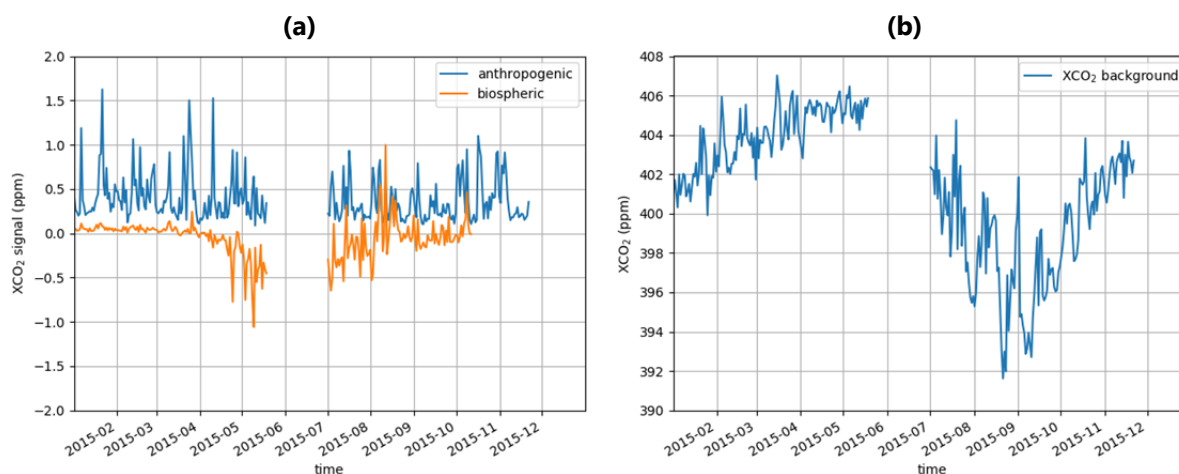


Figure 12: XCO₂ time series over Berlin (averaged) at satellite overpass (11 UTC).

Total XCO₂ is the sum of CO₂ signals from anthropogenic emissions ($XCO2_A + XCO2_BV + XCO2_JV$), biospheric fluxes ($XCO2_RA - XCO2_GPP^1$) and inflow from the background field at the model boundary ($XCO2_BG$). Figure 12 shows the time series of daily values of these tracers at 11 UTC, i.e. the expected overpass time of the Sentinel CO₂ satellite, averaged over Berlin. The anthropogenic signal has a baseline of about 0.2 ppm with peaks up to 1.5 ppm. The baseline is largely due to emissions within the model domain but outside the city of Berlin. The peaks are correlated with low wind speeds when CO₂ accumulates in the city area. The biospheric signal is the sum of (negative) gross primary product (GPP) and respiration (RA). In winter, the biospheric signal is slightly positive but much smaller than the anthropogenic signal, because GPP and RA are both small. In the growing season in spring and summer, both GPP and RA increase and their sum is negative because GPP dominates RA. In summer, the day-to-day variability of the biospheric signal has a similar magnitude as the anthropogenic signal. The annual cycle in the background signal is also driven by biospheric fluxes with a maximum just before the onset of the growing season and a minimum around September. The day-to-day variability of the background signal is of similar magnitude as the anthropogenic signal.

Figure 13 presents the time series of CO. The background signal has an annual cycle caused by the longer lifetime of CO in winter when concentrations of the OH radical, the main reactant of CO, are low. The anthropogenic signal over Berlin is rather small compared to the day-to-day variability of the background.

¹ GPP is generally defined as negative, but we define it positive because COSMO-GHG tracers need to be positive.

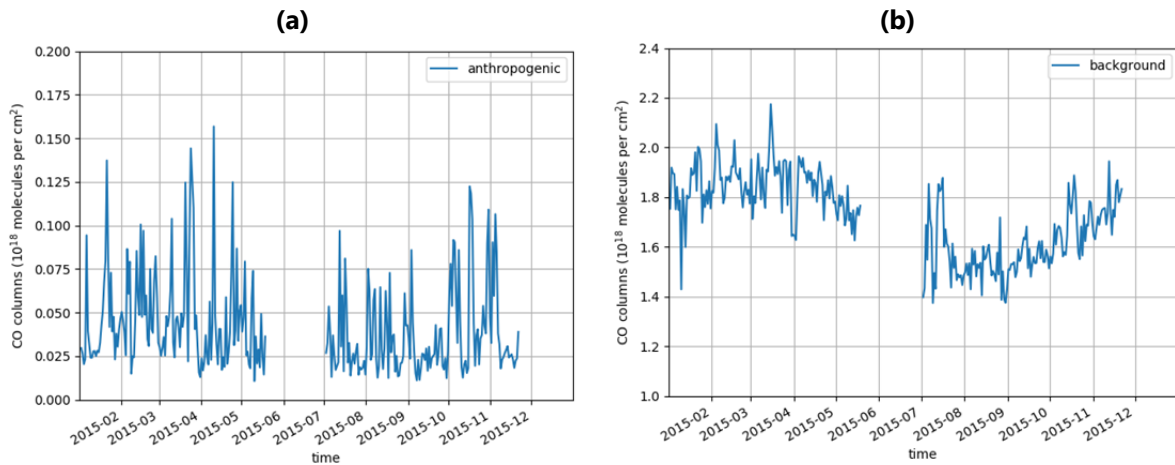


Figure 13: Time series of CO columns over Berlin at satellite overpass (11 UTC)

Figure 14 shows background and anthropogenic signals of NO_2 columns (NO_2_TOT and NO_2_BG). The anthropogenic signal is significantly larger than the background due to the short lifetime of NO_x . The background signal shows a weak annual cycle with higher values in winter caused by higher emissions and stronger winds transporting air from the domain boundaries more rapidly to the city of Berlin. In general, we would expect an even stronger annual cycle due to the longer lifetime of NO_x in winter, but this effect is missing in simulations assuming a constant lifetime. However, additional tracers (NOX_R00 , NOX_R02 , etc.) with different decay times were included which allow for analyzing this effect.

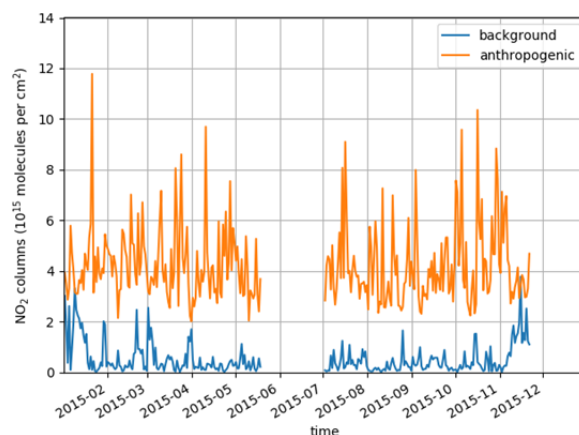


Figure 14: NO_2 time series over Berlin (averaged) at satellite overpass (11 UTC).

The spatial distribution of XCO_2 , CO and NO_2 columns at a given point in time is presented in Figure 15 for 2 July 2015 at 11 UTC. The left column shows the whole domain (without relaxation zone, about 50 km) and the right column shows a zoom-in over Berlin and the major power plants southeast of Berlin. Cloud fractions are shown as a white overlay.

The XCO_2 emissions from the power plants are easily discernible against the background field. The plume of the city of Berlin is comparatively weaker. The different tracers allow also for differentiating between anthropogenic, biospheric and background signals (Figure 16).

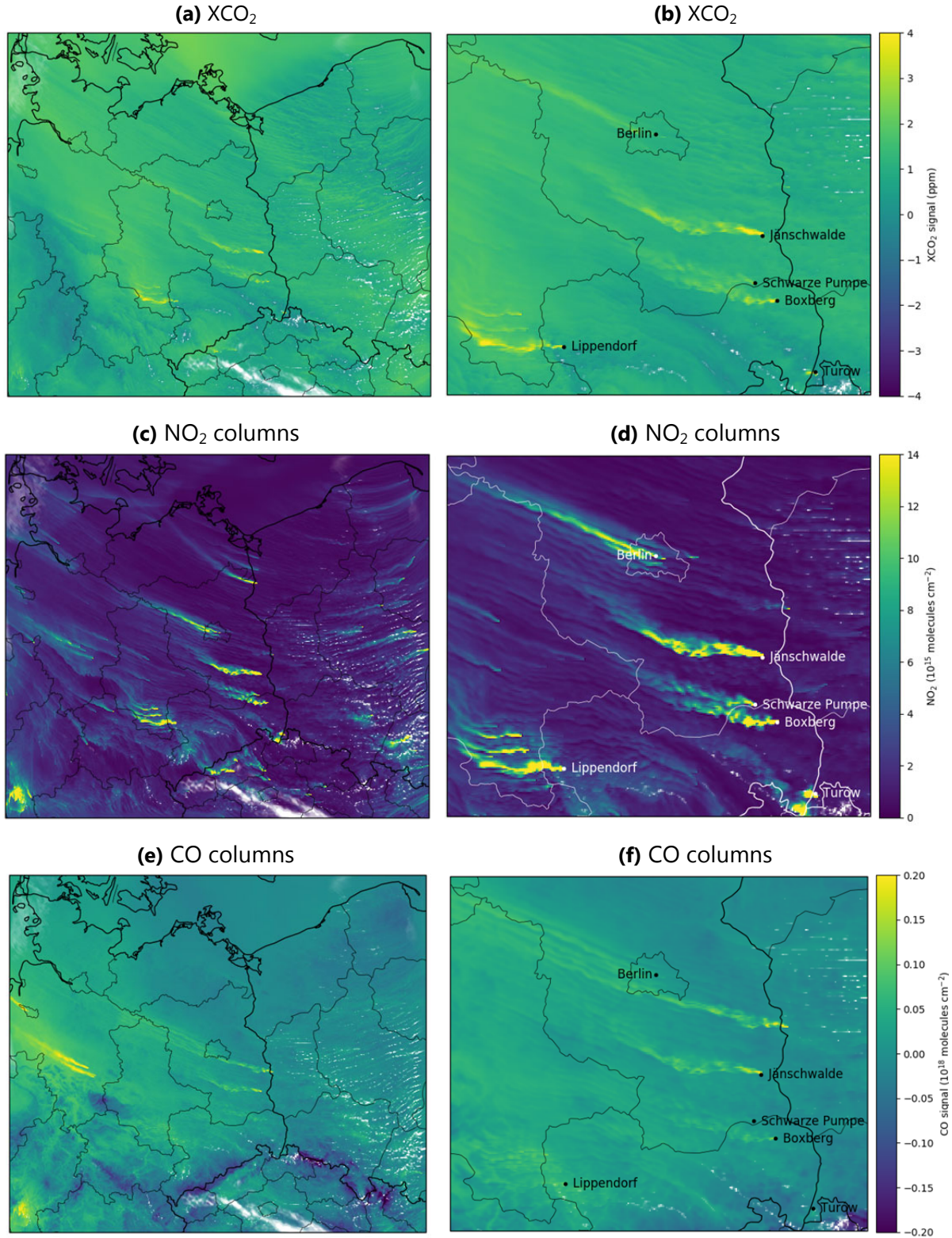


Figure 15: XCO₂ and NO₂ and CO columns on 2.7.2015 (11 UTC) with the full model domain in the left column and a zoom-in around Berlin and four major power plants in the right column.

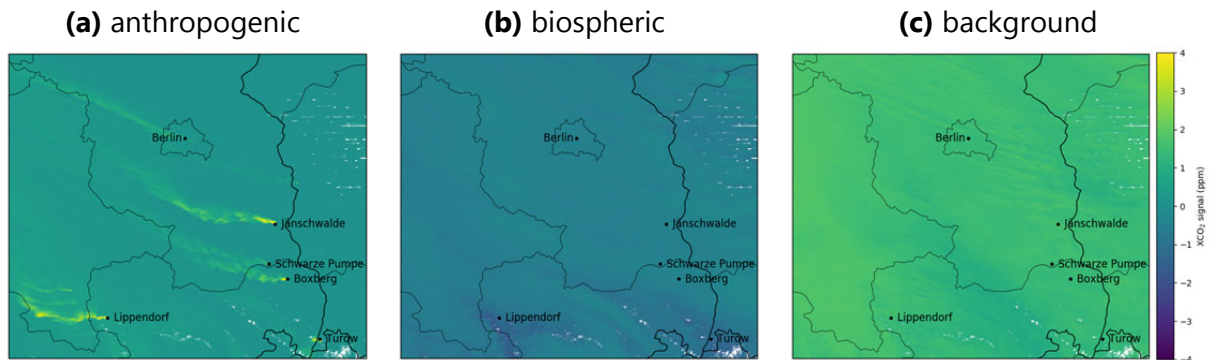


Figure 16: XCO₂ from anthropogenic emissions, biospheric fluxes and background fields (2 July 2015, 11 UTC).

In the NO₂ maps the anthropogenic signals due to emissions from the major point sources and Berlin are strongly enhanced above the respective backgrounds. Several smaller plumes are visible in the domain that were not seen in the CO₂ maps. The CO map shows only weak emissions from the power plants except for Jänschwalde.

Model evaluation

The simulated XCO₂ was compared with XCO₂ measurements at the TCCON site in Bremen (Figure 17). The model agrees well with the measurements ($r=0.95$) but overestimates the values especially in the first half of the year. The seasonal variability in the model is mainly driven by the boundary conditions and the bias is already present in the CAMS model used as boundary conditions.

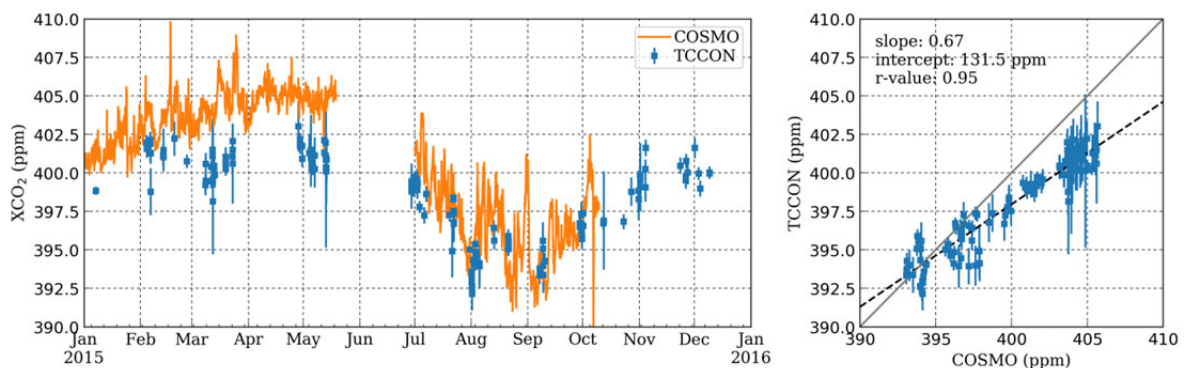


Figure 17: Comparison of XCO₂ from COSMO and TCCON site in Bremen. The data are well correlated ($r = 0.95$) but COSMO XCO₂ is overestimated.

Berlin plume

To differentiate emissions from different sectors in Berlin, separate tracers were defined for emissions from "industry" (B0), "heating" (B1) and "traffic" (B2). Figure 18 shows mean CO₂ emissions by sector and month for Berlin. Figure 19 shows CO₂ and NO₂ emissions from Berlin for southerly winds on 24 January 2015 (11 UTC). For southerly winds it is possible to distinguish the plumes from the largest point sources in the city which are aligned along an east-west axis. The largest emissions are from the industry sector which is dominated by a

few small power plants used for energy production. The heating sector has some strong point sources (public buildings and universities) but also area sources (residential heating) spread out more evenly over the city. Traffic emissions are an area source (line sources before rasterizing to the COSMO grid) with larger emission near the city center. Traffic emissions make up only about 10% in January and 25% in July of total CO₂ emissions in Berlin. The respective plume is, therefore, comparatively faint.

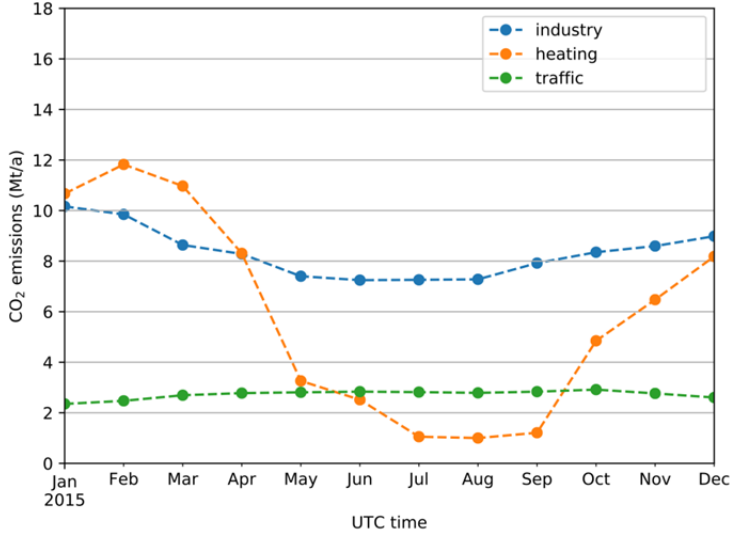


Figure 18: CO₂ emissions from Berlin by sector.

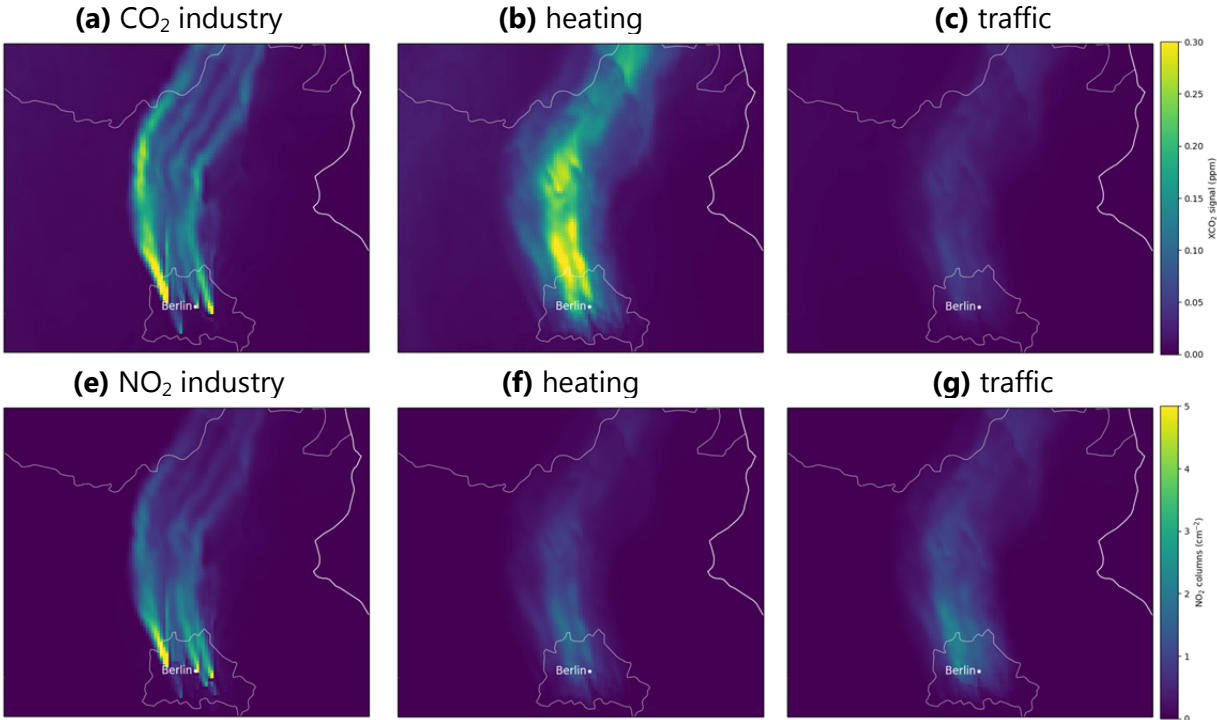


Figure 19: (a-c) XCO₂ and (e-g) NO₂ emissions (in 10¹⁵ cm⁻²) from industry, heating and traffic (24.1.2015, 11 UTC).

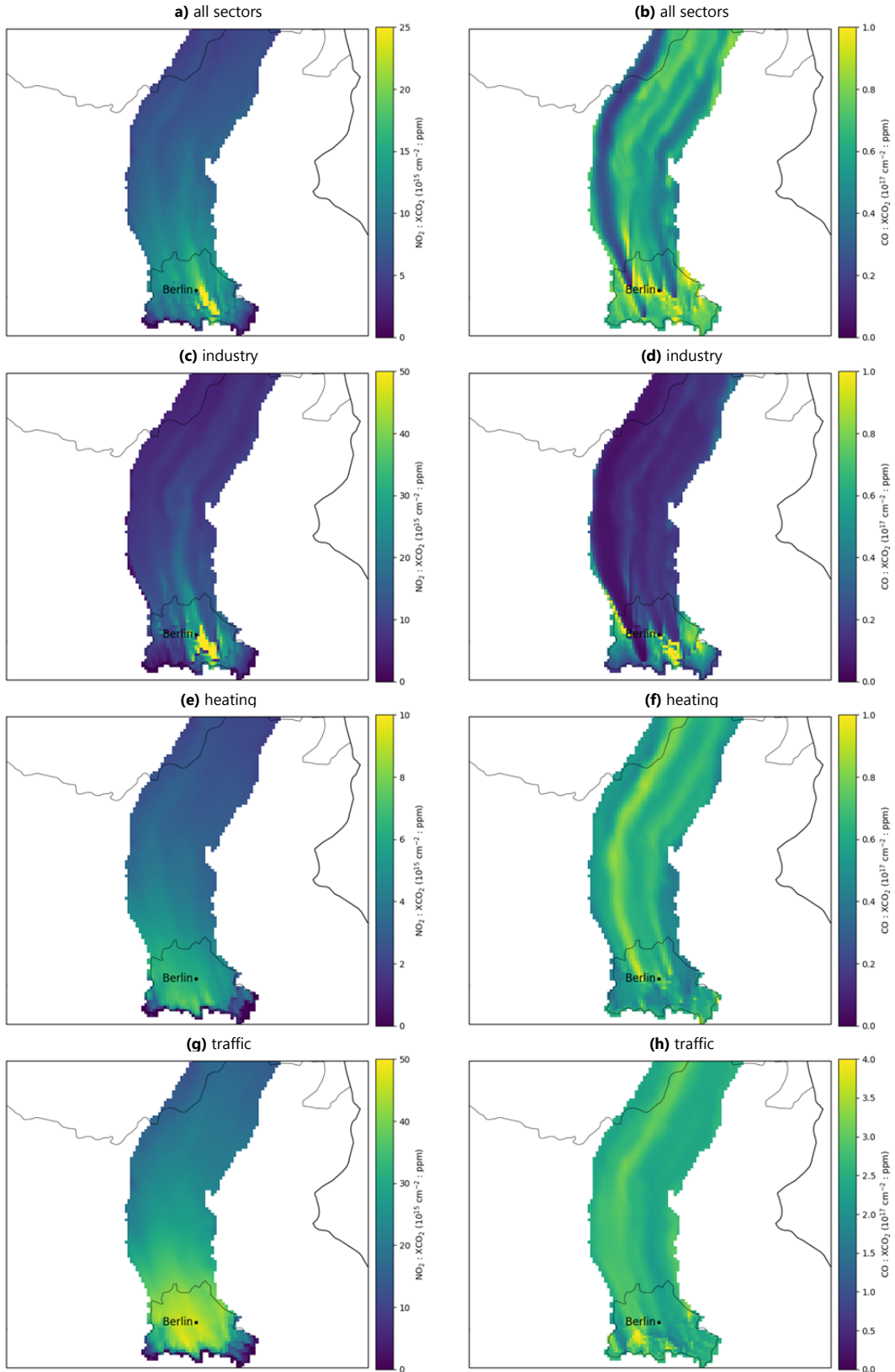


Figure 20: Tracer ratios for Berlin for different sectors.

Figure 20 shows $\text{NO}_2:\text{CO}_2$ (left column) and $\text{CO}:\text{CO}_2$ (right) ratios for the same plume. The different sectors have quite different emission ratios. For both NO_2 and CO the ratios are highest for traffic emissions and rather constant across the city. The ratios are smallest for the “industry” sector and are particularly small in the case of CO and the large point sources. The ratios are less uniform for the heating and especially for the industry sources compared to traffic. The $\text{NO}_2:\text{CO}_2$ ratios decrease downstream due to the NO_x decay (constant e-folding time of four hours). Typical ratios over the city for the sum of all emissions are of the order of 0.9 ppb NO_2 / ppm CO_2 and 3.6 ppb CO / ppm CO_2 .

Emission ratios from major power plants

Figure 21 shows the $\text{NO}_2:\text{CO}_2$ and $\text{CO}:\text{CO}_2$ ratios from the five largest power plants in the domain for 2 July 2015. The $\text{NO}_2:\text{CO}_2$ ratios are largest at the source and decrease downwind due to the NO_x decay (e-folding time: 4 hours). The power plants at Patnów and Turów in Poland have higher ratios and thus emit more NO_x per emitted CO_2 . These two plants emit via stacks while the other power plants release their emissions via cooling towers. CO emissions are generally very small, also in the case of the power plants in Poland.

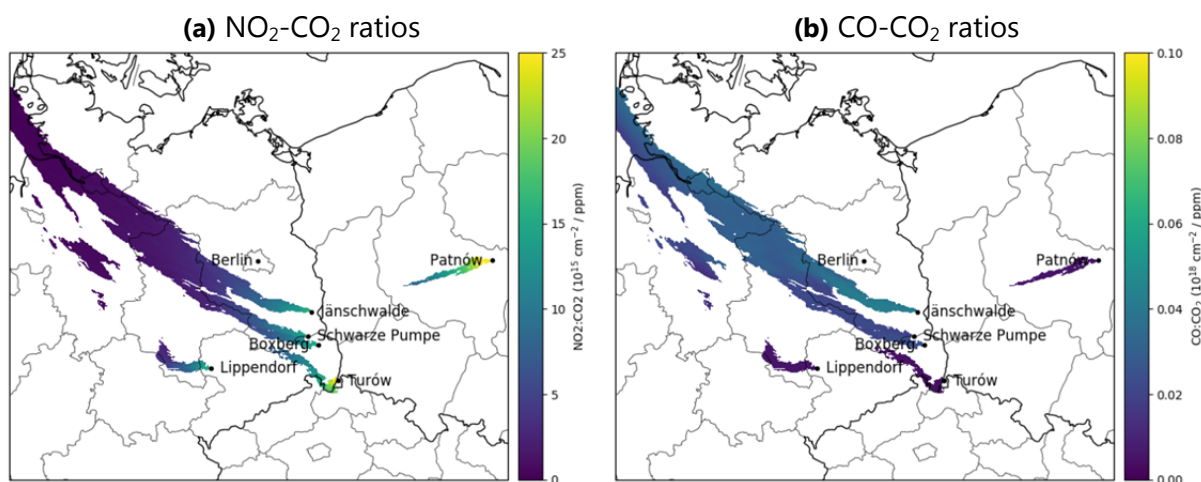


Figure 21: Ratios of NO_2 and CO to CO_2 from the five largest power plants in the domain (2 July 2015).

Cloud cover

The number of useful satellite measurements depends strongly on the fractional cloud cover. Figure 22 shows the number of days in Berlin with cloud fractions less than 30% at satellite overpass time (11 UTC). In addition, the number of days is shown where COSMO simulations were available. The number of cloud free days per month was 5 to 10 days most of the year. In some winter months (November and January) the number of cloud free days was as low as 1-2 days.

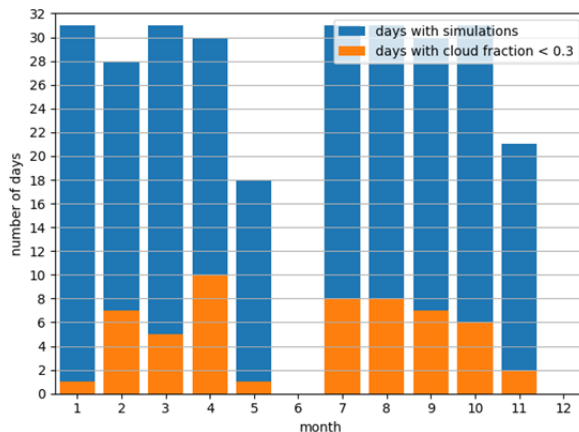


Figure 22: Number of days per month in 2015 with mean cloud fraction less than 30% in Berlin at 11:00 UTC. In addition, the number of days simulated per months are shown.

NO_x decay times

NO_x decay times affect the visibility of the NO₂ plumes. Tracers with different decay times were simulated which allows studying its effect on emission estimates. Figure 23 shows the NO₂ columns on 2 July 2015 (11 UTC) for different decay times. The major plumes remain visible even for short decay times (e.g. 2 hours) but their spatial extent is more restricted to the surroundings of the sources.

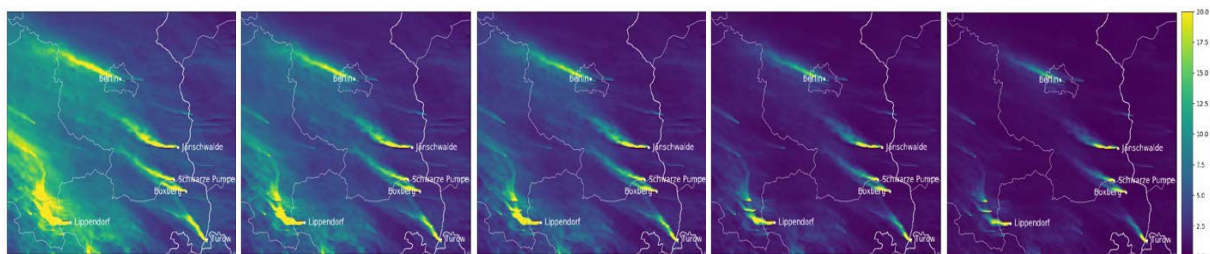





Figure 23: NO₂ for different decay times (no decay, 24h, 12 h, 4h and 2 h).

Plume rise

Tracers with different emission heights were simulated to estimate the impact of release height on the propagation of the plumes. The simulated scenarios are emissions at the surface, emissions based on fixed profiles for each SNAP category, and emissions based on plume rise calculations (only for major sources). The plume height affects the transport of the plumes because of the increase of wind speed with height but also due to changes of wind direction with height. Figure 24 illustrates the difference between plume rise calculations and fixed SNAP profiles for the five major plumes again for the case of 2 July 2015. The direction of propagation is clearly different for the two tracers. The plume height has large uncertainties because the stack parameters, especially effluent temperature, are not well known. As a result, the propagation of the plume in the model may deviate significantly from reality. In case of real satellite observations, the release height could potentially be adjusted in the model to optimally match the observations, as done already operationally for volcanic plume forecasting (Flemming and Inness, 2013).

Final Report	<p>ESA Project SMARTCARB</p> <p>Study on use of satellite measurements of auxiliary reactive trace gases for fossil fuel carbon dioxide emission estimation</p> <p>contract no 4000119599/16/NL/FF/mg</p>	  
---------------------	--	---

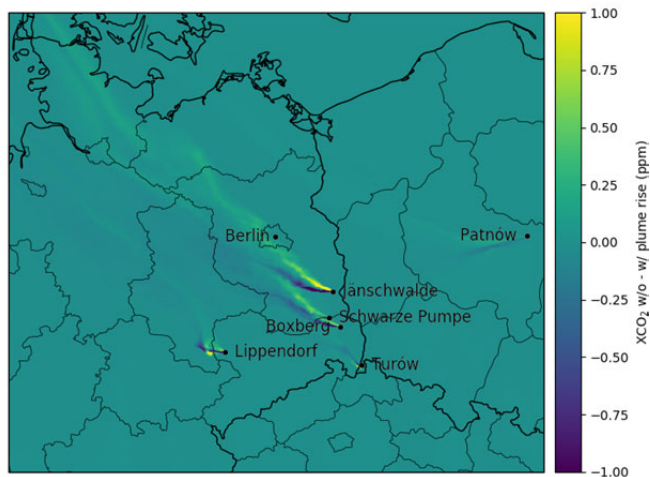


Figure 24: Example of the XCO₂ difference between no plume rise (fixed release height profile) and plume rise (2 July 2015, 11 UTC).

4.2.2 Synthetic Level-2 data

In this section, we present the synthetic Level-2 data and their uncertainties derived from the model simulations using the satellite orbit simulator. For the data1 package, Level-2 data were computed for a constellation of four Sentinel-7 instruments as well as for Sentinel-5.

Example of observations in July 2015

Figure 25 shows examples of Level-2 XCO₂ fields for all days in July 2015 that are not fully overcast.

Uncertainty scenarios

Uncertainty scenarios were defined for the satellite observations of XCO₂, NO₂ and CO (see Section 3.2). Figure 27 shows XCO₂, NO₂ and CO measurements for a single orbit without noise and for the low and high noise scenarios. For XCO₂, the plumes of the power plants are readily visible in the low noise scenario but are more difficult to detect with higher noise. The Berlin plume, which is quite weak in this example, is still discernable with low noise but difficult to detect in the high noise scenario. For NO₂, the plumes of Berlin and the power plants are well visible in both the low and high noise scenarios while for CO the plumes are invisible even in the low noise scenario. CO observations thus appear to be of little use to support CO₂ emission estimation with current instrument technology for the type of sources investigated here. Combustion processes are typically well-controlled in developed countries and CO emissions correspondingly small. In developing countries the situation will likely be different with relatively higher emissions of CO and lower emissions of NO₂. Additional NO₂ measurements, on the other hand, seem very suitable as auxiliary observations for characterizing the extent of a plume as well as detecting faint plumes beyond the limits of detection of the CO₂ measurements.

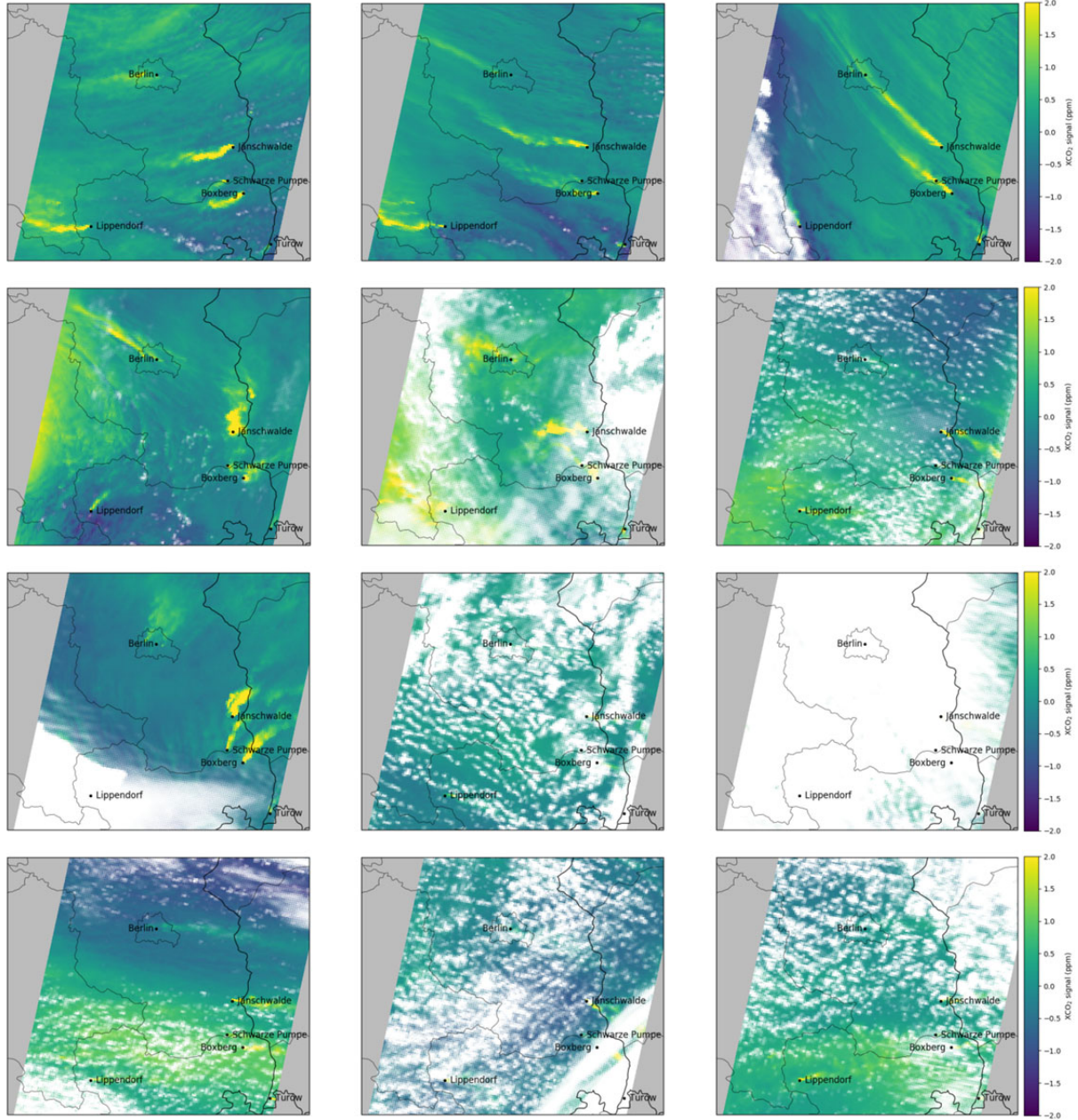





Figure 25: Examples of Sentinel CO₂ orbits on different days in July 2015 using the same orbit path on each day.

<p>Final Report</p>	<p align="center">ESA Project SMARTCARB</p> <p align="center">Study on use of satellite measurements of auxiliary reactive trace gases for fossil fuel carbon dioxide emission estimation</p> <p align="center">contract no 4000119599/16/NL/FF/mg</p>	<p align="center">  Empa Materials Science and Technology  Max Planck Institute for Biogeochemistry  </p>
----------------------------	---	---

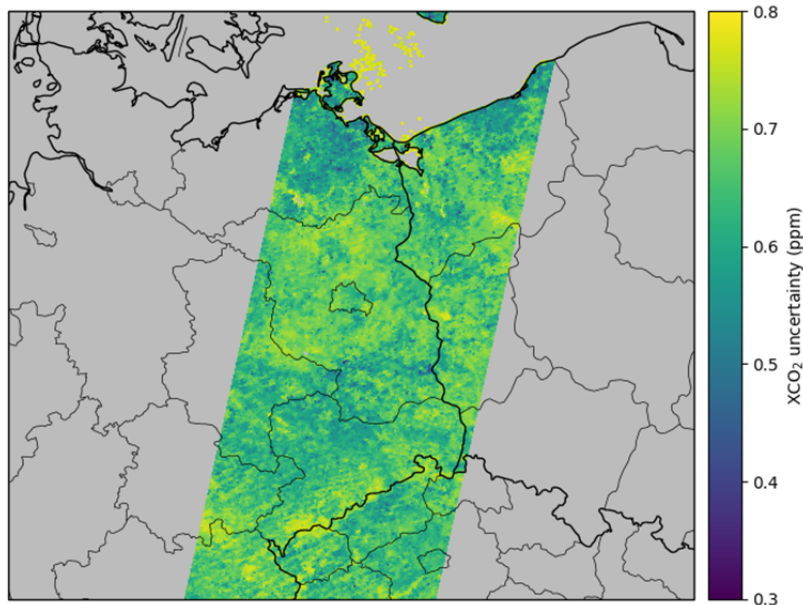


Figure 26: XCO₂ random uncertainty based on error parametrization formula with 0.7 ppm uncertainty for the VEG50 scenario (1 January 2015, 11 UTC).

In the analysis above, XCO₂ uncertainties were estimated by simply adding a Gaussian random noise. In addition, we also calculated a more realistic noise using empirical error formulas depending on solar zenith angle and surface reflectance. Figure 26 presents the random uncertainties of a single orbit. In this scenario, the uncertainty for the so-called VEG50 scenario, i.e. measurements over vegetation with a solar zenith angle of 50°, are 1.5 ppm. In order to obtain the scenarios defined in Section 3.2 with uncertainties of 0.5, 0.7 and 1.0 ppm, the uncertainty is scaled accordingly. The uncertainties show spatial patterns due to their dependency on surface reflectance with higher uncertainties over areas with low surface reflectance. Figure 28 shows the uncertainty scenarios applied to Sentinel CO₂ mission's Level-2 data (2015-06-17).

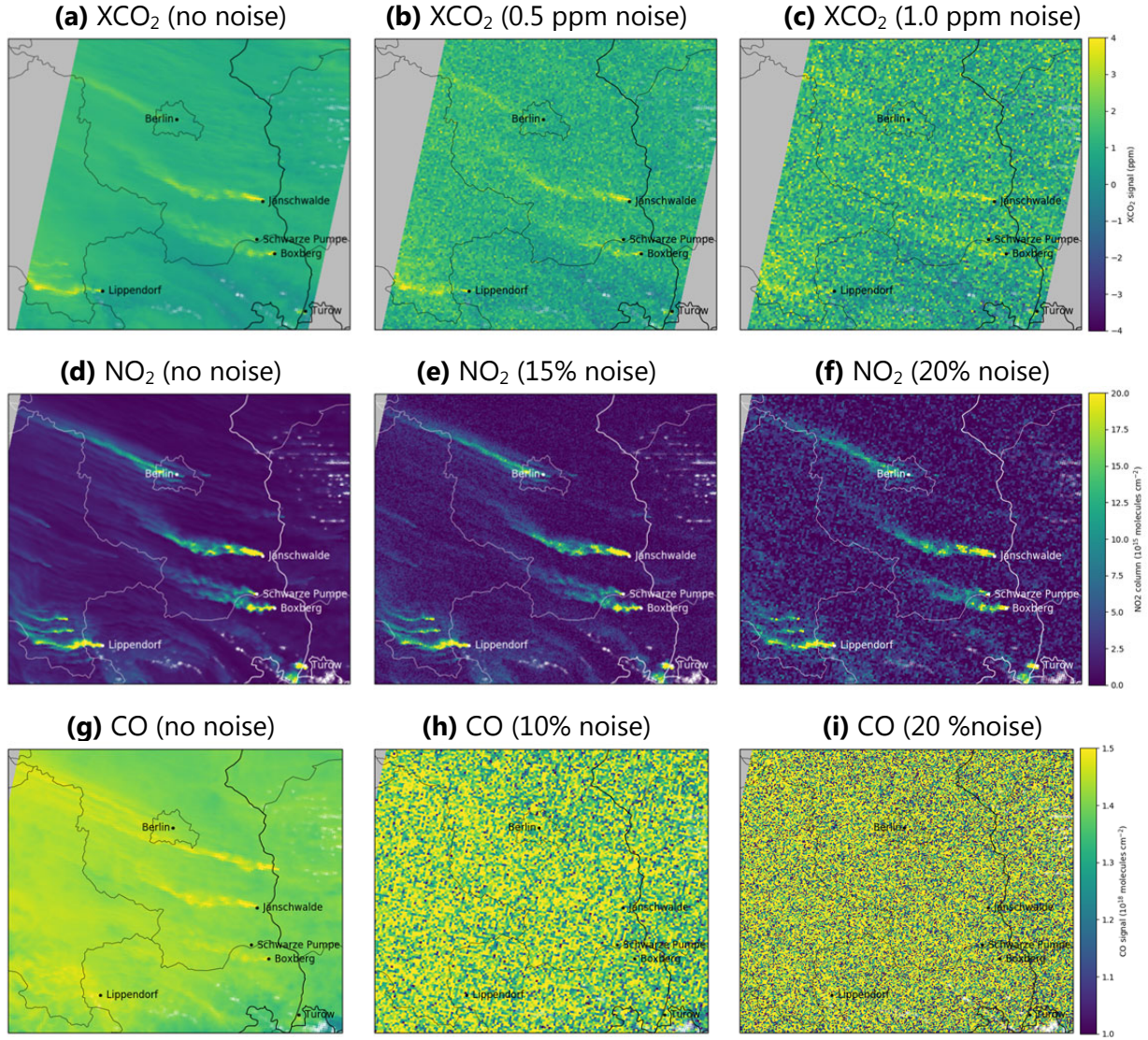


Figure 27: XCO₂, NO₂ and CO Level-2 on 2 July 2015 (11 UTC) without noise and with noise for a low and high noise scenario.

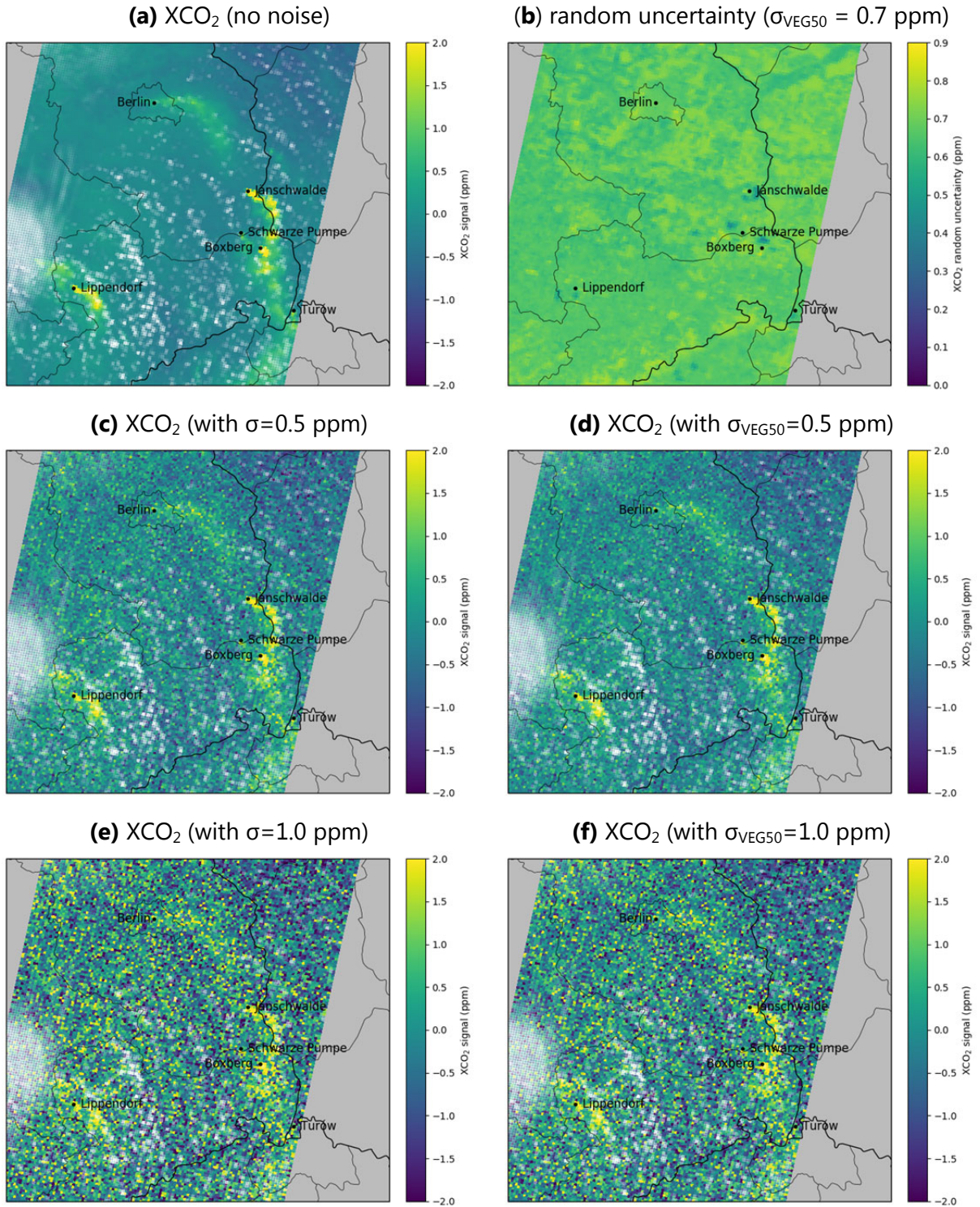


Figure 28: Sentinel CO₂ mission's Level-2 data (2015-06-17, 11 UTC) with different uncertainty scenarios: **(a)** XCO₂ fields without noise, **(b)** XCO₂ random uncertainties computed with error parametrization formula, **(c,e)** XCO₂ field with 0.5 ppm and 1.0 ppm noise, and **(d,f)** XCO₂ fields with random noise computed with scaled parametrization formula.

Impact of spatial resolution

The spatial resolution affects the detectability of smaller plumes, because larger pixels can smooth out small plumes and because the presence of scattered clouds reduces the chance for clear-sky observations when pixels are large. If a NO₂/CO instrument shall be used for detecting the location of the XCO₂ plume, a higher resolution than the CO₂ instrument can be useful, because XCO₂ and NO₂/CO ground pixels may not be overlapping exactly.

Figure 29 shows the influence of spatial resolution on the satellite observations for the scene of 2 July 2015. It shows noise-free NO₂ observations from the Sentinel CO₂ mission with 1, 2 and 4 km resolution as well as Sentinel-5 with 7 km resolution. The impact of resolution can best be illustrated for the plumes from the coal-fired power plant Lippendorf and two smaller point sources north of Lippendorf. The plumes are easily detectable at 1 and 2 km resolution but are more difficult to identify at 4 km resolution. In the Sentinel-5 scenario with 7 km resolution and a 2 hours later overpass, the three plumes are merged into a single one such that all emissions would potentially be falsely attributed to Lippendorf only. For Sentinel-5, it also becomes difficult to distinguish the two plumes from the power plants Schwarze Pumpe und Boxberg. Furthermore, it is not possible to accurately detect the origin of the CO₂, because of the lower resolution and the time gap of two hours.

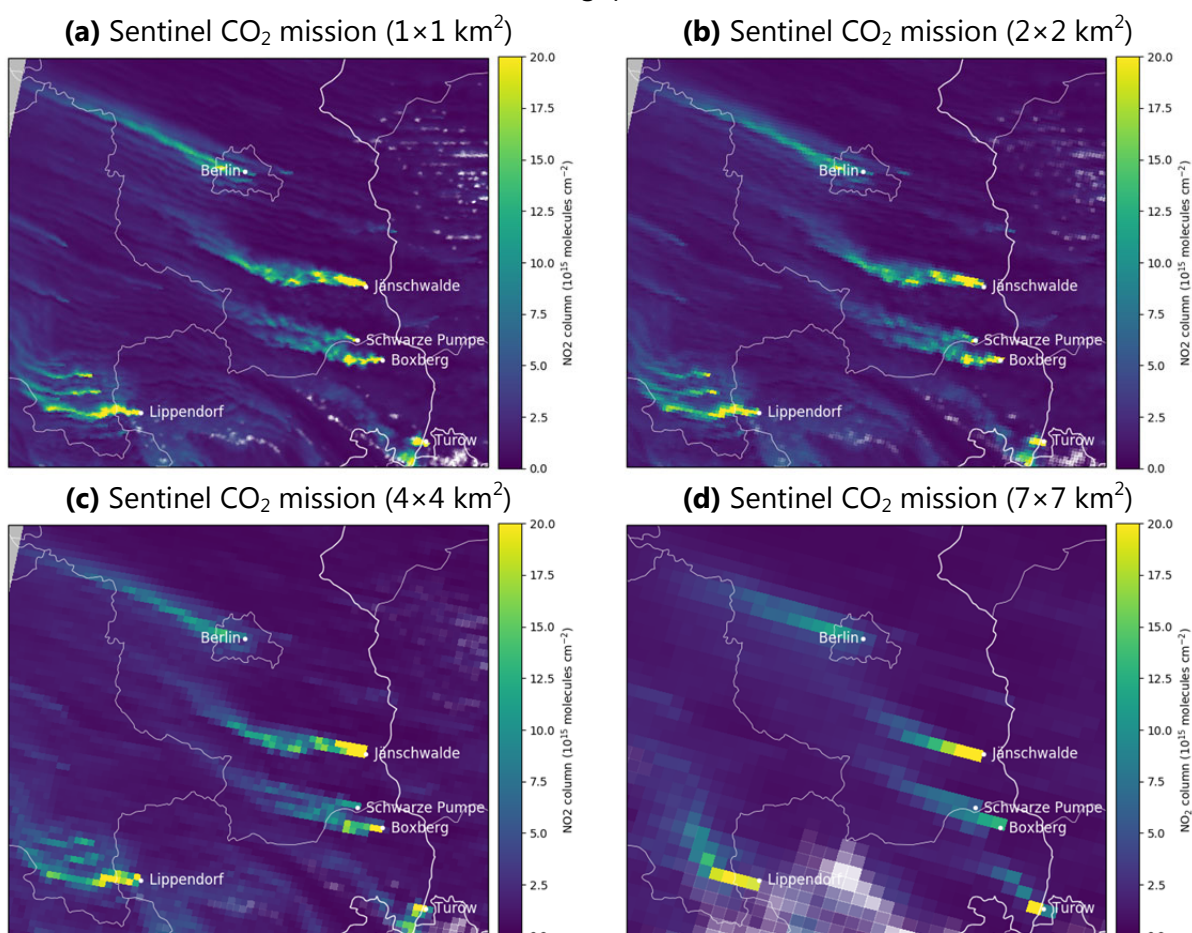





Figure 29: Synthetic NO₂ satellite observations for different spatial resolutions. (a-c) Sentinel CO₂ mission at 11 UTC and (d) Sentinel-5 at 9 UTC on 2 July 2015.

<p>Final Report</p>	<p>ESA Project SMARTCARB</p> <p>Study on use of satellite measurements of auxiliary reactive trace gases for fossil fuel carbon dioxide emission estimation</p> <p>contract no 4000119599/16/NL/FF/mg</p>	  
----------------------------	--	---

5. Estimating CO₂ emissions

This section analyzes the potential of different satellite configurations to estimate the CO₂ emissions of cities and power plants with a particular focus on the potential benefit of complementary NO₂ and/or CO observations. It first places the emissions from Berlin and the power plants in a global context by comparing with emissions in other parts of the world (Section 5.1). Next, the overall coverage of constellations of one to six satellites over the study domain and the potential for plume detection is analyzed (Section 0). An algorithm for detecting emission plumes in satellite trace gas observations is then presented and applied to the estimation of CO₂ emissions of Berlin and different power plants (Sections 5.3-5.5). The algorithm is applied to synthetic satellite observations of a constellation of up to six CO₂ satellites generated with a high-resolution atmospheric transport model and orbit simulations. In addition, NO₂ plumes observed by Sentinel-5 with an earlier overpass time are also analyzed. Finally, the potential for estimating CO₂ emissions from satellite observations is analyzed. The emissions of Berlin are estimated by analytical inversion using tracer information provided by the model and by computing fluxes through control surfaces (Section 5.4). The emissions of power plants are estimated by fitting a Gaussian plume model to the observations (Section 5.5).

5.1 Emissions from Berlin and power plants in a global context

In the SMARTCARB project we only analyze the situation for a region over Europe where emissions of CO₂ and especially the emission ratios of NO₂:CO₂ and CO:CO₂ may be different from other parts of the world. In order to place this study in a broader context, we compare the emissions from the city of Berlin to the emissions from the 387 most populated cities in the world with a population of more than 1 million. For this purpose, we calculated the total emissions within a circle of 25 km radius around the center of the cities using the EDGAR emission inventory for the year 2010 (EDGAR v4.2_FT2010 for CO₂ and EDGAR_v4.3.1 for NO_x and CO). The cumulative percentage of emissions from cities with an emission lower than a given threshold is shown in Figure 30 for CO₂ and NO_x and in Figure 31 for CO. The emissions of Berlin are highlighted by the blue dashed line and those of Paris and New York are shown for comparison. In terms of population Berlin is the 71th largest city in world (source: <https://www.maxmind.com/de/free-world-cities-database>). According to our analysis, Berlin's rank is similar in terms of CO₂ emissions being the 64th largest emitter worldwide. In terms of NO_x and CO emission, however, it is only ranked 151 and 198, respectively, suggesting that combustion processes are comparatively clean in Berlin. Its CO₂ emissions are comparable to those of Paris, but its NO_x and CO emissions are lower, possibly due to a smaller relative contribution from traffic emissions in Berlin. The largest CO-emitting cities are located in developing countries where biofuels and coal are frequently used for heating and cooking under poorly controlled combustion conditions.

It should be noted that the emissions in EDGAR as used previously e.g. in the LOGOFLUX project (RD-2, RD-3) are significantly higher than those reported by the official inventory of

the city of Berlin. According to the municipal inventory used in this study, the emissions in the year 2012 were 16.9 Mt for CO₂, 18.9 kt for NO_x, and 36.5 kt for CO.

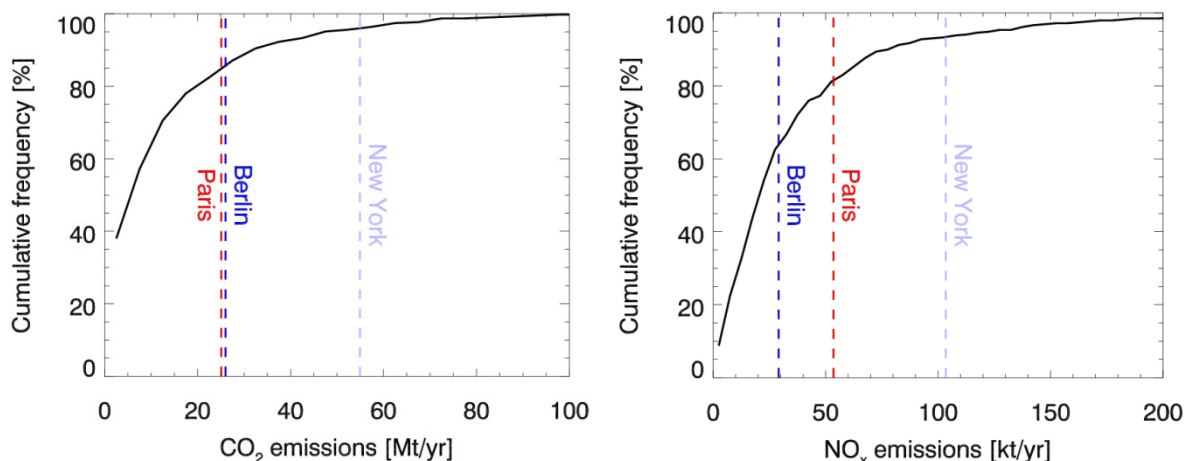


Figure 30: Cumulative distributions of (a) CO₂ and (b) NO_x emissions from the 387 most populated cities worldwide with a population > 1 million based on the EDGAR emission inventory for the year 2010. Binsize was chosen as 5 Mt/yr for CO₂ and 5 kt/yr for NO_x emissions.

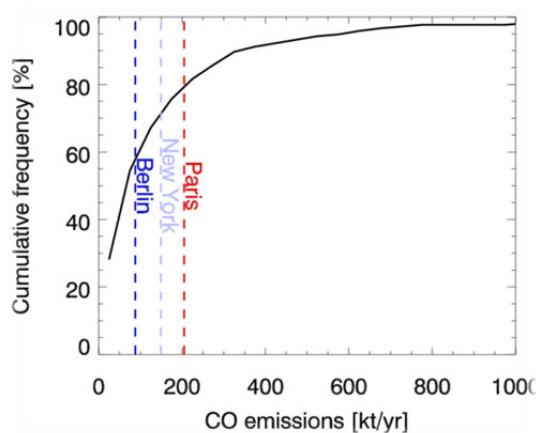


Figure 31: Cumulative distribution of CO emissions from the 387 largest cities worldwide with a population > 1 million based on the EDGAR emission inventory for the year 2010. Binsize is 25 kt/yr.

According to the Carbon Monitoring for Action (<http://carma.org>) global database of power plant emissions, the German power plant Jänschwalde, the main power plant investigated in this study, is the 16th largest power plant globally in terms of CO₂ emissions. In 2015, its emissions were 23.6 Mt, which is larger than the emissions from the whole city of Berlin. Table 13 shows CO₂ emissions and rank of the five largest power plants in our model domain based on the CARMA database.

The emissions used in the simulations were deduced from the TNO/MACC-3 inventory for the year 2011. For some power plants these emissions were significantly different from CARMA and the European Pollutant Release and Transfer Register (E-PRTR). Emissions for Jänschwalde, for example, were too high in the simulations, whereas those of Turów and Schwarze Pumpe were too low compared to officially reported numbers.




Final Report	ESA Project SMARTCARB Study on use of satellite measurements of auxiliary reactive trace gases for fossil fuel carbon dioxide emission estimation contract no 4000119599/16/NL/FF/mg	  
---------------------	---	---

Table 13: Emissions and global rank of largest power plants in model domain based on CARMA database. The rank is based on CO₂ emissions. Emissions as used in the simulations deduced from TNO/MACC-3 inventory for the year 2011 are also shown.

Power plant	Rank	Emissions in 2009 (CARMA & E-PRTR)			Emissions in 2011 (TNO/MACC-3) (used in this study)		
		CO ₂ (Mt/yr)	NO _x (kt/yr)	CO (kt/yr)	CO ₂ (Mt/yr)	NO _x (kt/yr)	CO (kt/yr)
Jämschwalde	16	23.6	18.2	11.9	33.3	26.9	44.1
Boxberg	63	15.3	9.8	4.5	19.0	15.4	14.4
Lippendorf	96	12.8	8.6	1.1	15.3	12.3	2.7
Turów	108	11.7	11.8	0.9	8.7	13.1	1.3
Schwarze Pumpe	137	10.7	4.2	1.9	8.2	6.6	5.3

5.2 Coverage and potential for plume detection

The frequency with which the CO₂ plumes of a given source can be observed by a satellite depends on how often it passes over a source and how often cloud-free conditions dominate during the overpass. The number of overpasses over a location scales with the number of satellites, the number of overpasses of each satellite within its assumed 11-day repeat cycle, and the swath width of the instrument. We define an overpass as an intersection between the satellite swath and the area of the source (e.g. the city center of Berlin). Here, we analyze a constellation of one to six satellites that are equally spaced in the same orbit and have a swath width of 250 km. The satellites in a constellation are distinguished by their starting longitude at the equator of the first orbit in the repeat cycle (see Section 3 for details).

Figure 32 shows the global number of overpasses and a zoom on Europe of one Sentinel CO₂ satellite for its 11-day repeat cycle. In the SMARTCARB model domain (white box), one or two overpasses occur within 11 days. The total number of overpasses in the simulation period (360 days) is about 33 and 65 for one and two overpasses in 11 days, respectively. The number of overpasses increases with additional satellites (Figure 33), but since an additional satellite adds either one or two overpasses per 11 days, the number of overpasses does not trivially scale with the number of satellites, but is roughly 1.75 multiplied with the number of satellites for the model domain.

shows the days during the 11-day cycle with overpasses over Berlin for the different number of satellites in a constellation together with the assumed starting longitude at the equator of each satellite. When a single satellite passes over a location twice in 11 days, the overpasses always occur on two consecutive days. Since satellites are equally spaced in orbit, changing the number of satellites changes the starting longitudes and overpass days of the satellites.

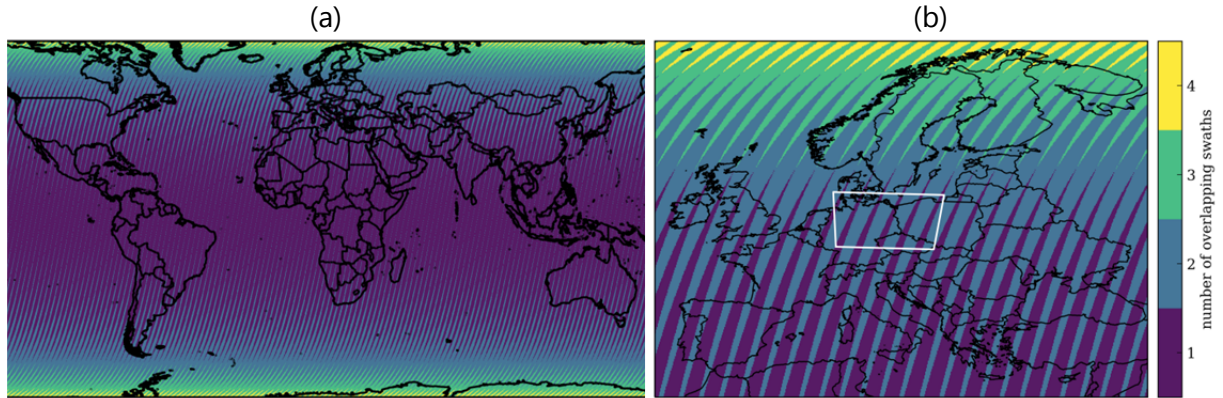


Figure 32: (a) Global and (b) European coverage of a single Sentinel CO₂ satellite for an 11-day cycle. The SMARTCARB model domain is shown as white box.

Table 14: Time profiles of satellite overpasses over Berlin for a constellation of one to six satellites equally spaced within the same orbit. Cells with numbers and colors have a satellite overpass on that day and empty cells have no overpass. The numbers are the (rounded) equator starting longitudes (in degrees east) of each satellite. Colors are used to highlight satellites with identical starting longitudes.

		Day of 11-day repeat cycle											
		1	2	3	4	5	6	7	8	9	10	11	
Number of satellites in constellation	1	0°	0°										
	2	0°	0°				12°	12°					
	3	0°	0°		8°	8°			16°	16°			
	4	0°	0°		6°		12°	12°		18°	18°		
	5	0°	0°	5°	5°	10°	10°	14°	14°		19°		
	6	0°	0°	4°	8°	8°	12°	12°	16°	16°	20°	20°	

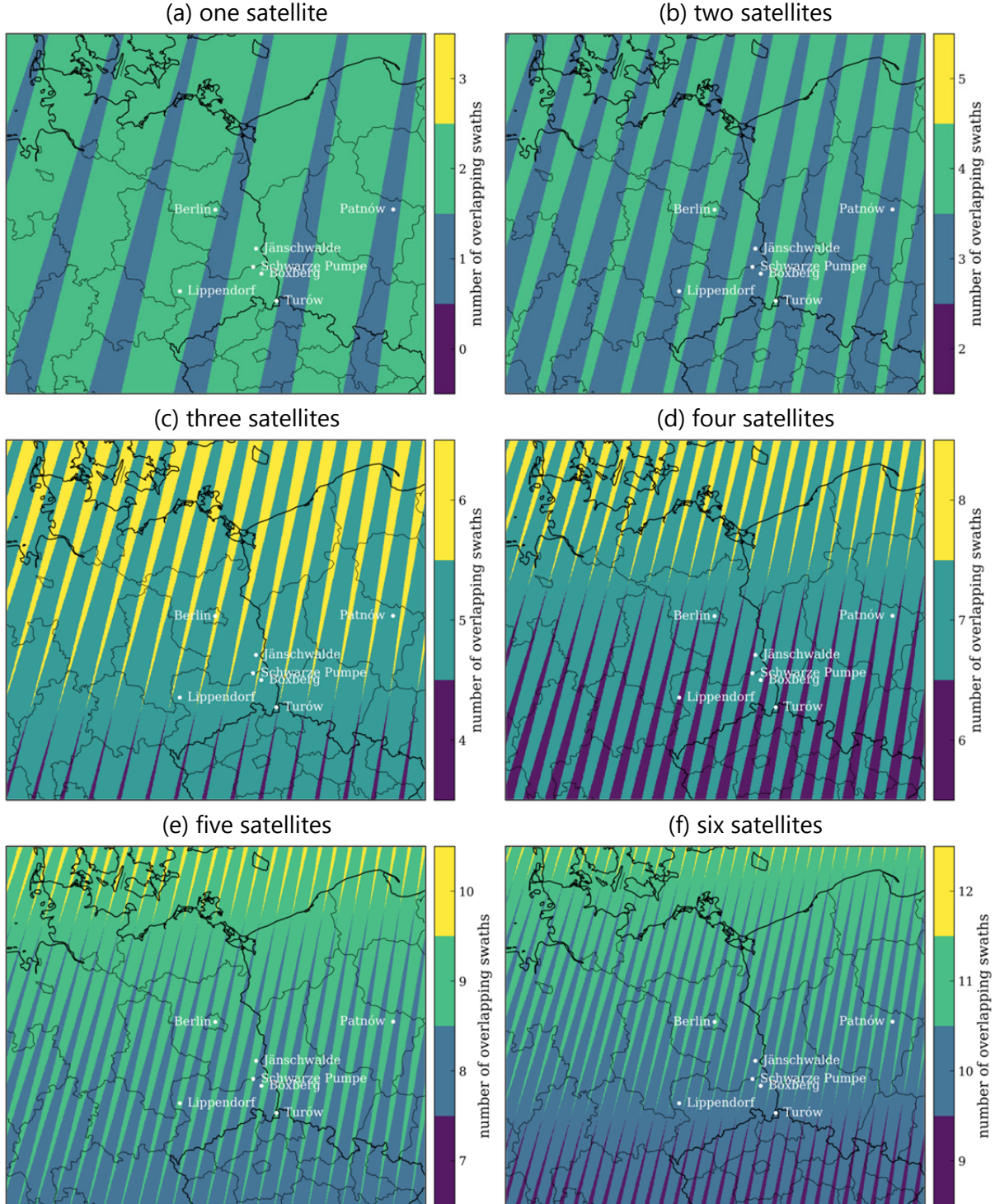


Figure 33: Number of overlapping swaths in an 11-day repeat cycle in the SMARTCARB model domain for a constellation of one to six satellites equally spaced (e.g. by 120° in the case of 3 satellites) in a common orbit. The locations of Berlin and six major power plants are marked. Six satellites would provide near-daily coverage in the model domain while at the equator only 6 or 7 out of 11 days (about 60%) are covered (not shown). The exact locations of the "stripes" are arbitrary and depend on the equator starting longitude (here: 0°E) of the first satellite in the constellation.




Final Report	ESA Project SMARTCARB Study on use of satellite measurements of auxiliary reactive trace gases for fossil fuel carbon dioxide emission estimation contract no 4000119599/16/NL/FF/mg	  Max Planck Institute for Biogeochemistry 
---------------------	---	---

Table 15: Statistics of XCO₂ and NO₂ time series of the standard deviations of the background fields in an area around Berlin (200 x 200 km²) at 11 UTC. The time series are shown in Figure 38c and d.

	XCO ₂ (ppm)	NO ₂ (10 ¹⁵ molecules cm ⁻²)
Mean	0.25	0.80
Standard deviation	0.16	0.44
Minimum	0.06	0.28
Maximum	1.38	3.38

To identify the number of CO₂ plumes that can be observed under cloud-free conditions (ignoring observation errors), the model tracer XCO₂_BV representing only emissions from Berlin (see Table 1) is used to define the location of the plumes. Berlin is chosen as an arbitrary example of a large source in the domain. The results for power plants, which emit comparable amounts of CO₂, would likely be similar. Satellite observations of CO₂ require rigorous filtering for clouds, which significantly reduces the number of observations available for plume detection (Taylor et al., 2016). Here, we remove all pixels with cloud fractions larger than 1%. The NO₂ retrieval can tolerate larger errors and is therefore less sensitive to clouds. For NO₂ plumes we use a cloud threshold of 30% as often applied in satellite NO₂ studies (e.g. Boersma et al. 2011). All cloud information in this study is obtained from COSMO-GHG, i.e., the same model as used for the tracer transport simulations.

To define the extent of the plume, we have to set a *signal threshold* for the tracer field (here: XCO₂_BV) above which a pixel is considered as belonging to the plume. A suitable threshold is the value at which the signal would become smaller than the variability of the background, i.e. where the signal is larger than the standard deviation of the background. Table 15 shows the statistics of the background field around Berlin extracted from the time series of the background (Figure 38). Based on these values, we used a threshold of 0.05 ppm for XCO₂ and 0.2×10¹⁵ cm⁻² for NO₂ approximately corresponding to the minimum of the standard deviation of the background field (Table 15). In addition, we required that Berlin is inside the swath of the instrument to be able to unambiguously assign a plume to the city. We also removed parts of plumes that re-entered the swath after leaving it, because it is often not possible to correctly assign these parts to their source.

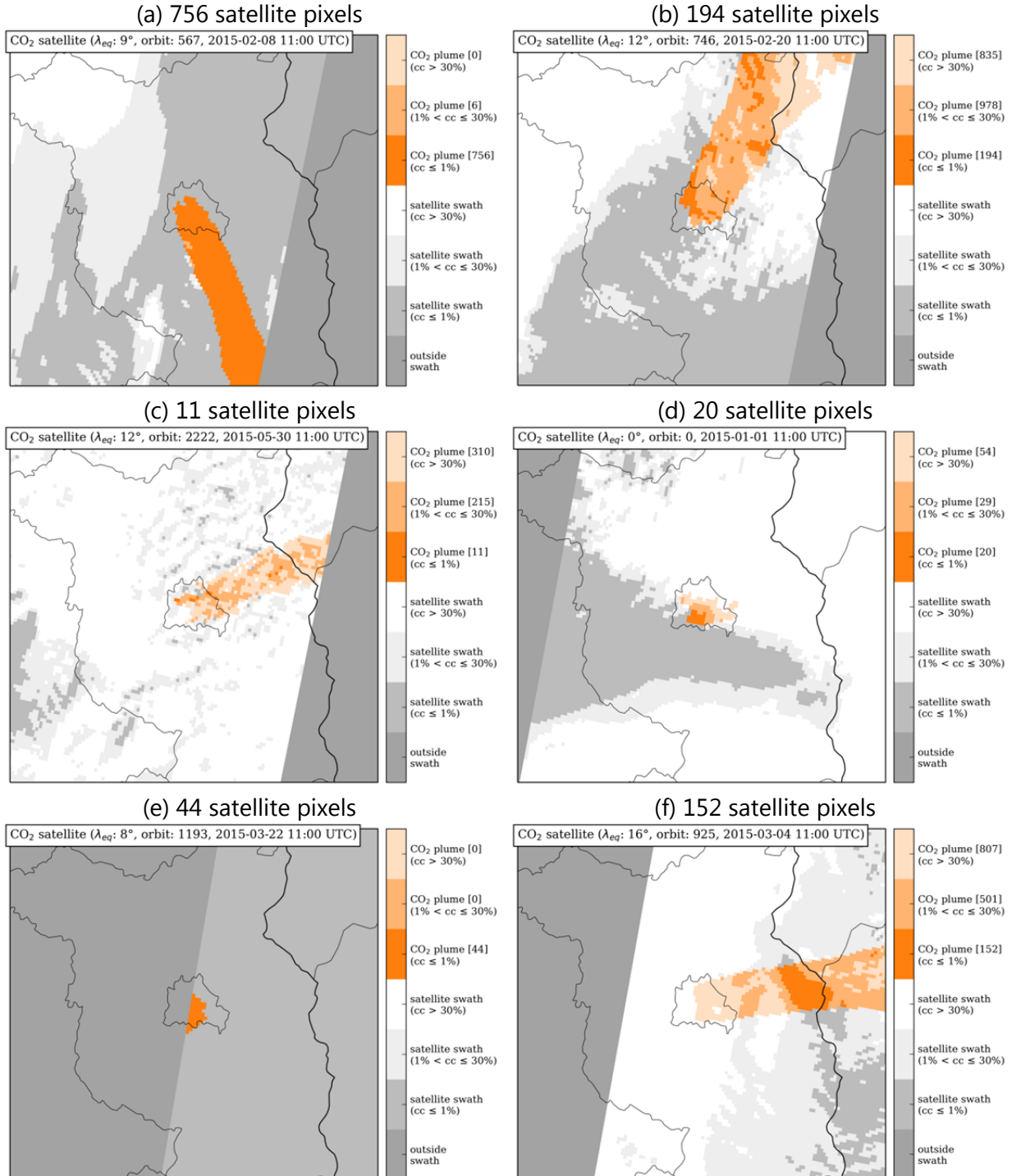


Figure 34: Examples of XCO₂ plumes of Berlin (XCO₂ signal > 0.05 ppm) with different cloud fractions (cc). The numbers of XCO₂ pixels are shown for cloud fractions ≤ 1%. (a-d) Three plumes with increasing cloud fraction, (e) plume close to the edge of the swath, (f) plume not connected to Berlin.

Without clouds, the Berlin plume can be identified on each individual overpass, but the presence of clouds reduces this rate considerably. Figure 34 presents examples of CO₂ plumes under different cloud conditions. Figure 34a-d show plumes with an increasing fraction of clouds and a corresponding decrease in the number of observable plume pixels. In Figure 34e, the plume is close to the edge of the swath and thus not fully visible. Finally, Figure 34f shows a plume where Berlin is cloudy, but a small part of the plume with 152 pixels is cloud free. The plume detection algorithm presented in next section would not be able to detect this plume, because it requires the plume to be connected to the source.

To define the number of plumes that can be observed with a satellite and have a size large enough to be used for emission estimation, we need to define how many pixels are needed to make up a "useful" plume. Figure 35 shows how the number of plumes for a constellation of one, three and six satellites reduces with increasing threshold for the number of pixels.

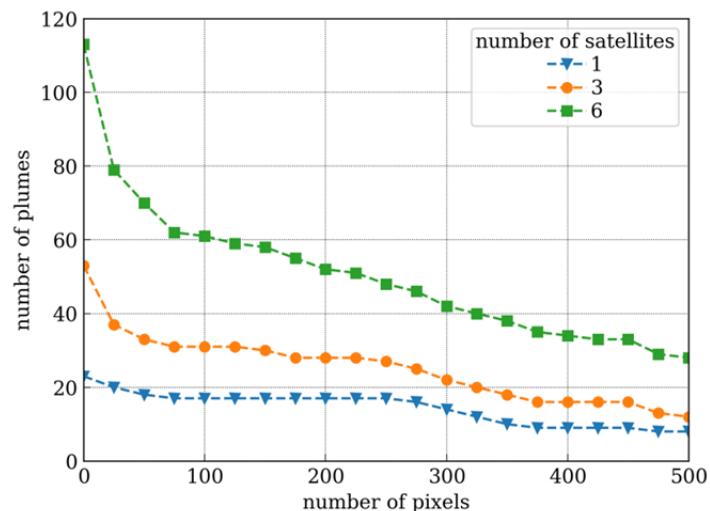


Figure 35: Number of plumes with more than a given number of XCO₂ pixels (XCO₂ > 0.05 ppm and cloud fraction ≤ 1%) observed by a constellation of one, three or six satellites during one year.

For emission estimation, the required number of pixels depends on the uncertainty of the CO₂ instrument and the signal strength of the source but also on the inversion approach. For example, a Gaussian plume model requires the number of pixels to be sufficiently large to infer the direction of propagation of the plume. Furthermore, to estimate emissions of cities, the plume must extend beyond the city limits to contain emissions from the whole city area. The plumes in Figure 34d and e, for example, are too small. For these reasons, we only consider CO₂ plumes with at least 100 CO₂ pixels to be useful. This excludes roughly 40% of the plumes. The cross-wind diameter of the plume of Berlin is typically about 20 km or 10 pixels, which is roughly the diameter of the part of the city with the highest emissions. Therefore, the threshold of 100 pixels is quickly reached and is almost always exceeded unless the plume is heavily obscured by clouds or very close to the swath edge. The threshold does not necessarily remove swaths with plumes in broken clouds (Figure 34b and c). However, for these plumes it might also be challenging to estimate emissions, because the high reflectance of adjacent cloudy pixels increases the XCO₂ uncertainty of the cloud-free pixels (Taylor et al., 2016).

Figure 36 presents the number of observable plumes per month for constellations of one to six satellites. A constellation of six satellites with approximately daily overpasses observes only 61 plumes within one year due to the small number of days with low cloud fractions in particular in winter months. If plumes not connected to the city area are removed, e.g. Figure 34f, the number of plumes is further reduced to 53 (not shown). The presence of clouds thus reduces the opportunity for plume detection by a factor as large as 5 to 6 and thus a constellation of at least three satellites is needed to have a good chance of observing at least one plume in months with many cloudy days.

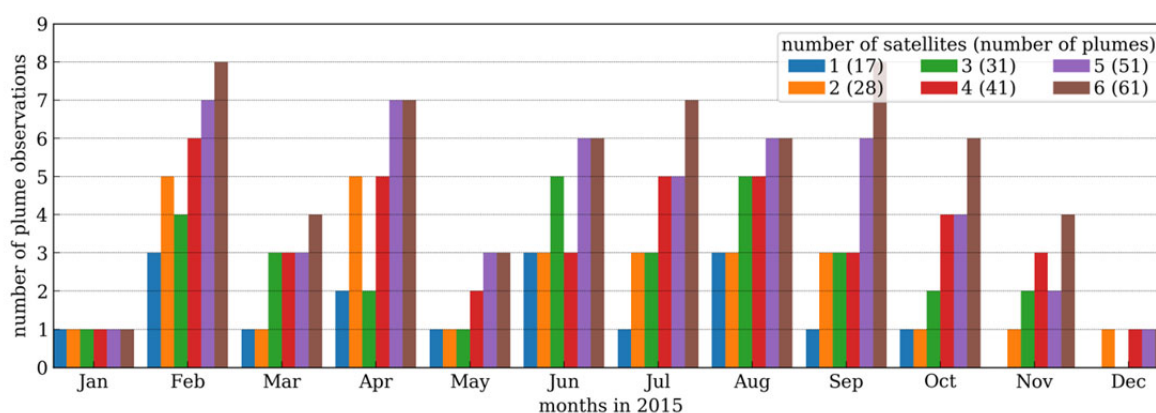





Figure 36: Number of potential observations of the Berlin plume with at least 100 pixels (XCO₂ signal > 0.05 ppm and cloud fraction < 1%) for constellations for constellations of one to six satellites. The number of plume observations is mainly constrained by the number of cloud-free days per month.

Besides clouds two additional factors affect the number of plume observations: First, the number is reduced when the source is close to the edge of the swath. For example, Figure 34e shows an orbit where Berlin is close to the edge and thus only a small number of pixels (<100) can be seen by the instrument for easterly winds. Since the satellites have a repeat cycle of 11 days and only 1-2 overpasses during a cycle, overpasses near the edge of the swath occur every 11 days. The satellite with equator starting position of 8° longitude (Figure 34e), for example, overpasses Berlin twice in 11-days but only sees 57 instead of 66 plumes with 100 pixels (-14%) if we ignore clouds. Second, since the number of cloud-free days is small, statistical fluctuations can have a large effect on the number of plume observations of a given satellite. According to Figure 36, for example, a constellation of two satellites seems almost equivalent to a constellation of three, but this result is merely a consequence of the fact that cloud cover was often large during these overpasses and Berlin is at the edge of the swath for the satellite with starting position of 8°. The result would be different for another starting longitude of the first satellite, another city, or another year. To fully quantify the influence of statistical fluctuations on the number of observable plumes, the number of Level-2 data created for this study is too small. A much larger ensemble of Level-2 data would have to be created with varying starting longitudes for the different constellations.

<p>Final Report</p>	<p align="center">ESA Project SMARTCARB</p> <p align="center">Study on use of satellite measurements of auxiliary reactive trace gases for fossil fuel carbon dioxide emission estimation</p> <p align="center">contract no 4000119599/16/NL/FF/mg</p>	  
----------------------------	---	---

5.3 Plume detection from satellite images

In the previous section, plumes were defined by the extent of a model tracer released only from the respective source. However, in practice, model simulated plumes will never perfectly match the real plumes observed by the satellites. In this section, we therefore describe an algorithm for detecting CO₂ emission plumes directly from the (synthetic) satellite observations using an image processing technique. The algorithm does not require any a priori information but retrieves the plume extension based on the CO₂ enhancements within the plume with respect to the background. The source of the plume can be either a point source (e.g. a power plant) or a city with emissions spread over a larger area.

5.3.1 Detection limit

In a satellite image, a CO₂ plume can be seen as a collection of connected pixels with elevated signals starting at a source. Whether and how frequently the plume of a given source can be detected depends on several, partly interdependent factors:

- (1) The number of satellites and the instrument's swath width, as they determine the number of overpasses over the plume.
- (2) The intensity of the plume, i.e. the amplitude of the enhancement above background.
- (3) The single sounding precision of the instrument, which determines if the enhancement within the plume can be detected
- (4) The variability of the background, which is caused by other anthropogenic emissions and biospheric fluxes and which is additionally affected by meteorology.
- (5) Clouds affect the detectability of the plume by partially or fully covering the plume.
- (6) The size of the plume, because larger plumes consist of more pixels.

Since most of these factors vary with season, the detectability also depends on the time of the year. When a plume is below the detection limit, measurements of co-emitted gases like NO₂ and CO might be used for detecting the location of the plume. The expected enhancements (signals) in XCO₂ and auxiliary trace gases for Berlin and Jänschwalde are shown in Table 16. The CO₂ signal-to-noise ratio (SNR) is 0.5 and 1.0 for σ_{VEG50} of 1.0 and 0.5 ppm, respectively, for Berlin and is slightly smaller if the variance of the background field (i.e. other anthropogenic and biospheric signals) is added to the noise. For Jänschwalde, CO₂ SNR are larger due to the higher signal. For the CO instrument, the SNRs of 0.08 and 0.28 for Berlin and Jänschwalde, respectively, are smaller than for the CO₂ instrument even for the low noise scenario, which makes the CO instrument less suitable for detecting the plumes than the CO₂ instrument. In contrast, the NO₂ instrument has much higher SNRs of 5.0 and 6.7 for both the high and low noise scenario, respectively. Therefore, we only investigate the potential benefit of supplementary NO₂ observations for plume detection since the assumed single sounding precision of the CO instrument was too low for the CO measurements to add any useful information in the considered simulation domain.




Final Report	ESA Project SMARTCARB Study on use of satellite measurements of auxiliary reactive trace gases for fossil fuel carbon dioxide emission estimation contract no 4000119599/16/NL/FF/mg	 Materials Science and Technology  Max Planck Institute for Biogeochemistry 
---------------------	---	--

Table 16: Statistics of XCO₂, CO and NO₂ enhancements in the plumes of Berlin and Jänschwalde extracted from Level-2 data of a constellation of six satellites. Individual enhancements were computed as mean of the 10 and 5 highest values within the area of Berlin and Jänschwalde, respectively.

Percentile	XCO ₂ (ppm)			CO (10 ¹⁷ cm ⁻²)			NO ₂ (10 ¹⁶ cm ⁻²)		
	5 th	50 th	95 th	5 th	50 th	95 th	5 th	50 th	95 th
Berlin	0.2	0.5	1.3	0.2	0.3	1.2	0.4	0.9	2.0
Jänschwalde	1.0	2.5	7.1	0.4	1.1	3.1	1.7	4.0	10.8

5.3.2 Plume detection algorithm

The plume detection algorithm finds satellite pixels with CO₂ or NO₂ values significantly larger than the background using a Z-test. The Z-test is a statistical test for which the distribution of the test statistic can be approximated by a normal distribution. It computes the normalized difference between the mean value of n_p pixels X_p and the background X_{bg} and compares the difference to the z-value:

$$\frac{X_p - X_{bg}}{\sqrt{\frac{s_{ssp}^2}{n_p} + s_{bg}^2}} > z(q), \quad (1)$$

where $z(q)$ is the value for which X_p is larger than X_{bg} with probability q , s_{ssp}^2 is the squared single sounding precision (SSP) of the satellite measurements, s_{bg}^2 is the variance of the background field.

To take advantage on the size of the plume, we do not compare single pixels but compute X_p as the mean of a local neighborhood. Figure 37 shows examples of neighborhoods with different sizes n_s that have been used for testing the algorithm.

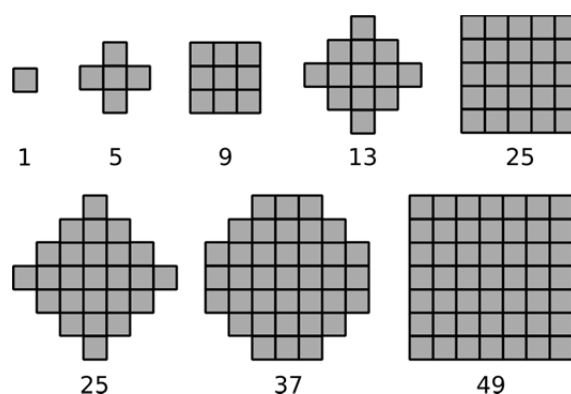


Figure 37: Neighborhoods for computing local mean value.

The difference between the mean of the neighborhood and the mean of the background within the neighborhood is normalized by the square root of the variance of the data, i.e. the standard deviation that would be expected without the presence of a plume. This variance is the sum of single sounding precision s_{ssp}^2 of the satellite measurements inversely scaled by the number of pixels n_p assuming random errors, and the spatial variance of the

background σ_{bg}^2 , which is assumed to be mostly systematic and thus does not change with neighborhood size. Since some pixels in a neighborhood might be missing, for example due to clouds, n_p can be smaller than the size of the neighborhood n_s .

For simplicity, mean and variance of background are estimated from the model tracers excluding the emissions of the source for a $200 \times 200 \text{ km}^2$ square around cities and a $100 \times 100 \text{ km}^2$ square around each power plant. Figure 38 shows the mean and standard deviation of background XCO_2 and NO_2 columns around Berlin. XCO_2 has a strong annual cycle with an amplitude of about 16 ppm. The background variability, on the other hand, is typically only of the order of a few tenths of a ppm (Figure 38c). Despite higher XCO_2 in winter than in summer, the variability is somewhat larger in summer possibly due to biospheric activity in combination with lower average wind speeds, especially in July and August. For NO_2 , the variability in the background is relatively constant over the year, at least for our idealized NO_2 tracer with a constant lifetime of 4 hours. Since Berlin's XCO_2 signal is typically only about 0.5 to 1 ppm (Figure 39a), it is critical to accurately estimate the background XCO_2 value and its variance. On the other hand, Berlin's NO_2 signal is typically ten times larger than the standard deviation of the background (Figure 38d and Figure 39b).

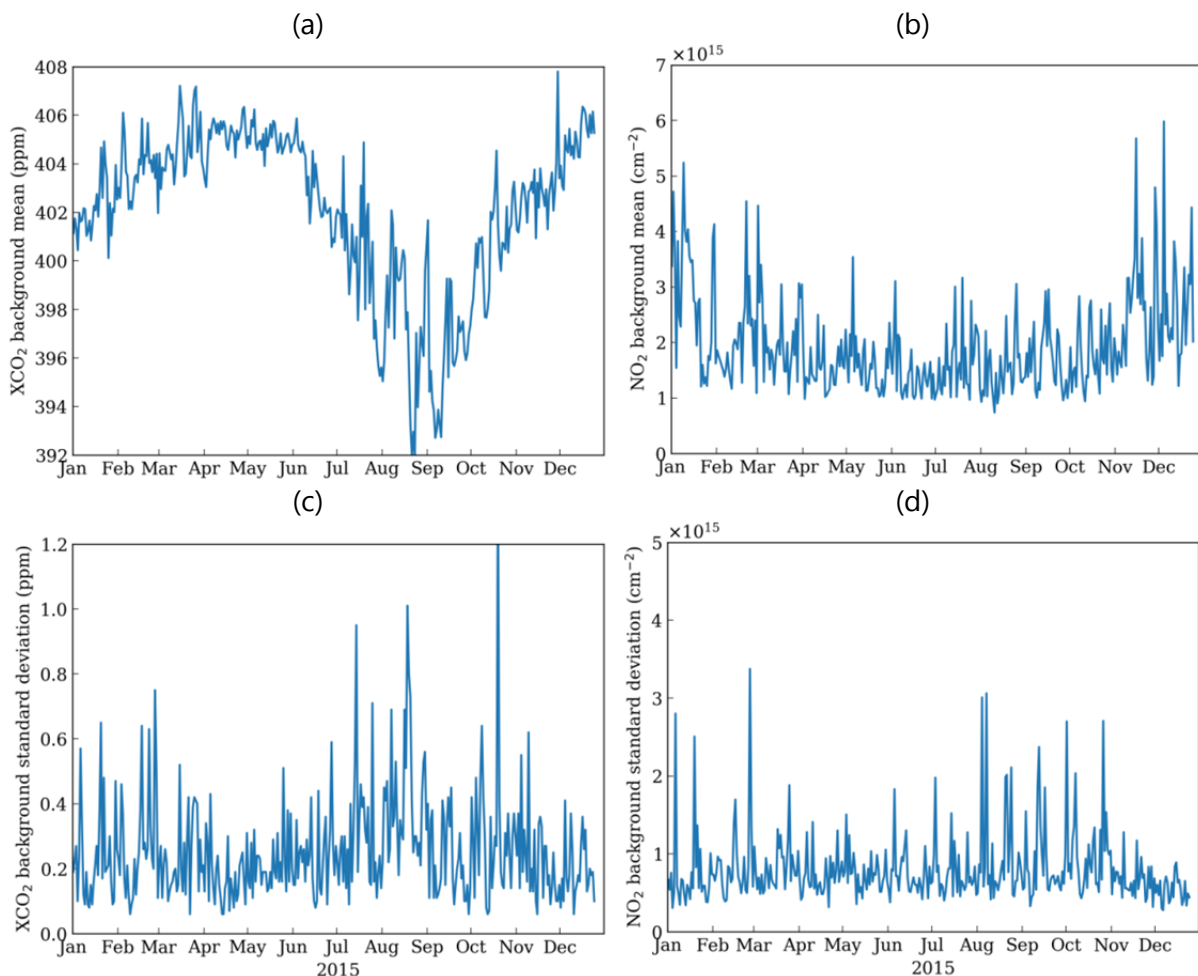


Figure 38: (a,b) CO_2 and NO_2 mean value of the background in a $200 \times 200 \text{ km}^2$ area around Berlin and (c,d) the standard deviation of the background (total XCO_2 or NO_2 minus Berlin emission tracer) in the same area.

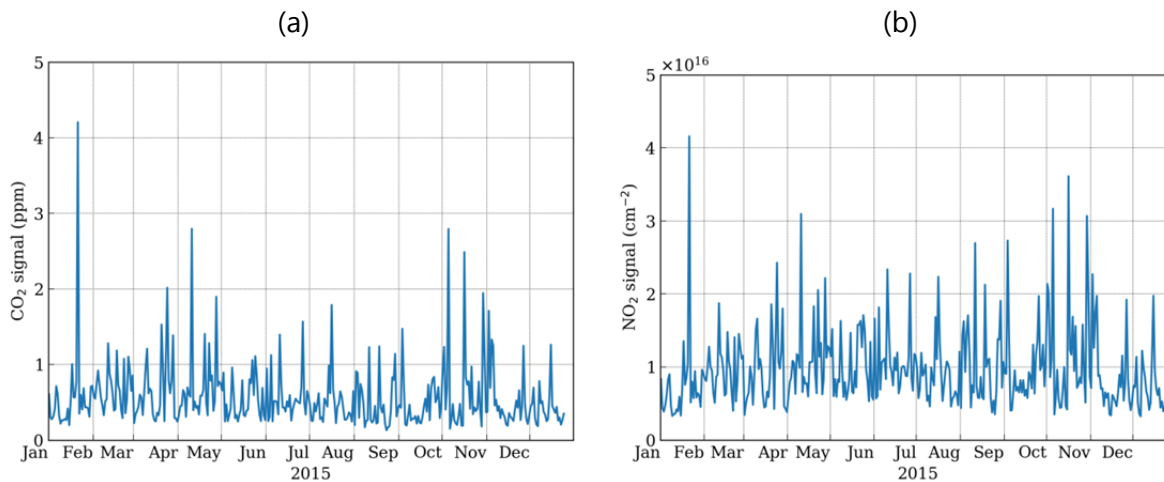


Figure 39: Time series of Berlin's (a) CO₂ and (b) NO₂ signals (XCO₂_BV and NO₂_BV tracer) calculated as mean of the ten highest values in the Level-2 data of six satellites over the area of Berlin (~15 km radius, i.e. about 130 satellite pixels).

The result of the Z-test is a binary image with "true" values where pixels are enhanced above the background and "false" values where they aren't. The connected true pixels are assumed to belong to the same plume and are labelled using a Moore neighborhood where each pixel has eight potential neighbors. The labelling algorithm assigns each connected region a unique integer value. In order to identify the source of the plume, we select all regions that intersect with the source. For cities we use a circle with a radius of 15 km and for point sources a circle with a radius of 5 km around the source. The last step removes all regions not connected to a source, which may include parts of a real plume separated from the source by clouds.

Figure 40 shows an example of plume detection for Berlin. Figure 40a shows the XCO₂ observations for a noise scenario of 0.7 ppm, i.e. $\sigma_{\text{VEG50}} = 0.7$ ppm. Figure 40b shows the calculated z-values for a neighborhood with 49 pixels and Figure 40c shows the labelled regions using z-values larger than 2.33 ($q = 99\%$). In the last step, only plumes are used that intersect with Berlin (Figure 40d).

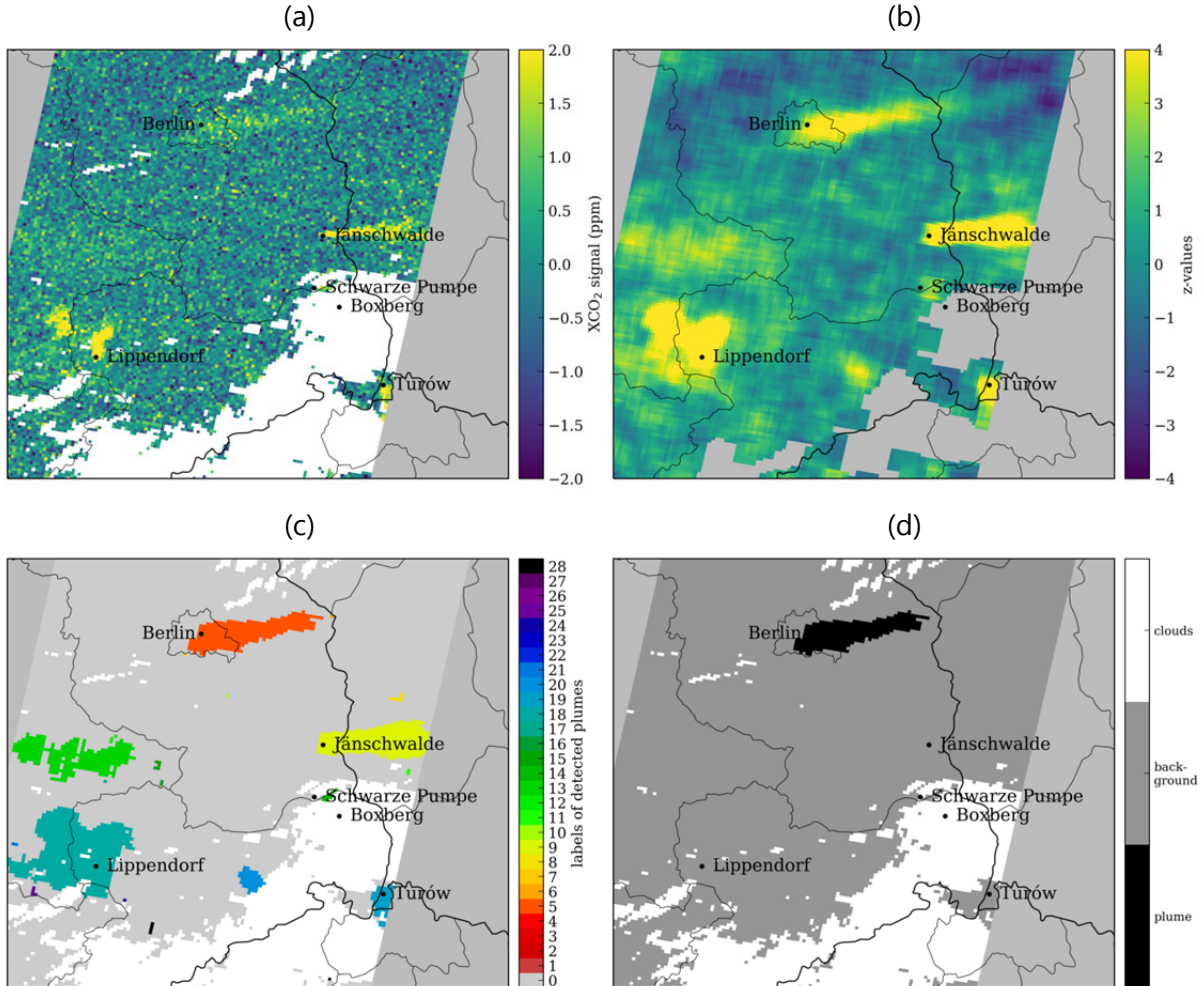


Figure 40: The plume detection algorithm used to detect Berlin's CO₂ plume on 23 April 2015, 11 UTC. (a) XCO₂ field with σ_{VEG50} of 0.7 ppm and pixels with cloud fractions larger than 0.01 in white. (b) z-values with n_s of 49. (c) 28 labelled plumes in the area. (d) The final plume assigned to Berlin.

5.3.3 Berlin plume

The plume detection algorithm is applied to the plumes of Berlin, using CO₂ and NO₂ observations of Sentinel CO₂ satellite and NO₂ observations of Sentinel-5 with the uncertainty scenarios defined in Section 3.2. The p-value is set to 1% ($q=0.99$) and the size of neighborhood n_s is varied between 1 and 121. For CO₂ we apply a cloud fraction threshold of 1% and for NO₂ a much larger threshold of 30%, since for NO₂ a larger retrieval error due to clouds can be tolerated.

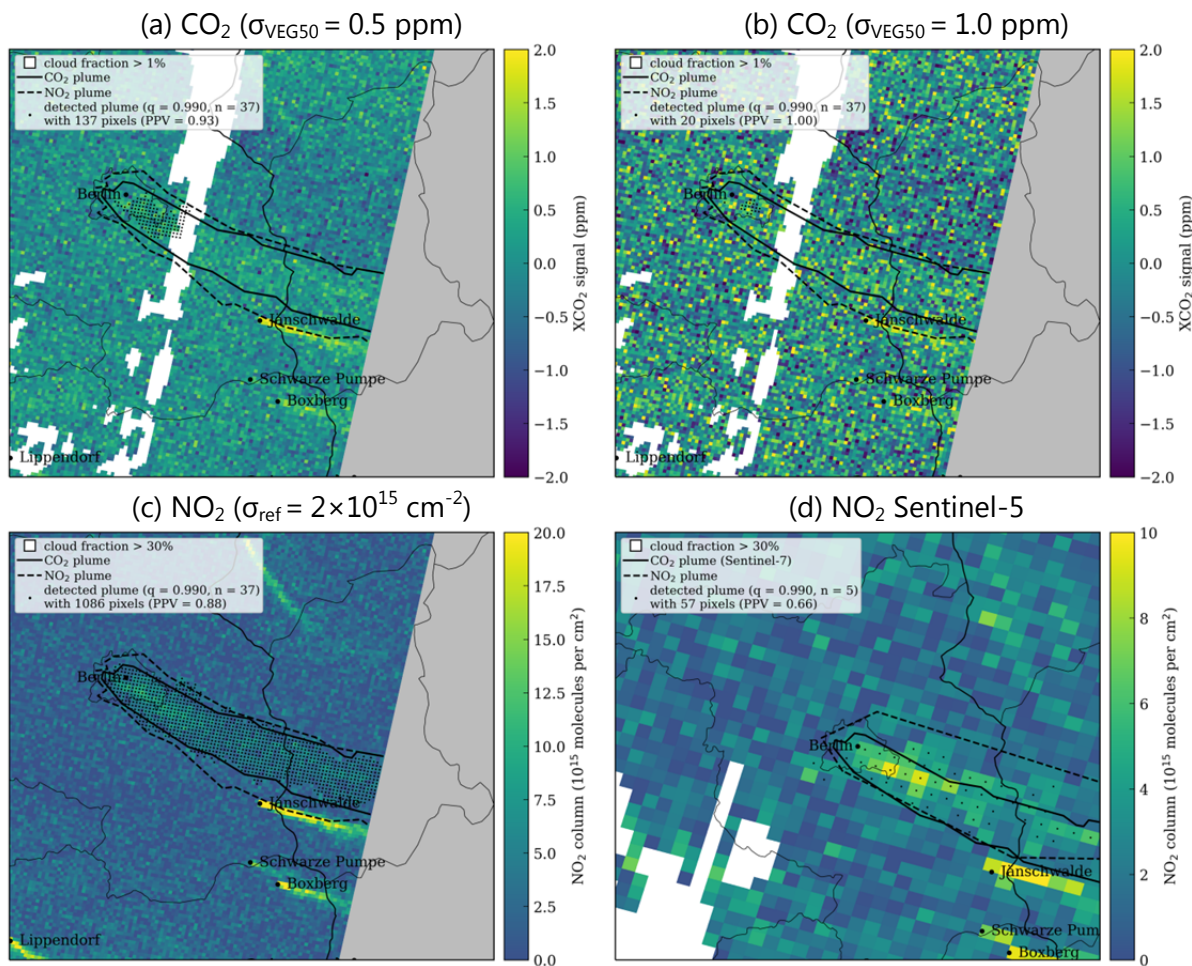


Figure 41: Example for plume detection with Sentinel CO₂ mission's CO₂ and NO₂ instrument and Sentinel-5's NO₂ instrument on 21 April 2015 (Satellite A, orbit 1640.). NB: the outlines of the true CO₂ and NO₂ plumes are smoothed and thus cannot be used for counting the number in- and outside the plume.

Plume detection examples

Figure 41 shows Berlin's CO₂ plume on 21 April 2015. A CO₂ instrument detects 137, 90 and 20 pixels with noise scenarios σ_{VEG50} of 0.5, 0.7 and 1.0 ppm, respectively (Figure 41a and b). A band of clouds prevents the detection further downwind. However, if the clouds were removed still only 210 pixel would be detected with the best CO₂ instrument ($\sigma_{\text{VEG50}} = 0.5$ ppm). The NO₂ instruments are less sensitive to clouds and thus can detect 1215 and 1086 pixels with the low and the high noise scenario (Figure 41c). The NO₂ tracer used here and in all subsequent analyzes has a lifetime of 4 hours. The Sentinel-5 NO₂ instrument also detects the plume with 57 Sentinel-5 pixels, but since it is measured two hours earlier, the NO₂ plume seen by Sentinel-5 (dashed line in Figure 41d) is slightly shifted with respect to the CO₂ plume (solid line).

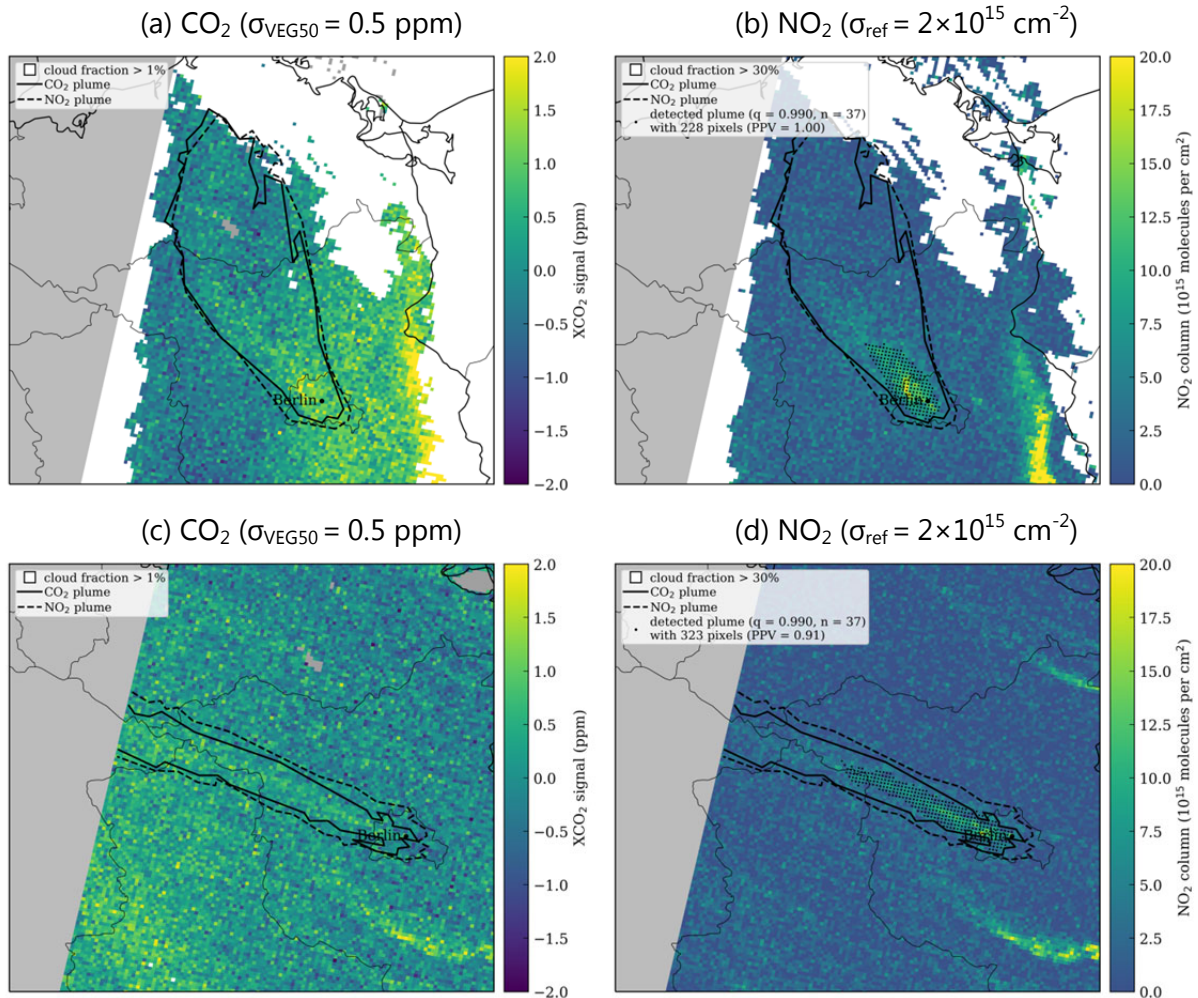


Figure 42: (a) Example where plume detection with a CO_2 instruments fails because of pronounced horizontal gradients in the CO_2 background field (27 February 2015). (c). Example where the plume detection fails due small CO_2 signals as a result of high wind speeds (2 July 2015). In both cases, the plume can readily be detected by the NO_2 instrument.

Figure 42 presents two examples where the CO_2 instrument fails to detect the CO_2 plume of Berlin. In Figure 42a, the CO_2 field has a pronounced spatial gradient resulting in a high variance of the background field preventing the detection of the plume. This gradient is not present in the NO_2 field which makes it possible to detect the plume using the NO_2 instrument (Figure 42b). Such situations occur in roughly 20% of cloud-free swaths. Figure 42c and d show a second example where the CO_2 instrument cannot detect the plume, because the signal is very weak due to strong winds. The NO_2 instrument has a better signal-to-noise ratio and is able to detect the plume also in these situations.

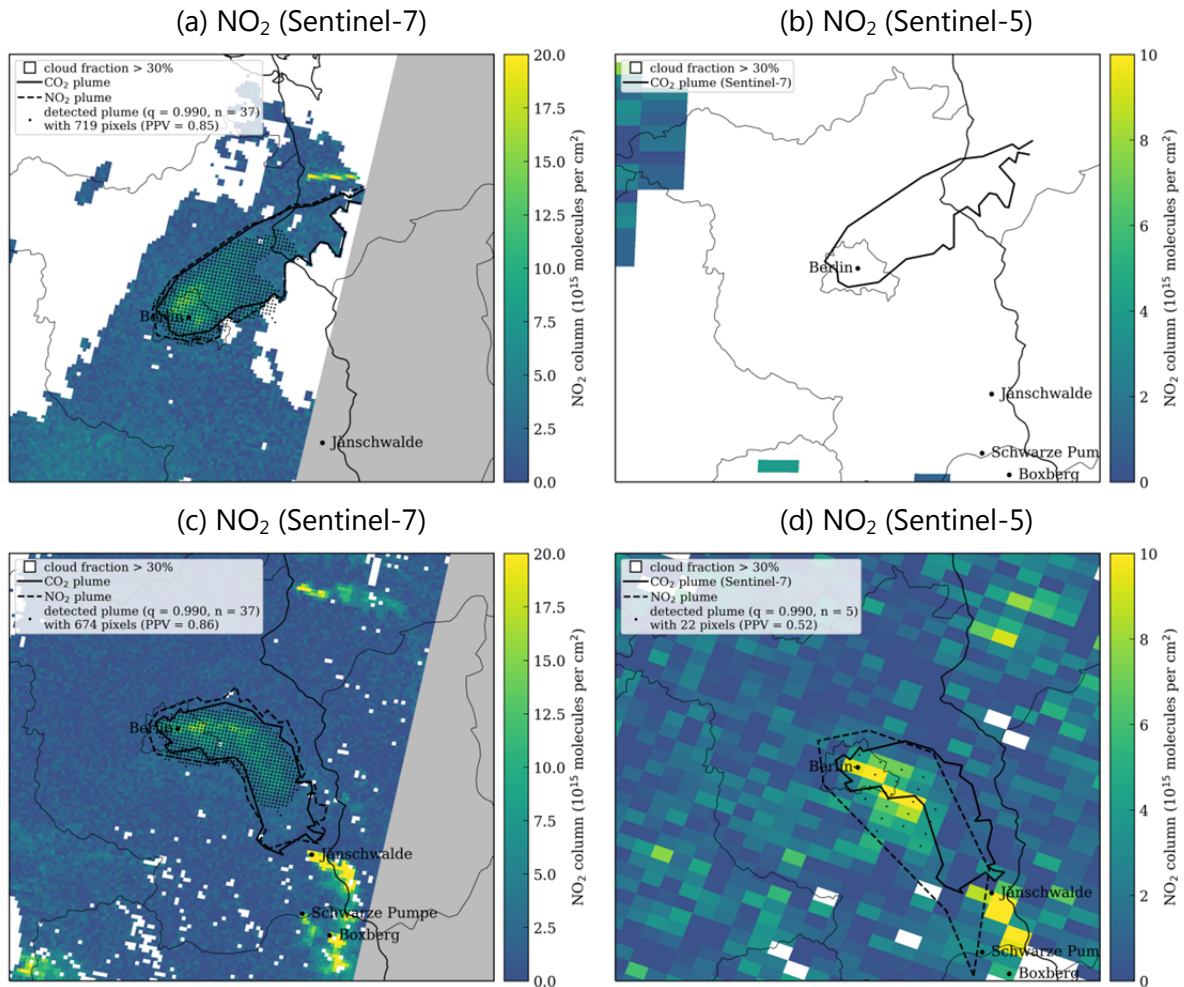


Figure 43: Examples of comparing plume detection with the Sentinel-5 and Sentinel-7 NO₂ instrument (a, b) Due to time-lag between overpasses, the Sentinel-5 is cloudy (3 December 2015). (c, d) The plume position clearly changed between the two overpasses (17 June 2015).

Figure 43 presents two examples comparing the NO₂ plume observed by Sentinel-5 to the CO₂ plume (solid black line) observed two hours later by the Sentinel CO₂ satellite. In the first example (sub-panels a and b), Sentinel-5 fails to detect any plume due to clouds, which have largely disappeared by the time of the Sentinel CO₂ satellite overpass. In the second example, both the Sentinel-5 and the Sentinel CO₂ satellite detect a plume of similar size, but the Sentinel-5 plume is significantly displaced due to changes in the prevailing winds between the two overpasses.

Effect of neighborhood size on plume detection

The neighborhood approach computes the mean at a given location by not only considering a single pixel but also its surrounding pixels, which reduces random noise and thus makes it possible to detect smaller CO₂ enhancements above the background. On the other hand, this approach is equivalent to a spatial smoothing making it difficult to correctly assign pixels at

the edge of the plume. Furthermore, plumes smaller than the size of the neighborhood become more difficult to detect.

The performance of the plume detection algorithm has been evaluated using both visual inspection and confusion tables which compare the predicted plume with the true plume. The confusion table computes the number of true positives (TP), false positives (FP), false negatives (FN) and true negatives (TN) (Table 17).

The true plume is defined here as the plume within the swath of Sentinel CO₂ satellite with XCO₂ values of the Berlin tracer above 0.05 ppm as described in Section 0. The extent of the plume is limited to the area connected to Berlin with cloud coverage below 30%, since at higher cloud coverage it can be neither detected by an XCO₂ nor by an NO₂ instrument. Furthermore, we only consider reasonably large plumes with at least 100 pixels with cloud coverage below 1% to be useful for source estimation. For a NO₂ instrument on Sentinel-5, detected pixels are projected onto the pixels of a Sentinel CO₂ satellite's XCO₂ instrument.

Table 17: Confusion table of plume detection algorithm against true plume as directly estimated from Berlin tracer.

		true class	
		plume	no plume
predicted class	plume	true positives (TP)	false positives (FP)
	no plume	false negatives (FN)	true negatives (TN)

Two key quality indicators can be obtained from the confusion table:

- The true positive rate (TPR) or sensitivity is the fraction of pixels of the real plume that are successfully detected by the algorithm:

$$TPR = \frac{TP}{P} \text{ with } P = TP + FN. \quad (2)$$

- The positive predictive value (PPV) or precision is the fraction of all detected pixels that are true positives:

$$PPV = \frac{TP}{TP+FP}. \quad (3)$$

Figure 44, Figure 45 and Figure 46 show the effect of neighborhood size on true and false positives, true positive rate and positive predictive value. A visual inspection of all plumes showed that a PPV of less than 0.8 typically means that plume detection failed due to a large fraction of detected pixels actually belonging to other plumes or the background. The latter is typically observed when background XCO₂ has a strong horizontal gradient. Therefore, a vertical dashed line was added to the figures indicating a PPV of 0.80 and, hence, a threshold for successful plume detection.

Figure 44 shows that for a CO₂ instrument, TP increases with neighborhood size. However, the median of true positives is zero for all neighborhoods sizes suggesting that more than half of the plumes are not detectable at all with a CO₂ instrument. The PPV is mostly close to one for all sizes. Very small PPVs are caused by detections with small true positives.

Instead of detecting the plume with the CO₂ instrument, it could also be detected with an NO₂ instrument. Note that in this case the plume detection algorithm is applied to NO₂ observations but the confusion table statistics are computed by comparing the detected pixels to the true CO₂ plume, not the NO₂ plume. With an NO₂ instrument the number of true positives and the TPR is much larger than for a CO₂ instrument, because the instrument has a better signal-to-noise ratio and is less affected by clouds (Figure 45). The number of true positives increases with neighborhood size, but levels off at about 400 pixels (TPR = 0.5) for neighborhoods larger than 25 pixels. The number of false positives increases and the PPV decreases with neighborhood size, respectively.

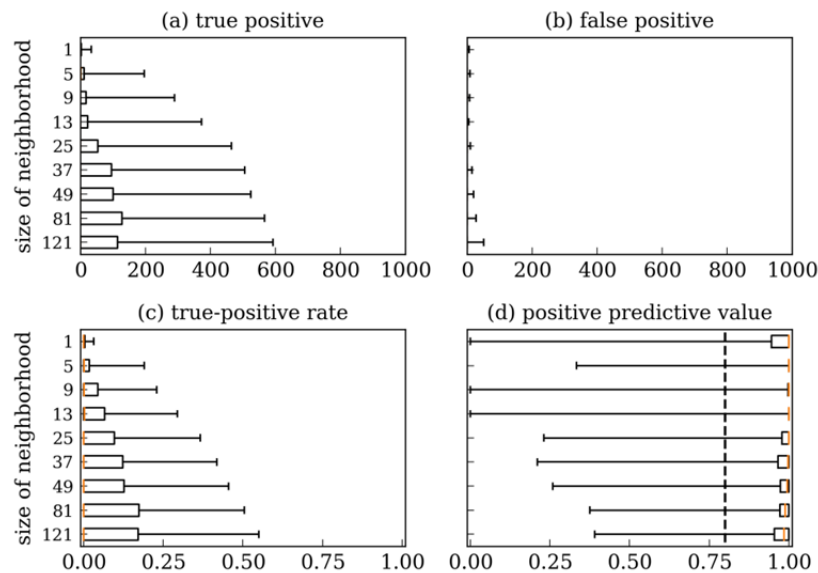


Figure 44: Elements of the confusion matrix for detection of Berlin's CO₂ plume (<30% cloud fraction) with a CO₂ instrument ($\sigma_{\text{VEG50}} = 0.5$ ppm, 1% cloud threshold and six satellites) for different-sized neighborhoods and a total of 61 analyzed scenes. Boxes denote the range between the 25% and 75% percentiles. The whiskers show the full range of values. The black dashed line marks a PPV of 0.80.

Figure 46 presents the same analysis for an NO₂ instrument on Sentinel-5. Since this instrument has a lower spatial resolution (7.5×7.5 km²), the area covered by a given neighborhood is much larger than for Sentinel-7 (2×2 km²), and therefore only neighborhood sizes between 1 and 13 were analyzed. TP is largest for neighborhoods of 5, 9 and 13. However, the PPV is quite small for these neighborhoods, which is a result of the spatial mismatch between CO₂ plume of the Sentinel CO₂ satellite and Sentinel-5's NO₂ plume caused primarily by the different overpass times (Sentinel-7: 11:30 local time and Sentinel-5: 9:30 local time).

As optimal neighborhood size for detecting Berlin's CO₂ plume, we chose a value of 37, since the number of true-positives levels off at larger sizes for plume detection with the NO₂ instrument (Figure 45). This neighborhood size is applied to both the CO₂ and the NO₂ instrument. For Sentinel-5, conversely, we chose a much smaller neighborhood size of either 1 or 5 due to the coarser pixels. The optimal size depends not only on the size of the pixels but also on the size of the plume. The Berlin plume has a typical initial diameter of 20-25 km.

The 37-neighborhood has a somewhat smaller diameter of about 14 km which leads to a good compromise between sensitivity (TPR) and precision (PPV).

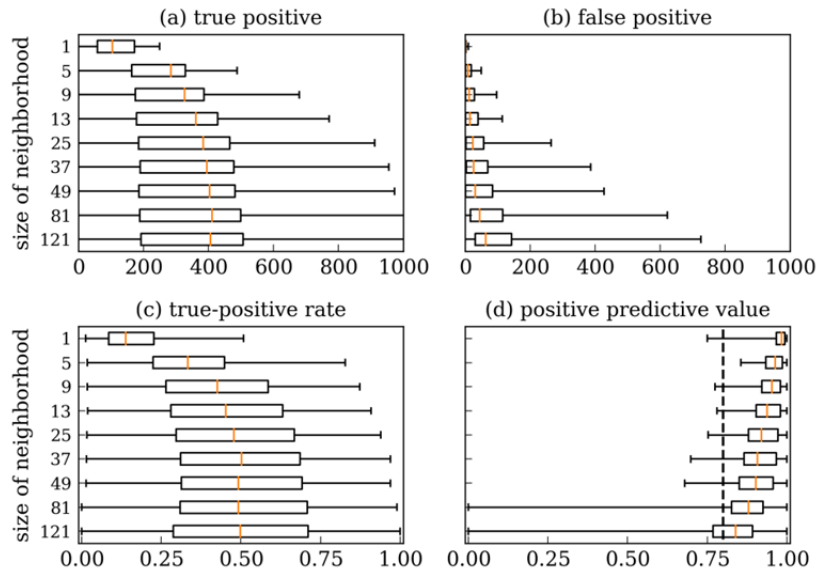


Figure 45: Confusion matrix for detection of Berlin's CO₂ plume (<30% cloud fraction) with a NO₂ instrument (high noise, 30% cloud threshold and six satellites). Boxes denote the range between the 25% and 75% percentiles. The whiskers show the full range of values. The black dashed line marks a PPV of 0.80.

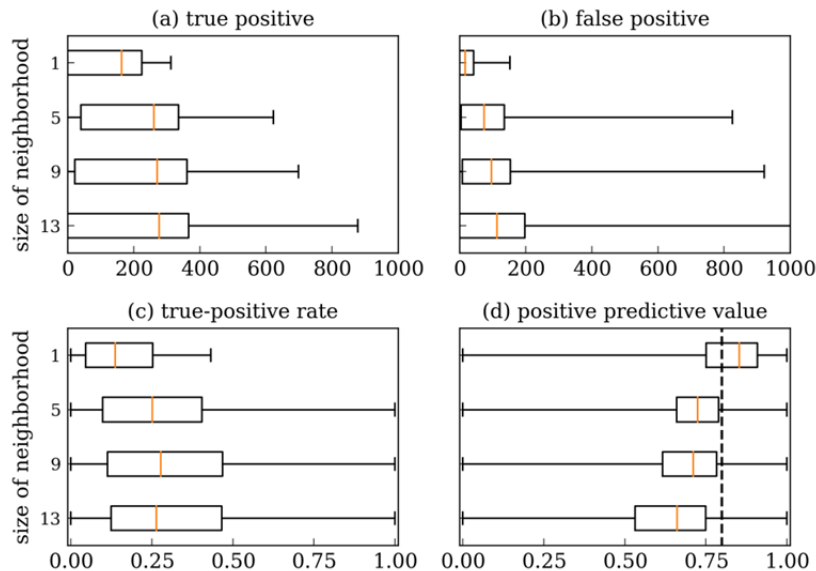


Figure 46: Confusion matrix for detection of Berlin's CO₂ plume (<30% cloud fraction) with the Sentinel-5 NO₂ instrument (30% cloud threshold and one satellite). Boxes denote the range between the 25% and 75% percentiles. The whiskers show the full range of values. The black dashed line marks a PPV of 0.80.

Number and sizes of detected Berlin plumes

In this section, we analyze in detail how many plumes can be detected with the CO₂ and NO₂ instrument for different instrument noise scenarios. Figure 47 shows the number of

detectable plumes during one year as a function of plume size for a constellation of six satellites. For smaller constellations the numbers would be accordingly smaller. Plumes with a large number of false positives (PPV < 0.80) are not included. Figure 47a counts only pixels that have valid CO₂ observations using a cloud threshold of 1%. In contrast, Figure 47b also includes pixels with a cloud cover of up to 30% applicable to an NO₂ instrument that do not provide valid CO₂ observations but can provide potentially useful information about plume shape and orientation for the inversion framework (see Sections 5.4.2 and 5.5.1). Table 18 summarizes the total number of plumes with more than 0 and 100 successfully detected pixels, respectively, and the mean and median sizes of the plumes for the case with a 1% cloud threshold.

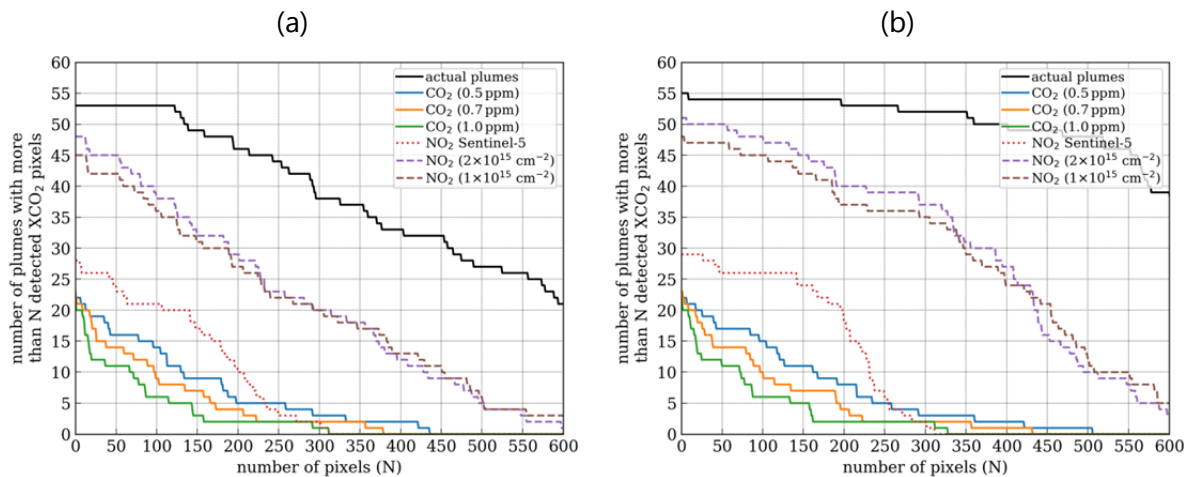
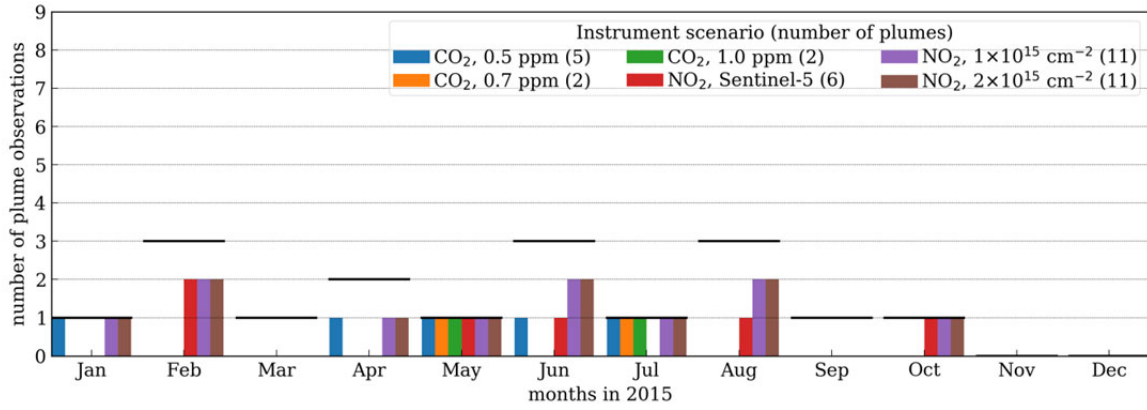


Figure 47: The number of plumes with more than N detected (true positive) CO₂ pixels (only plumes with PPV ≥ 0.8). The neighborhood size is $n_s = 37$ for the Sentinel CO₂ mission and $n_s = 1$ for Sentinel-5. (a) for a 1% cloud threshold for both NO₂ and XCO₂ and (b) using a 1% threshold for XCO₂ and a 30% threshold for NO₂.

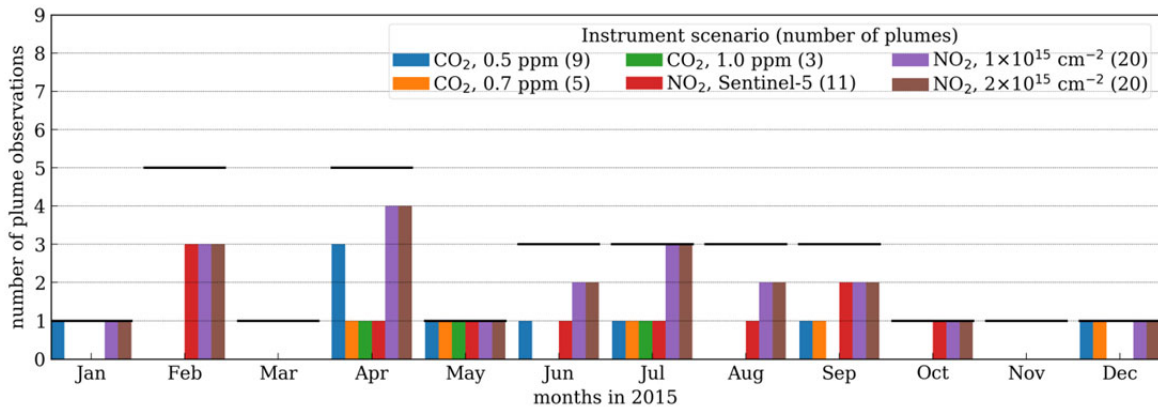
Table 18: Number of Berlin's CO₂ plumes and the mean/median number of detected CO₂ pixels (TP if PPV ≥ 0.8 and cloud fraction < 1%) for different instruments (constellation of six Sentinel CO₂ satellites or one Sentinel-5 satellite). The neighborhood size is $n_s = 37$ for the Sentinel CO₂ mission and $n_s = 1$ for Sentinel-5. Real plumes are all plumes with at least 100 cloud free (<1%) pixels with XCO₂ > 0.05 ppm.

Instrument (uncertainty)	Number of plumes (percentage of all plumes)		True positives (TP)	
	>0 pixels	>100 pixels	Mean number of pixels	Median number of pixels
real CO ₂ plumes	53 (100%)	53 (100%)	628	458
CO ₂ ($\sigma_{\text{VEG50}} = 0.5$ ppm)	23 (43%)	14 (26%)	148	113
CO ₂ ($\sigma_{\text{VEG50}} = 0.7$ ppm)	23 (43%)	9 (16%)	107	89
CO ₂ ($\sigma_{\text{VEG50}} = 1.0$ ppm)	22 (42%)	6 (10%)	77	52
NO ₂ Sentinel-5	29 (55%)	21 (39%)	156	179
NO ₂ (low noise)	48 (91%)	36 (67%)	271	231
NO ₂ (high noise)	51 (96%)	38 (71%)	261	228

(a) 1 satellite



(b) 2 satellites



(c) 3 satellites

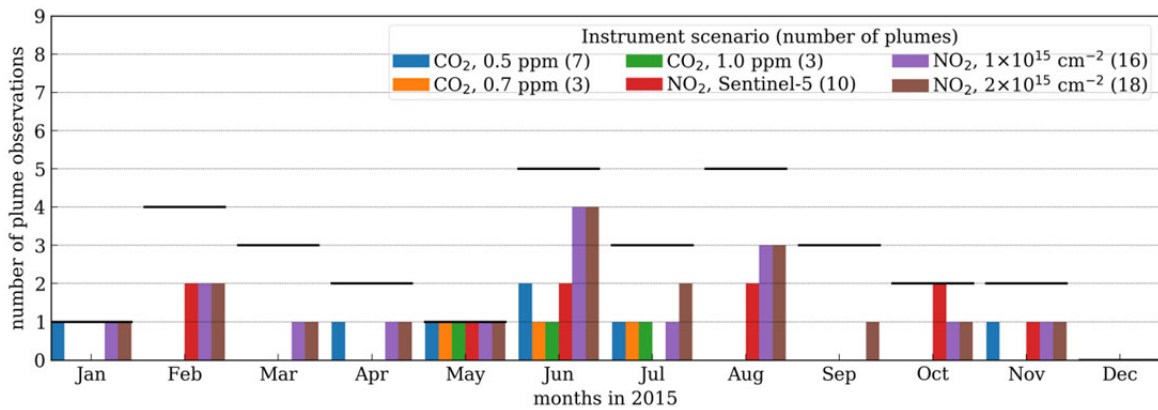
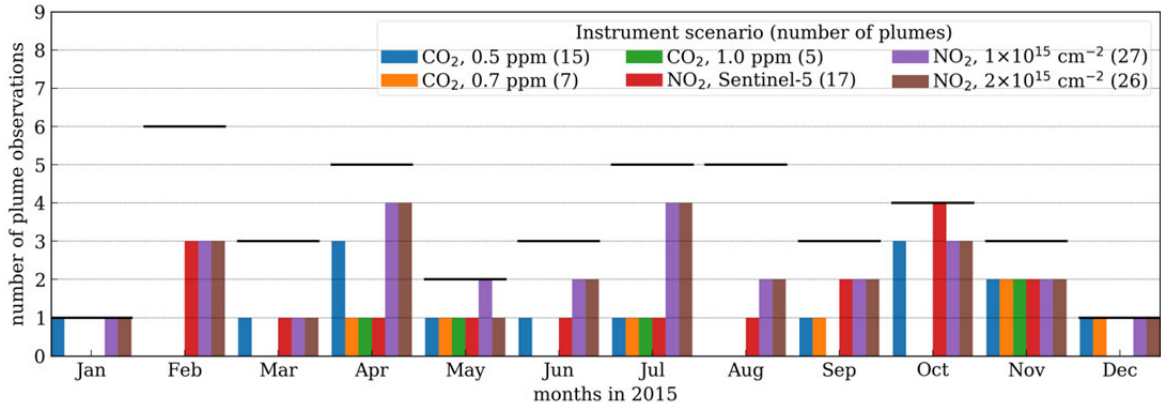
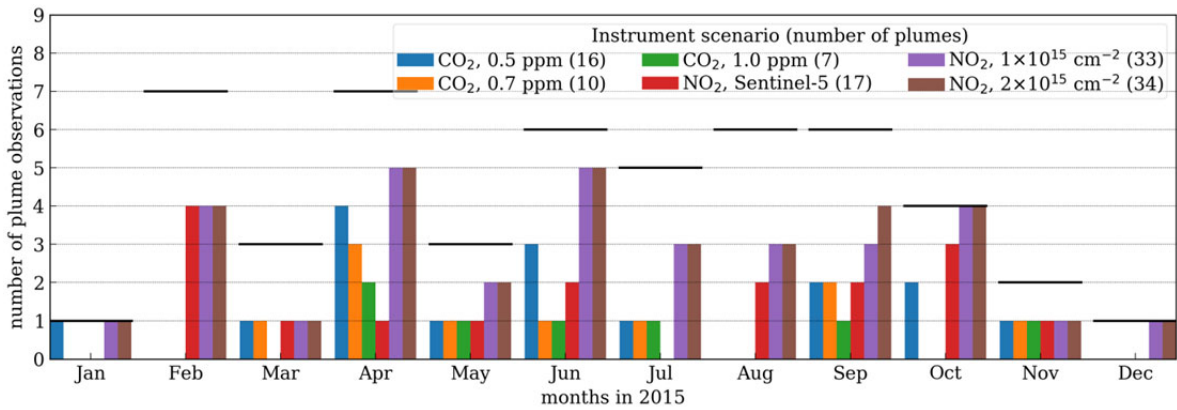


Figure 48: Number of detected plumes with at least 100 pixels for different instrument scenarios for (a) one, (b) two and (c) three satellites. The instrument scenarios are the CO₂ instrument with 0.5, 0.7 or 1.0 ppm uncertainty, NO₂ observations from Sentinel-5 and NO₂ from the Sentinel CO₂ mission with low and high noise. The black line is the maximum number of plumes that could potentially be detected in each month (Figure 36).

(a) 4 satellites



(b) 5 satellites



(c) 6 satellites

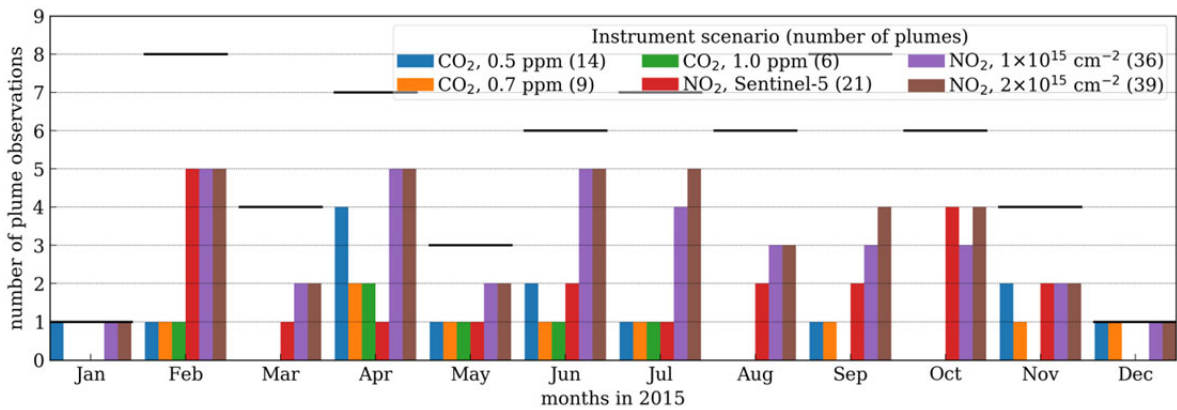


Figure 49: Number of detected plumes with at least 100 pixels for different instrument scenarios for (a) four, (b) five and (c) six satellites. The instrument scenarios are the CO₂ instrument with 0.5, 0.7 or 1.0 ppm uncertainty, NO₂ observations from Sentinel-5 and NO₂ from the Sentinel CO₂ mission with low and high noise. The black line is the maximum number of plumes that could potentially be detected in each month (Figure 36).

The CO₂ instruments detect significantly fewer plumes than the NO₂ instruments. Depending on noise scenario, the CO₂ instruments detect plumes with more than 100 pixels with a success rate of only 10% to 26%, while for the NO₂ instruments the success rates are 67% to 71%. The NO₂ instrument with low noise performs worse than the high noise instrument. This is an artefact of the algorithm often detecting small plumes not related to emissions from Berlin in the case of a low-noise instrument that results in a PPV below 0.80. The Sentinel-5 NO₂ instrument detects 39% of the plumes, thus only little more than half the success rate of the NO₂ instruments of the Sentinel CO₂ satellite.

Figure 48 and Figure 49 show the number of plumes per month with at least 100 detected pixels for different constellations between one and six satellites. The number of plume detections per month is small and therefore highly sensitive to the specific orbit configuration. For example, two satellites seem to detect more plumes than three, but this result is caused by an unfavorable orbit for observing Berlin for the constellation with three satellites and unfavorable cloud cover as already discussed in Section 0. Figure 50 shows the increase of the number of plume observations with the number of satellites. The standard deviation was estimated by bootstrapping for different starting longitudes (i.e. east-west displacements of all orbits). The figure shows that the number of observed plumes generally increases with the number of satellites as expected, but statistical noise can mask the increase from one constellation to the next. The figure confirms the much lower success rates of the CO₂ instruments as compared to the NO₂ instruments. The plumes of Berlin are often too weak to be detectable with an area of at least 400 km² (100 pixels) even with a low noise CO₂ instrument.

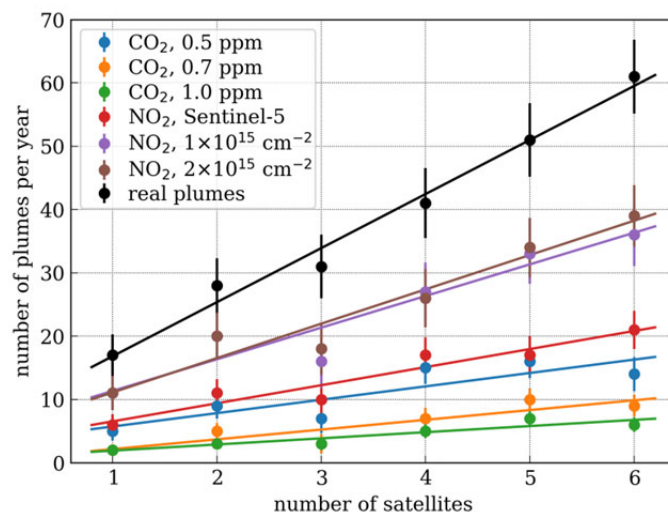


Figure 50: Number of CO₂ plumes (TP ≥ 100 and PPV ≥ 0.8) for different number of satellites. The dots are number of plumes for the standard starting longitudes (

Table 14). The standard deviations were roughly estimated by bootstrapping from the 12 unique starting longitudes. Straight lines represent the results of standard linear regression.

5.3.4 Power plant plumes

There are six major power plants in the model domain: Jänschwalde, Boxberg, Schwarze Pumpe, Lippendorf, Turów and Patnow. Because no model tracer was defined for individual power plants but only for the sum of all of them, the true plume of an individual power plant is not known. Therefore, visual inspection was used to identify those plume detections which erroneously included neighboring plumes.

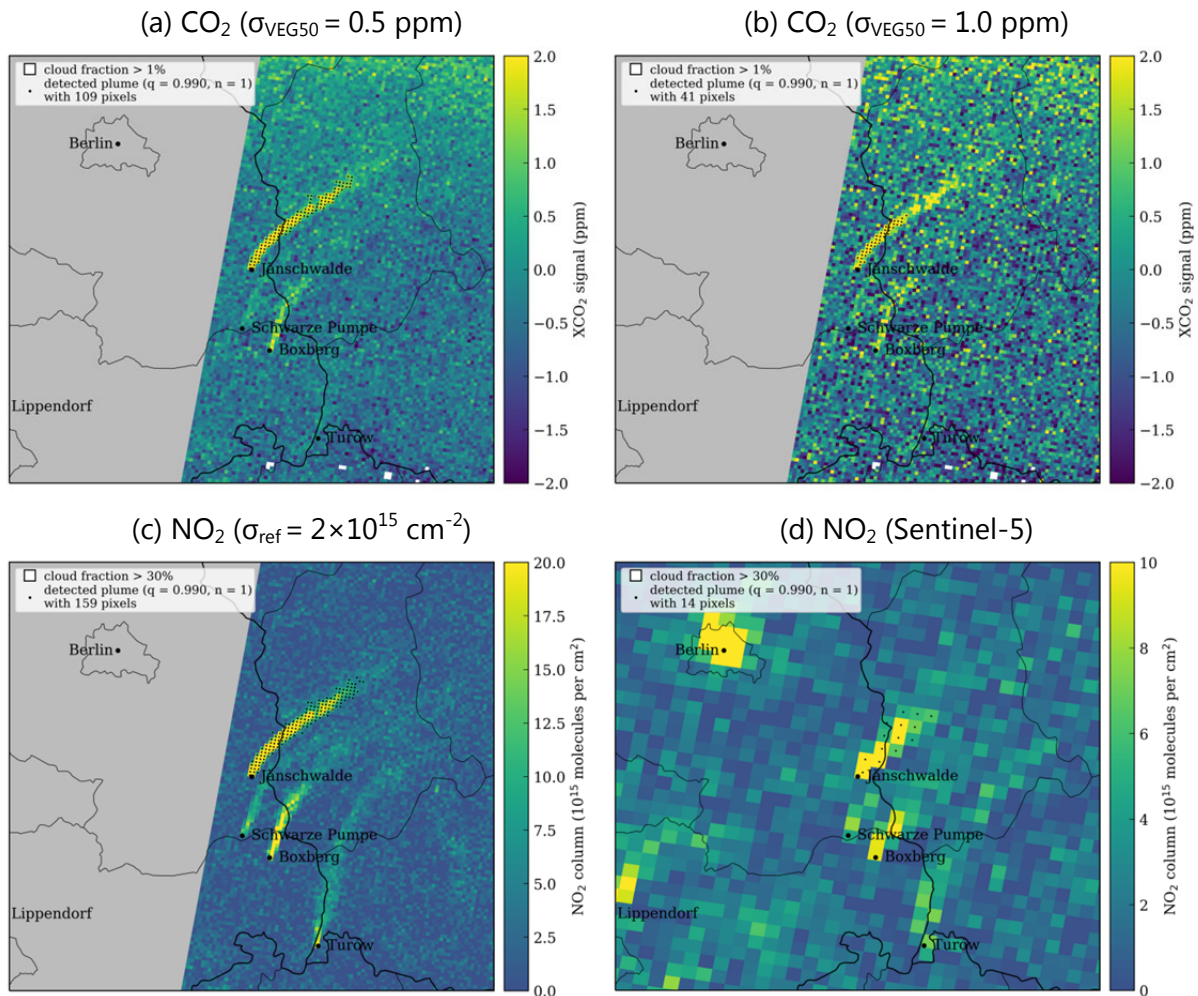


Figure 51: Example of plume detection for Jänschwalde power plant on 2 November 2015 using (a, b) the CO_2 instrument with σ_{VEG50} of 0.5 and 1.0 ppm, (c) the NO_2 instrument with the high noise scenario and (d) the NO_2 instrument on Sentinel-5.

As an example, Figure 51 shows the successful detection of the CO_2 plume of Jänschwalde on 2 November 2015 using different instruments. Since CO_2 emissions of Jänschwalde are high, the XCO_2 signal is very strong and can be detected well even with a high noise instrument (σ_{VEG50} of 1.0 ppm). With low noise (σ_{VEG50} of 0.5 ppm) the weaker plumes of Schwarze Pumpe and Boxberg are visible as well. The NO_2 instrument detects the four plumes in the region well. On this day also the Sentinel-5 NO_2 instrument successfully detects the plume of Jänschwalde and other point sources.

Figure 52 presents a second example for 17 February 2015. The CO₂ instrument successfully detects the plume with 0.5 ppm uncertainty, but with 1.0 ppm uncertainty, the number of detected pixels is likely too small to be useful for emission estimation. The NO₂ instrument detects the plume, but because the NO₂ plume of Jänschwalde overlaps with neighboring plumes, these plumes are erroneously assigned to Jänschwalde as well. At the coarser resolution of Sentinel-5 the plumes can hardly be separated and, moreover, the time difference of two hours results in a plume location that is shifted with respect to Sentinel-7.

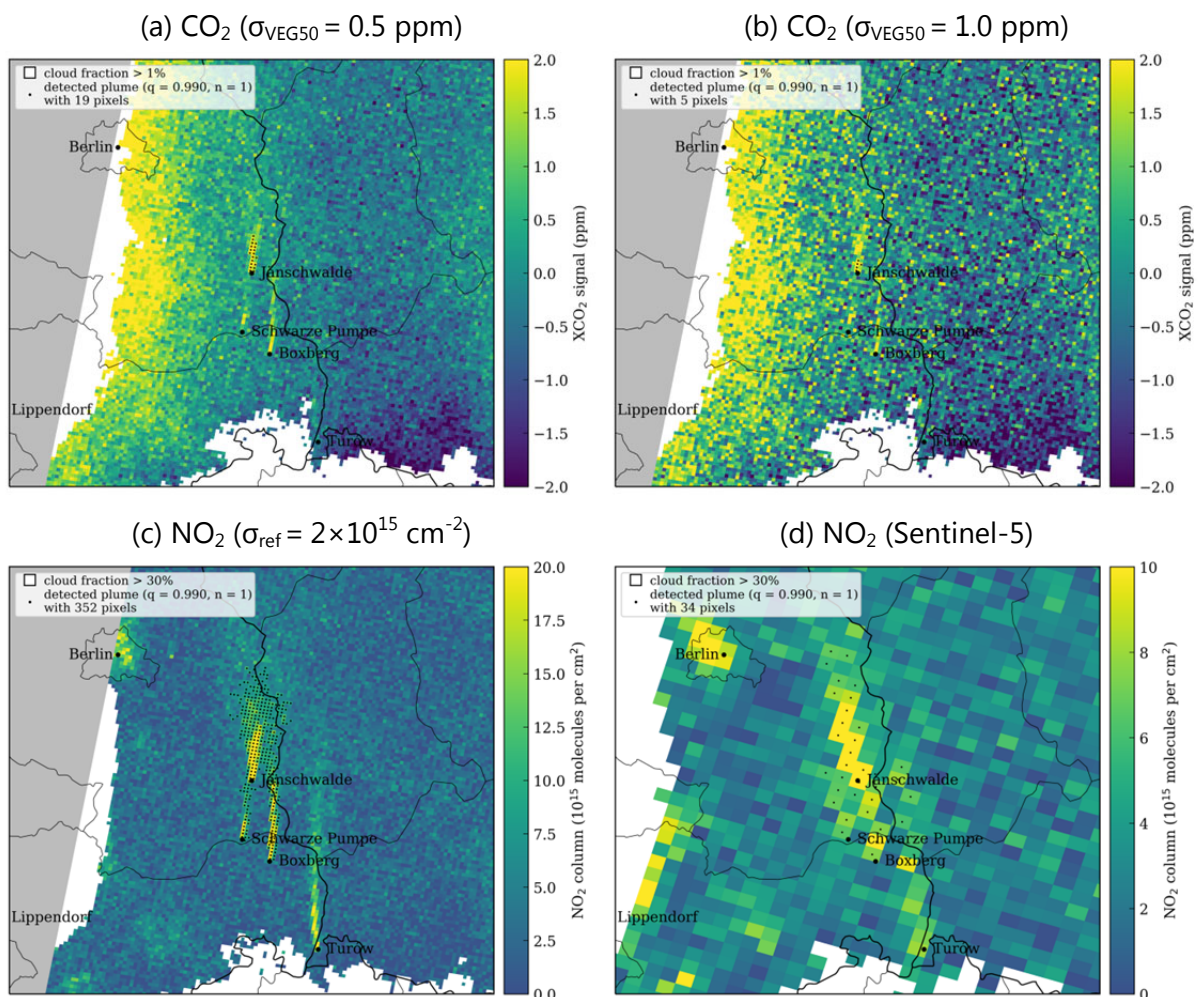





Figure 52: Example of plume detection for Jänschwalde power plant on 17 February 2015 using (a, b) the CO₂ instrument with σ_{VEG50} of 0.5 and 1.0 ppm, (c) the NO₂ instrument with the high noise scenario and (d) the NO₂ instrument on Sentinel-5.

Table 19 summarizes the results of the plume detection for Jänschwalde with different instrument scenarios and neighborhood sizes n_s . It shows the number of detected CO₂ plumes with at least 1 and 10 pixels. Note that in the case of the much narrower plumes from power plants, a comparatively low threshold for the number of detectable pixels is sufficient for the plume to be useful for emission estimation. A visual inspection was used to identify cases where the algorithm detected, in addition to the plume of Jänschwalde, parts of the

Final Report	ESA Project SMARTCARB Study on use of satellite measurements of auxiliary reactive trace gases for fossil fuel carbon dioxide emission estimation contract no 4000119599/16/NL/FF/mg	  Max Planck Institute for Biogeochemistry 
---------------------	---	---

background or other plumes (e.g. Figure 52b). We classified detections that include large parts of the background as failed, but counted plume detections that include neighboring plumes as successful detections, because they are, in principle, suitable for estimating emissions, although for simplicity they are not used for estimating CO₂ emissions in this study.

Table 19: Number of plumes detected for Jänschwalde with six satellites. The total number of detected plumes is provided for plumes with at least 1 and 10 detected CO₂ pixels (cloud cover <1%) and includes plumes where other plumes were detected in addition to Jänschwalde (“multiple plumes”). The number of multiple plumes is shown separately, as well. The median plume size is provided for plumes with at least one CO₂ pixel.

Instrument scenario	Number of detected plumes that include valid CO ₂ pixels (cloud cover < 1%)			Median plume size (≥1 pixels)
	Number of pixels ≥1	Number of pixels ≥10	Multiple plumes	
CO ₂ (σ = 0.5 ppm, n _s =1)	45	37	2	32
CO ₂ (σ = 0.5 ppm, n _s =5)	42	38	7	73
CO ₂ (σ = 0.7 ppm, n _s =1)	46	33	1	21
CO ₂ (σ = 0.7 ppm, n _s =5)	43	38	6	61
CO ₂ (σ = 1.0 ppm, n _s =1)	44	21	0	8
CO ₂ (σ = 1.0 ppm, n _s =5)	44	39	4	42
NO ₂ (low noise, n _s =1)	60	53	23	62
NO ₂ (low noise, n _s =5)	58	52	28	76
NO ₂ (high noise, n _s =1)	62	55	12	56
NO ₂ (high noise, n _s =5)	57	53	25	74

In the year 2015, the numbers of detectable plumes with more than 10 pixels for a constellation of six satellites are 37, 33 and 21 for a CO₂ instrument with σ_{VEG50} of 0.5, 0.7 and 1.0 ppm and neighborhood size n_s of 1. The NO₂ instrument detects 55 plumes for the high noise scenario with six satellites. For a smaller number of satellites, the number of detectable plumes would be correspondingly smaller. The NO₂ instrument detects more plumes because of its lower sensitivity to clouds, which makes it possible to trace the plume to the source even for partly cloudy scenes. More plumes can be detected with a neighborhood of 5 pixels, but the number of cases where multiple plumes are detected increases as well. In particular, the NO₂ instrument often detects nearby plumes (e.g. Boxberg and Schwarze Pumpe), because the instrument is much more sensitive to small signals than the CO₂ instrument. The median plume size is 8-73 and 56-74 pixels for CO₂ and NO₂, respectively.

As last example, the instrument can also detect weaker plumes like Lippendorf (12.8 Mt CO₂ / yr). Figure 53 shows a corresponding example.

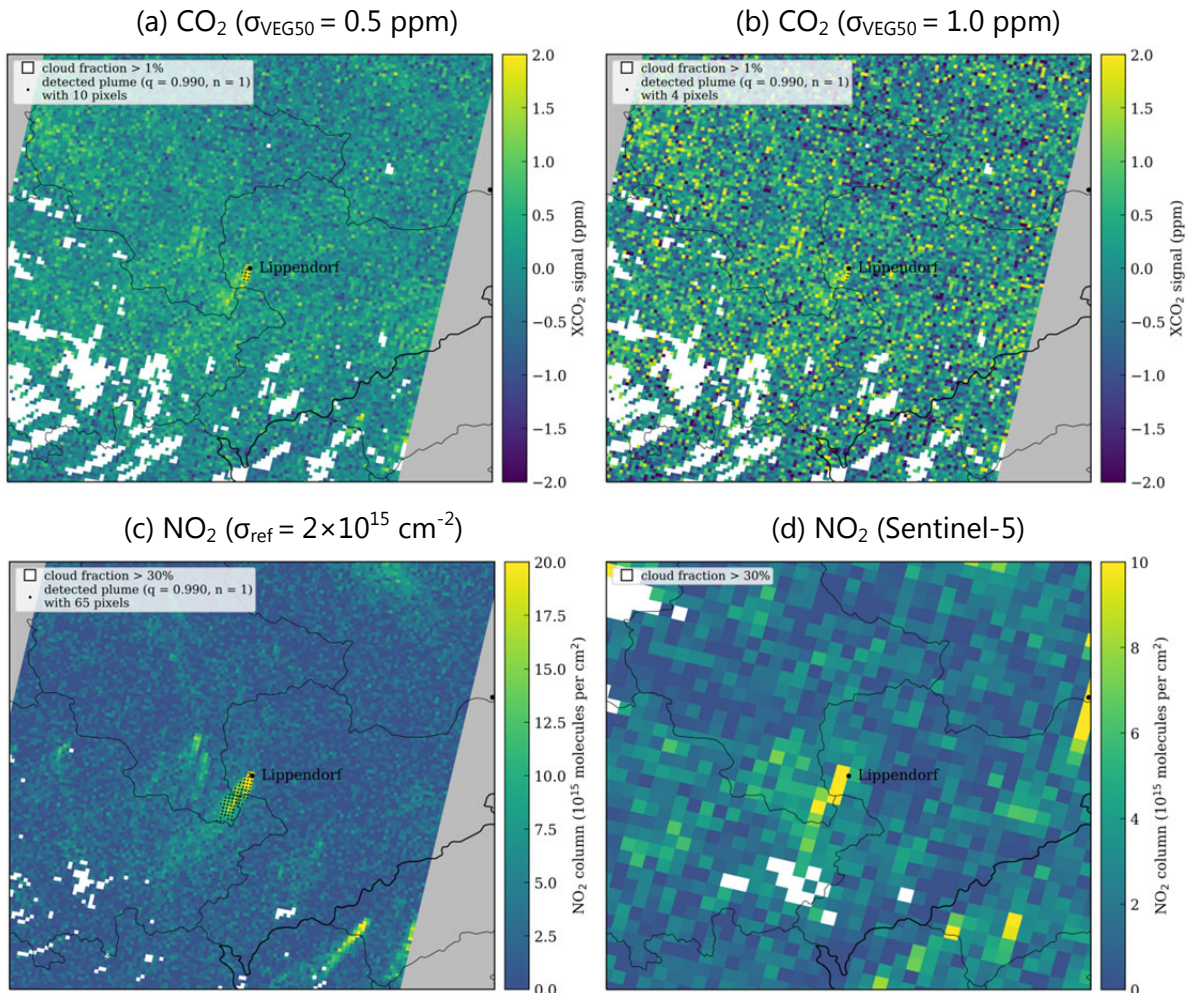


Figure 53: Example of plume detection for the power plant Lippendorf on 28 September 2015 using (a, b) the CO₂ instrument with σ_{VEG50} of 0.5 and 1.0 ppm, (c) the NO₂ instrument with the high noise scenario and (d) the NO₂ instrument on Sentinel-5.




5.4 Estimating the emissions of the city of Berlin

CO₂ emissions of Berlin are estimated in two alternative ways: (a) by an analytical inversion making use of the tracer information provided by the model and (b) by a mass balance approach using the plume detection algorithm and estimating the flux of CO₂ through control surfaces perpendicular to the main flow direction. Method (a) is similar to the methods applied e.g. in the LOGOFLUX project (RD-2, RD-3), whereas method (b) draws on ideas formulated in Krings et al. (2013) but required significant new developments.

5.4.1 Analytical inversion using tracer information provided by the model

Method

The analytical inversion uses Berlin's CO₂ signal simulated by the model, which provides perfect knowledge of the location of the plume. The method thus assumes a perfect

Final Report	ESA Project SMARTCARB Study on use of satellite measurements of auxiliary reactive trace gases for fossil fuel carbon dioxide emission estimation contract no 4000119599/16/NL/FF/mg	  
---------------------	---	---

transport model and allows isolating the uncertainties in the flux inversion due to instrument noise.

The inversion uses a simple forward model that computes the measurement vector \mathbf{y} of size m which contains all XCO_2 observations within the plume (i.e. $XCO_2_BV > 0.05$ and cloud fraction ≤ 0.01):

$$\mathbf{y} = \mathbf{H}\mathbf{x} + \mathbf{y}_{BG} \quad (4)$$

\mathbf{x} is the state vector, which in our case is a scalar x representing the CO_2 emissions of Berlin. \mathbf{H} is the observation operator representing the sensitivity of the XCO_2 signal to emissions x . It is easily obtained as the ratio between the XCO_2 tracer simulated with COSMO-GHG for the given source to the emissions x . \mathbf{y}_{BG} is the CO_2 background and a vector of size m (background varies within the plume). It is computed from the model simulated fields excluding the emissions from Berlin, consistent with the assumption of a perfect transport model (i.e. perfect knowledge of emissions, fluxes and boundary conditions).

The optimal state vector is found as maximum likelihood (ML) optimal estimate by minimizing the following cost function:

$$\chi^2(\mathbf{x}) = (\mathbf{y} - \mathbf{H}\mathbf{x} - \mathbf{y}_{BG})^T \mathbf{S}_\varepsilon^{-1} (\mathbf{y} - \mathbf{H}\mathbf{x} - \mathbf{y}_{BG}). \quad (5)$$

The uncertainty of the estimated CO_2 emissions is computed by error propagation as part of the algorithm. \mathbf{S}_ε is the error covariance matrix of the model-observation mismatch, which in our case of a perfect transport model corresponds to the measurement error covariance matrix. As a second measure of uncertainty, we compute mean biases (MB) and standard deviations (SD) of the differences between estimated and true emissions over all plumes considered. Thereby, the true emissions for each plume are taken as the average of CO_2 emissions at 10 and 11 UTC. The plume may also contain CO_2 emitted earlier in the day, but this information is not available from the model. Relative errors are computed relative to the annual mean at overpass (10-11 UTC) which is 16.9 Mt yr^{-1} for constant and 20.0 Mt yr^{-1} for time-varying emissions.

To estimate annual emissions and their uncertainties, the temporal variability of emissions has to be considered, for example, by applying correction factors for the diurnal, weekly and annual cycles of emissions. If the number of satellite observations is large enough, weekly and annual cycles can be estimated from the satellite data. The diurnal cycle, conversely, cannot be estimated from satellite observations with a fixed overpass time. For Berlin, CO_2 emissions at overpass are about 3.1 Mt yr^{-1} ($\sim 20\%$) larger than the annual mean.

In this study, we only estimate the skill of the inversion defined as the uncertainty of the mean of the estimates, which can be approximated by the root mean square deviation (RMSD):

$$RMSD = \sqrt{MB^2 + \frac{SD^2}{n}} \quad (6)$$

where n is the number of plumes. Please note that the RMSD is only an approximate measure, because we do not account for the (unknown) diurnal, weekly and seasonal cycle.

Results

The analytical inversion was applied to all CO₂ plumes of the Sentinel CO₂ satellites for constant and time-varying emissions (tracers XCO₂_BC and XCO₂_BV) and noise scenarios σ_{VEG50} of 0.5, 0.7 and 1.0 ppm. Figure 54 and Figure 55 show the time series of estimated CO₂ emissions for constant and time-varying emissions ($\sigma_{\text{VEG50}} = 0.7$ ppm) with a constellation of up to six satellites. Temporally varying emissions account for diurnal, day-of-week and monthly variations. CO₂ estimates with uncertainties larger than 8.4 Mt yr⁻¹ (50% of annual emissions) were removed. The boxplots (panel b) show the differences between estimated and true emissions. Detailed statistics are summarized in Table 20.

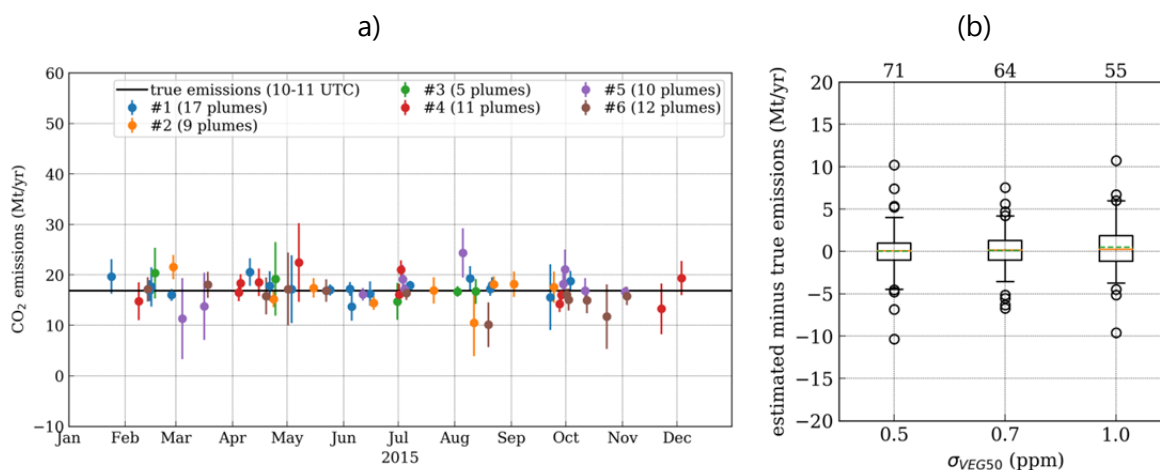


Figure 54: (a) Time series of estimated CO₂ emissions of Berlin using six satellites with σ_{VEG50} of 0.7 ppm. The emissions were constant. Emission estimates with uncertainties larger than 8.4 Mt yr⁻¹ (50% of annual emissions) were removed. (b) The boxplots show the difference between estimated and true CO₂ emissions of Berlin using six satellites for the different instrument noise scenarios. The boxes denote the range between 25th and 75th percentiles, orange lines are median values, the dashed lines are the mean values, and whiskers are 5th and 95th percentiles.

The constant emissions are generally well captured within the uncertainty range determined by the measurement noise. The uncertainties of the individual estimates vary strongly because the amplitudes and sizes of the plumes differ from case to case due to differences in wind speeds, cloud cover, and incomplete coverage of the plume by the swath. The median biases are zero whereas the mean biases are slightly positive.

In case of time-varying emissions, the seasonal cycle of the emissions can be reproduced quite accurately because many plumes can be observed with six satellites per season and because the individual estimates have an average uncertainty of only 17-22% depending on instrument noise scenario. The rare opportunities for plume detection in winter, however, can easily be missed by a small constellation of satellites, which will make it difficult to reliably trace the seasonal cycle. The median and mean biases slightly deviate from zero (Table 20). The mean bias has a weak seasonal cycle, because the observation operator \mathbf{H} was calculated from the tracer with constant emissions, which does not perfectly match the response of the XCO₂ signal to time-varying emissions. The mean bias is positive in October to April (+1.4 Mt yr⁻¹) when time-varying emissions are larger than the annual mean of emissions (16.9 Mt yr⁻¹)

and negative in May to September (-1.3 Mt yr^{-1}) when time-varying emissions are smaller than the annual mean.

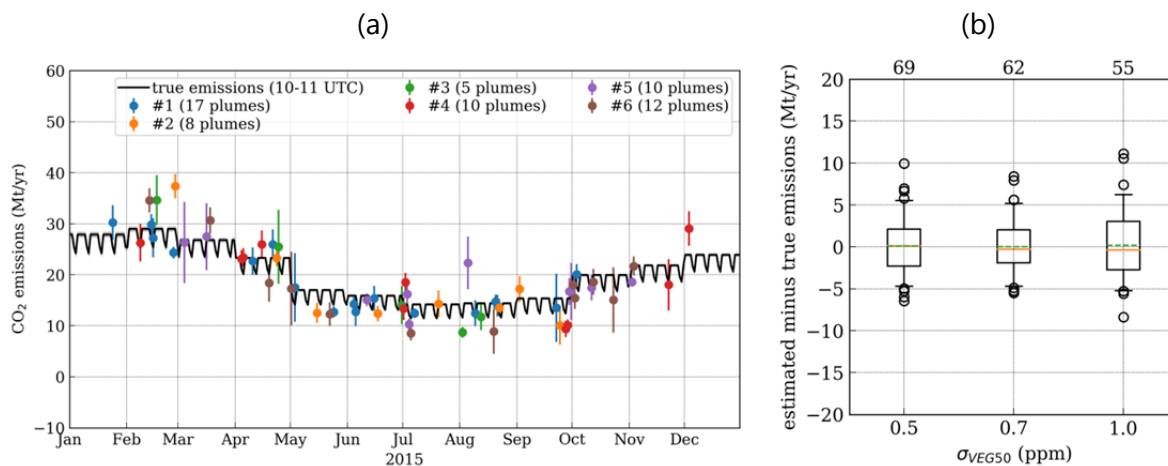


Figure 55: (a) Time series of estimated CO_2 emissions of Berlin using six satellites with σ_{VEG50} of 0.7 ppm. The emissions were time-varying. Emission estimates with estimated uncertainties larger than 8.4 Mt yr^{-1} (50% of annual emissions) have been removed. (b) The boxplots show the difference between estimated and true CO_2 emissions of Berlin using six satellites for the different instrument noise scenarios. The boxes denote the range between 25th and 75th percentiles, orange lines are median values, the dashed lines are the mean, and whiskers are 5th and 95th percentiles.

The number of plumes per satellite varies strongly due to one or two overpasses of the satellites per 11 day repeat cycle for the different orbits (see Section 0). The numbers slightly differ between constant and time-varying emissions due to different plume sizes defined by the XCO_2_{BV} and XCO_2_{BC} tracers. For time-varying emissions the number of useful plumes per satellite is 9 on average with σ_{VEG50} of 1.0 ppm but ranges from 4 to 15 for the different satellites. Useful plumes are defined here as plumes that resulted in CO_2 emission estimates with an uncertainty $< 8.4 \text{ Mt yr}^{-1}$ (50% of annual emissions). The number is similar to the results of the LOGOFLUX-2 study which estimated about 14 useful plumes for a satellite with a swath of 240 km where useful plumes were defined as plumes with $< 25\%$ CO_2 emission uncertainty, i.e. $< 11 \text{ Mt yr}^{-1}$ for annual emissions of 43 Mt yr^{-1} . The difference may be explained by the higher CO_2 emissions and thus higher CO_2 signal-to-noise ratios in the LOGOFLUX-2 study.

For time-varying emissions, the standard deviations (SD) of the differences between the individual emission estimates and the true emissions are 2.9, 2.6 and 3.2 Mt yr^{-1} for σ_{VEG50} of 0.5, 0.7 and 1.0 ppm, respectively (Table 20). These values agree well with the mean of the estimated uncertainties suggesting that the error propagation yields a realistic estimate of uncertainties. The number of plumes is larger for instruments with lower instrument noise, because emission estimates with uncertainties larger than 8.4 Mt yr^{-1} have been removed. As a result, the SD for σ_{VEG50} of 0.5 ppm is slightly larger than for 0.7 ppm, but for the same number of plumes would be smaller.




Final Report	ESA Project SMARTCARB Study on use of satellite measurements of auxiliary reactive trace gases for fossil fuel carbon dioxide emission estimation contract no 4000119599/16/NL/FF/mg	  Max Planck Institute for Biogeochemistry 
---------------------	---	--

Table 20: Mean bias, standard deviation and root mean square deviation of differences between estimated and true CO₂ emissions as well as mean of estimated uncertainties of Berlin based on observations with six satellites. Emission estimates with estimated uncertainties larger than 8.4 Mt yr⁻¹ (50% of annual emissions) have been removed.

Emissions	σ_{VEG50} (ppm)	Number of plumes	MB		SD		RMSD		Mean of est. uncertainty	
			Mt yr ⁻¹	%	Mt yr ⁻¹	%	Mt yr ⁻¹	%	Mt yr ⁻¹	%
1) Time-constant	0.5	71	0.0	0.1	2.9	17	0.3	2.0	2.6	16
	0.7	64	0.1	0.6	2.6	16	0.3	2.0	3.0	18
	1.0	55	0.5	2.9	3.2	19	0.7	3.9	3.4	20
2) Time-varying	0.5	69	0.1	0.6	3.3	17	0.4	2.1	2.6	13
	0.7	62	0.0	0.1	3.2	16	0.4	2.1	3.0	15
	1.0	55	0.2	0.9	4.1	20	0.6	2.9	3.5	18

The mean emissions can be estimated with a very low uncertainty with a RMSD of 0.3 to 0.7 Mt/yr (<2-4%) for the low and high CO₂ noise scenarios, respectively. This is a result of the large number of plumes (~60) observed by 6 satellites. For a smaller constellation of n_c satellites, the uncertainties would scale approximately with $\sqrt{6/n_c}$.

The uncertainty computed by the inversion framework can be used to estimate the minimum number of pixels required in a plume to estimate the emissions during a single overpass with a certain precision for a given instrument scenario. Figure 56 shows the CO₂ uncertainty for different plume sizes. Since uncertainties are assumed to be caused by random noise, the uncertainty should scale with the inverse square root of the number of pixels. The black line is the corresponding fit with 3σ uncertainty. Table 21 summarizes the resulting pixel numbers ($\pm 1\sigma$) for different levels of relative uncertainty. A CO₂ instrument with 0.7 ppm uncertainty, for example, requires at least 315 pixels to estimate CO₂ emissions with 25% precision.

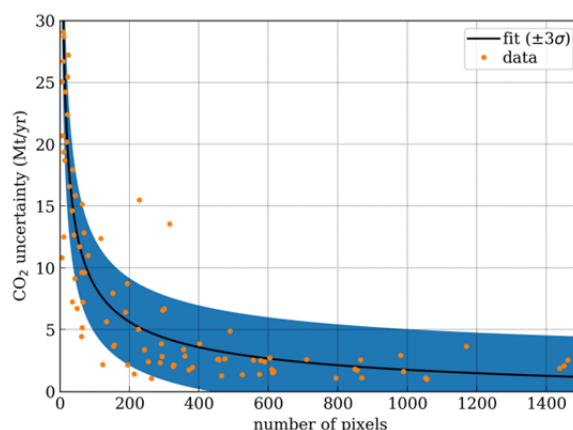


Figure 56: Estimated CO₂ uncertainties for 0.7 ppm (variable emissions) otherwise perfect model and fit assuming uncertainty is proportional to the inverse square root of the number of pixels.




Final Report	ESA Project SMARTCARB Study on use of satellite measurements of auxiliary reactive trace gases for fossil fuel carbon dioxide emission estimation contract no 4000119599/16/NL/FF/mg	  Max Planck Institute for Biogeochemistry 
---------------------	---	---

Table 21: Number of pixels ($\pm 1\sigma$) required for estimating Berlin's CO₂ emissions in a single overpass with an accuracy better than a given threshold in percentage of the annual mean emissions of 16.9 Mt/yr. The analysis is based on time-varying emissions. The estimated uncertainties only include the random noise of the instrument (single sounding precision) and assume a perfect transport model.

Required uncertainty	XCO ₂ single sounding precision		
	0.5 ppm	0.7 ppm	1.0 ppm
<10%	703 ⁺⁷¹¹ ₋₂₈₄	1044 ⁺¹⁴⁷⁶ ₋₄₇₆	1494 ⁺³⁰⁰⁹ ₋₇₅₇
<25%	186 ⁺⁷⁹ ₋₄₈	315 ⁺¹⁸² ₋₉₈	525 ⁺⁴²⁶ ₋₁₉₃
<50%	57 ⁺¹⁴ ₋₁₀	103 ⁺³³ ₋₂₂	186 ⁺⁷⁹ ₋₄₈
<100%	16 ⁺³ ₋₂	30 ⁺⁶ ₋₅	57 ⁺¹⁴ ₋₁₀

5.4.2 CO₂ emissions estimated by mass balance

In this section, a completely different approach is taken. The CO₂ emissions of Berlin are estimated from the plumes detected by the algorithm described in Section 5.3 and by calculating the fluxes through vertical control surfaces that intersect the plume. A similar method was used by Krings et al. (2013) for estimating CH₄ emissions from airborne measurements. The advantage of the method is that it does not require a dispersion model and thus helps to overcome modelling uncertainties. It only requires an estimate of the mean wind speed within the plume, which can be obtained, for example, from a numerical weather forecast model.

Method

The method computes CO₂ emissions from the total CO₂ mass flux through a vertical surface by integrating the XCO₂ field (converted from ppm to kg/m²) perpendicular to the direction of propagation of the plume:

$$M_p = \int_{y_{min}}^{y_{max}} c_p(x, y) dy \quad (8)$$

where c_p is the plume signal (in kg/m²). The quantity M_p has units of kg m⁻¹, i.e. mass of CO₂ within a slice of thickness of 1 m. Next, M_p is converted to a total mass flux using the wind speed u perpendicular to the control surface:

$$F_p = M_p u \quad (9)$$

To obtain the signal c_p , the plume needs to be identified using the plume detection algorithm described in Section 5.3 and the background needs to be subtracted from the XCO₂ observations. The background is estimated from the pixels surrounding the plume assuming that it is spatially smooth. First, the detected pixels of the plume as well as other pixels with z-values above the threshold are removed and the gaps are then filled using normalized convolution with a Gaussian filter with $\sigma = 10$ pixels. Since the signal c_p can have data gaps, e.g. due to clouds, gaps are filled with normalized convolution ($\sigma = 2$ pixels).

To obtain the location of the control surfaces, the center line of the plume is computed by fitting a 2D polynomial to the point cloud of detected pixels using z-values as weights. Figure 57 shows an example of a plume with detected plume pixels (dots) and center line (yellow). The control surfaces are then selected as cross-sections perpendicular to the center line every

2 km along the plume. Only a subset of cross-sections is shown in Figure 57 for clarity. For each cross-section, the flux is computed by integrating the XCO₂ signal above background along the cross-section and assuming a mean wind speed along the center line. The computed flux is only used if at least 50% of the pixels along the integral originate directly from measurements, i.e. are not obtained by gap filling. Figure 58 presents an example of CO₂ values along a cross-section.

For all cross-sections we use the same wind speed at overpass time calculated as the mean between 0 and 500 m above ground at the source origin taken from the COSMO-GHG simulations. Not taking the wind speeds directly at the locations of the cross-sections is an attempt to account for uncertainties in model-simulated winds that will be encountered with real rather than synthetic observations. Finally, the individual total fluxes F_p are averaged to obtain an estimate of the mean source strength. Since Berlin is an area source, we only consider values more than 15 km downstream of the city center such that the fluxes cover all emissions in the city area.

Uncertainties are estimated from XCO₂ uncertainties (σ_{VEG50} of 0.5, 0.7 and 1.0 ppm) and wind uncertainty ($\sigma_{\text{wind}} = 2$ m/s) (Sharp et al., 2015). The estimated uncertainties, however, do not include uncertainties from the estimated CO₂ background and model errors, which are difficult to determine and discussed separately in the following section. Model errors would be errors in the method described here. For example, wind direction might not be perpendicular to the center line, because the line is not estimated well. In that case the flux is not parallel to the wind direction.

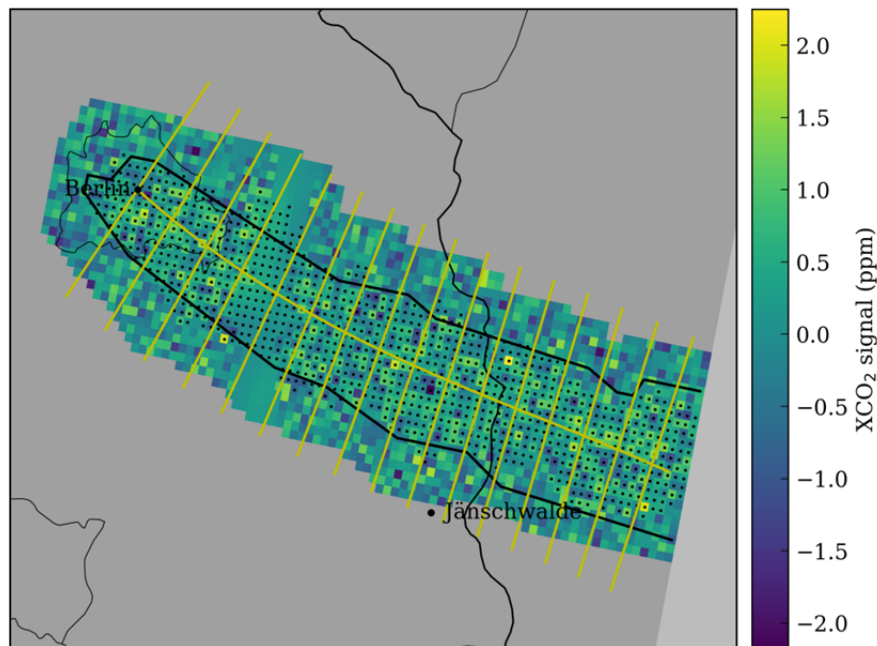


Figure 57: Example of plume with center line and slices (here every 10 km). The black dots are pixels within the plume detected by the detection algorithm using NO₂, while the black line is the true CO₂ plume. The yellow lines represent the center line and the cross sections of the plume. Values between 20 and 40 km downstream were obtained by spatial smoothing to bridge the gap caused by the presence of a narrow band of clouds.

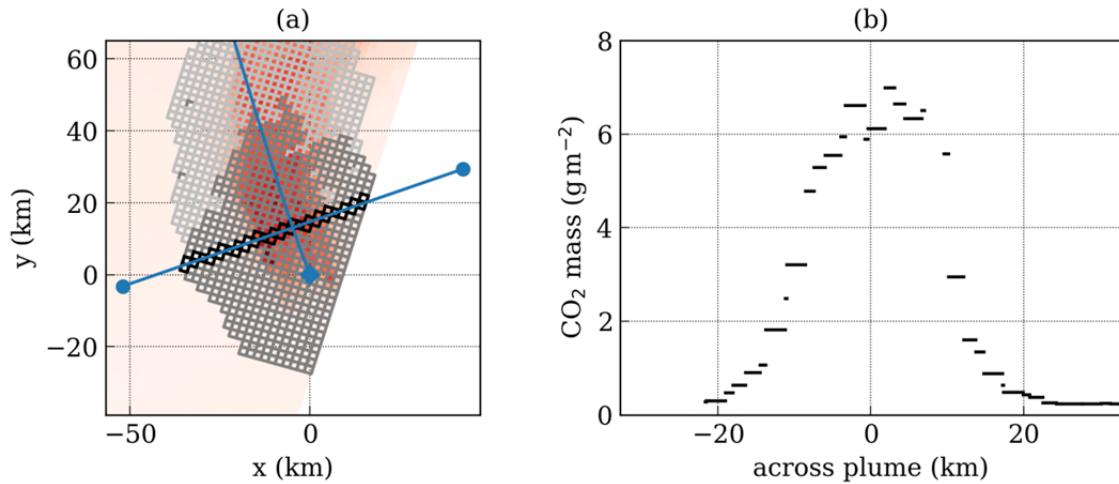


Figure 58: (a) Example of CO₂ plume of Berlin (red shading) with center line and cross section (blue) and with selected pixels along the cross section (black squares). Also shown are valid observation (dark gray) and observations missing due to clouds (light gray). (b) CO₂ mass along cross section (black pixels) for true CO₂ signals without noise. Uncertainties for single pixels have a standard deviation of about 10 g m⁻² for σ_{VEG50} of 0.7 ppm (not shown).

Results

The method was applied to synthetic CO₂ observations of the Sentinel CO₂ satellites using the uncertainty scenarios with σ_{VEG50} of 0.5, 0.7 and 1.0 ppm. The plume was detected either by the CO₂ instrument or the NO₂ instrument (high noise scenario; $\sigma_{\text{ref}} = 2 \times 10^{15} \text{ cm}^{-2}$).

CO₂ background and other sources of uncertainty

The CO₂ background has a strong impact on the estimated emissions. Figure 59 presents an example of estimated and true CO₂ background where the estimated field has only a small mean bias of -0.03 ppm and a standard deviation of 0.06 ppm. Figure 61 is a second example where the CO₂ field has a strong spatial gradient that results in a large mean bias of +0.13 ppm. Both plumes were detected with the NO₂ instrument. The bias of the estimated background results in an error in the integrated field M_p and, consequently in an error in the estimated emissions. The first example with a bias of -0.03 ppm results in CO₂ emissions that are overestimated by about 5.0 Mt yr⁻¹ (Figure 59). The large bias in the second example results in CO₂ emissions that are underestimated by about 25.4 Mt yr⁻¹, i.e. by more than 100% of the true emissions of Berlin.

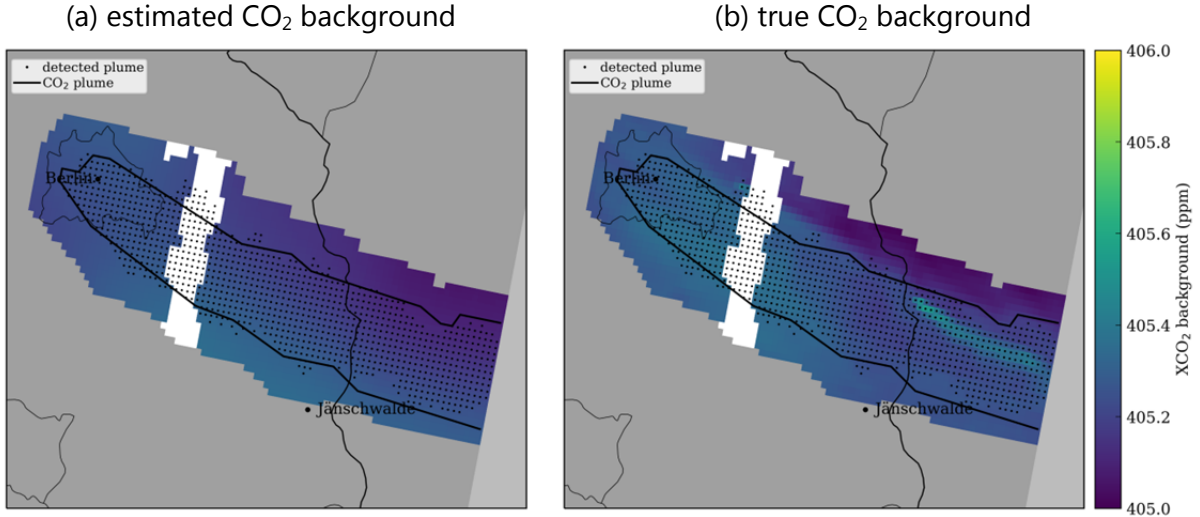


Figure 59: Estimated and true CO₂ background with mean bias of -0.03 ppm and standard deviation of 0.06 ppm of a Berlin plume (21 April 2015). Notable is the small plume in the true background. The plume was detected with the NO₂ instrument.

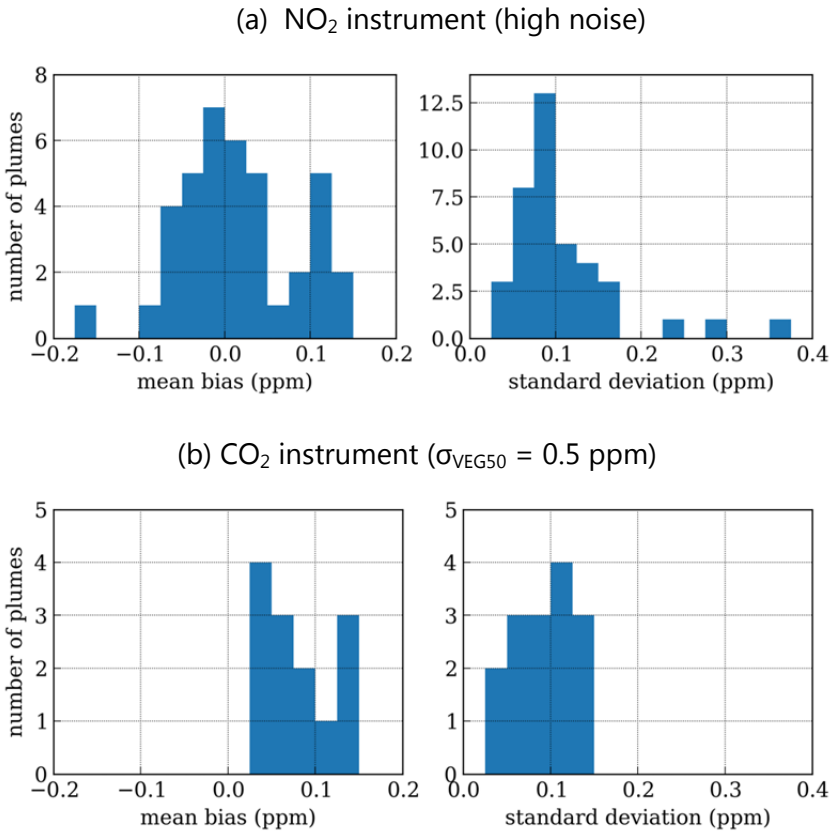


Figure 60: Histograms of mean bias and standard deviation of CO₂ background estimated from CO₂ observations with $\sigma_{VEG50} = 0.5$ ppm for all plumes detected in 2015 with a constellation of 6 satellites. (a) Plume detection by NO₂ instrument (high noise) and (b) by CO₂ instrument ($\sigma_{VEG50} = 0.5$ ppm). Only plumes with at least 100 pixels were used.

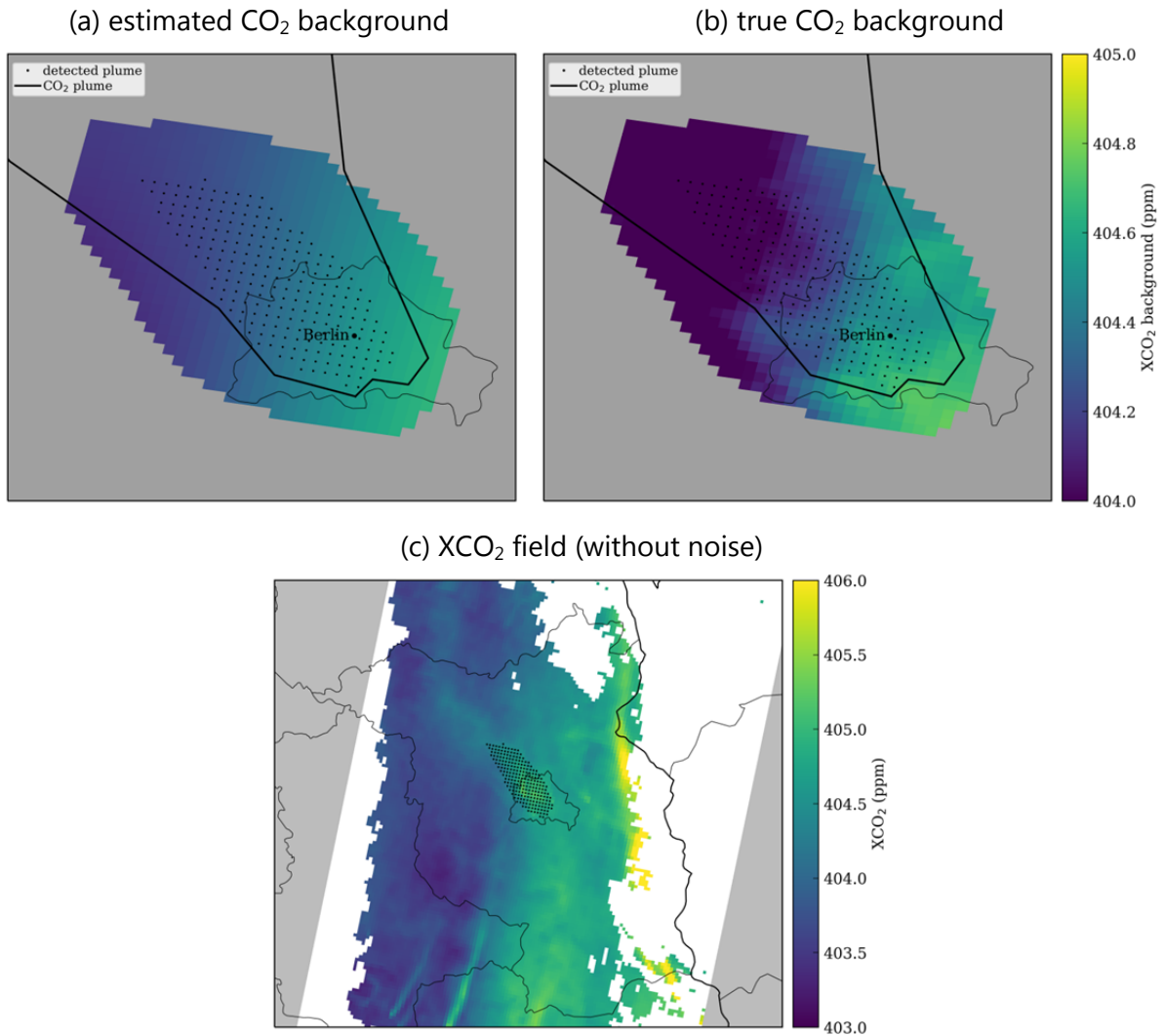


Figure 61: (a) Estimated and (b) true XCO₂ background on 27 February 2015. The true XCO₂ background has a strong gradient that is not correctly estimated by the algorithm resulting in a bias of 0.13 ppm and standard deviation of 0.15 ppm. In result, the XCO₂ values of the Berlin plume are underestimated resulting in a negative bias of 25.5 Mt yr⁻¹ in estimated CO₂ emissions. (c) Noise-free XCO₂ showing the strong spatial gradient.

Figure 60 presents histograms of mean bias and standard deviation between estimated and true XCO₂ background for all plumes detected in 2015 with a constellation of six satellites using either the NO₂ instrument or the CO₂ instrument with σ_{VEG50} of 0.5 ppm. CO₂ background fields estimated from the plumes detected by the NO₂ instrument have on average only a small positive bias of +0.02 ppm on a background of about 400 ppm. In contrast, the estimates based on the CO₂ instrument have a much larger positive bias of +0.11 ppm due to the fact that the plume detected by the CO₂ instrument only covers a fraction of the real plume. As a result, pixels with enhanced XCO₂, which are part of the real but not detected plume, are included in the estimation of the background. The estimated backgrounds have a similar mean standard deviation of about 0.10 and 0.11 ppm for CO₂ and

NO₂ based plume detection. The NO₂-based backgrounds have a few outliers that are caused by strong horizontal gradients in the CO₂ field. The CO₂-based plume detection fails to detect plumes in such challenging situations.

A second major source of error in the method is how well the center line is fitted to the detected pixels. If the center line is not parallel to the wind direction, the cross sections will not be perpendicular to the flow and consequently the path of the integral becomes longer and the source strength will be overestimated. The fitted center line depends on the number of pixels identified as part of the plume, which in turn depends on the performance of the plume detection algorithm for the different instrument scenarios. The error of these effects was estimated by computing the source strength using the noise-free XCO₂ tracer of Berlin. The estimate also includes errors from the assumption that emissions are constant. These errors were found to be mostly independent of NO₂- and CO₂-based plume detection with mean and standard deviation of about 3±8 Mt/yr. The reason might be that for larger plumes detected by the NO₂ instrument, the center line might be more accurate but other error sources, like time-varying winds and emissions and larger gaps in the CO₂ field, become more important within increasing distance from the origin of the source. In addition, the error is larger for plumes that are difficult to detect and these plumes can only be detected by the NO₂ instrument.

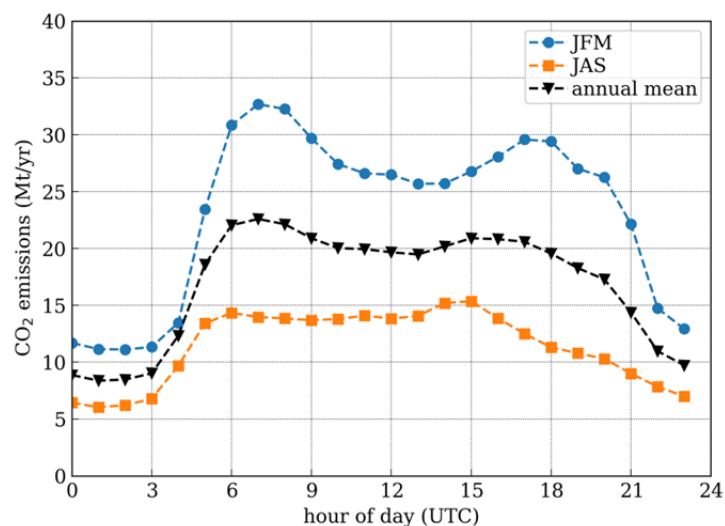


Figure 62: Diurnal cycle of Berlin's CO₂ emissions for winter (JFM: January, February and March) and summer (JAS: July, August and September).

The satellite overpass occurs around 11:30 local time (10:30 UTC at Berlin) but the CO₂ in the plume was emitted earlier depending on wind speed and distance from the source. Figure 62 shows the diurnal cycle of emissions for summer and winter as used in the simulations, which are different due to a different composition of sources. In winter, CO₂ emissions have a strong morning peak (around 7 UTC) at which emissions are 7 Mt yr⁻¹ higher than at 11 UTC. In summer, the morning peak is not as pronounced and emissions are nearly constant between 7 and 11 UTC. However, the differences in emissions are small compared to errors due to CO₂ background and model.

Estimated CO₂ emissions

Figure 63a and Figure 64a present the time series of estimated CO₂ emissions using a constellation of six satellites compared to the time series of true emissions (average of emissions at 10-11 UTC average). Emissions were only estimated for plumes with at least 100 detected pixels. The CO₂ instrument alone only detects about two plumes per satellite with at least 100 pixels resulting in 14, 10 and 6 plumes for a constellation of six satellites with σ_{VEG50} of 0.5, 0.7 and 1.0 ppm, respectively (Figure 63a). In contrast, when using the NO₂ instrument for plume detection, 7 ± 3 plumes are observed per satellite resulting in 39 plumes with six satellites (Figure 64a). The number of plumes detected per satellite varies strongly due to the differences between the orbits as mentioned earlier.

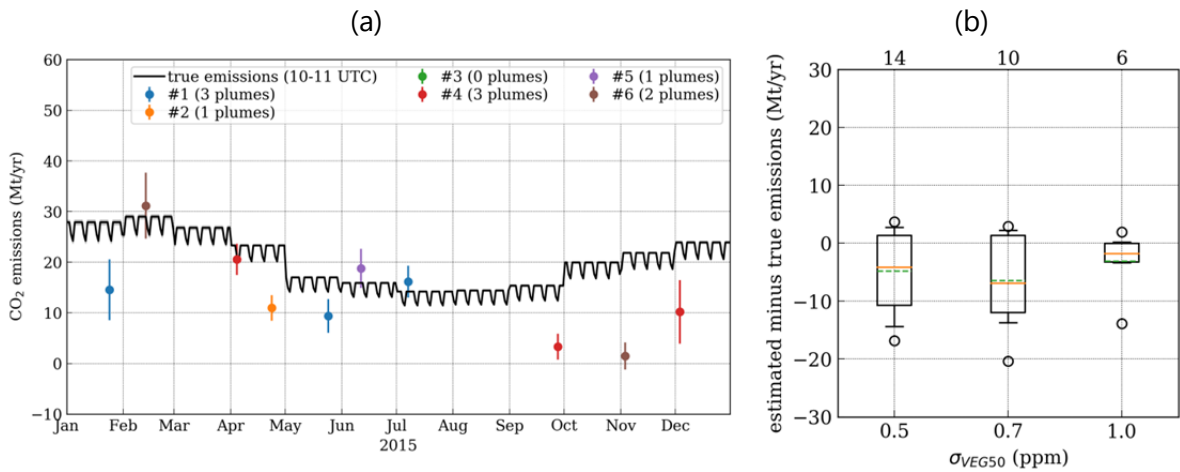


Figure 63: (a) Time series of estimated CO₂ emissions of Berlin using six satellites with σ_{VEG50} of 0.7 ppm. The emissions were time-varying. The plumes were detected by the CO₂ instrument and estimates from plumes with less than 100 pixels and negative emissions were removed. (b) The boxplots show the difference between estimated and true CO₂ emissions of Berlin. The boxes denote the range between 25th and 75th percentiles, orange lines are median values, and whiskers are 5th and 95th percentiles.

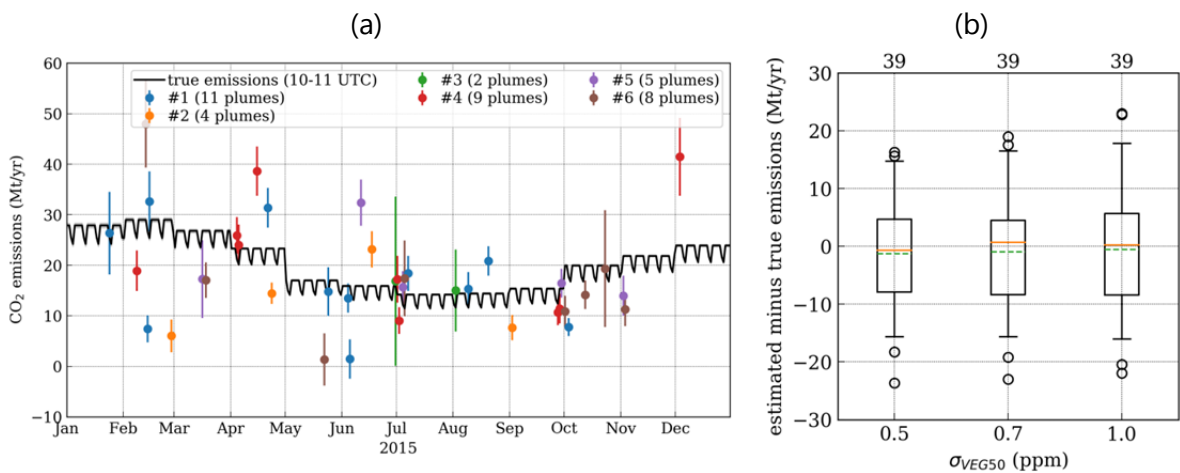


Figure 64: (a) Time series of estimated CO₂ emissions of Berlin using six satellites with σ_{VEG50} of 0.7 ppm. The emissions were time-varying. The plumes were detected by an NO₂ instrument (high noise) and estimates from plumes with less than 100 pixels and negative emissions were removed. (b) The boxplots show the difference between estimated and true CO₂ emissions of Berlin. The boxes denote the range between 25th and 75th percentiles, orange lines are median values, and whiskers are 5th and 95th percentiles.




Final Report	ESA Project SMARTCARB Study on use of satellite measurements of auxiliary reactive trace gases for fossil fuel carbon dioxide emission estimation contract no 4000119599/16/NL/FF/mg	  Max Planck Institute for Biogeochemistry 
---------------------	---	--

Table 22: Mean bias, standard deviation and root mean squared deviations of differences between estimated and true CO₂ emissions (10-11 UTC) as well as mean of estimated uncertainties of Berlin based on observations with six satellites and using all plumes with at least 100 detected pixels. The noise assumed for the NO₂ instrument σ_{ref} was $2 \times 10^{-15} \text{ cm}^{-2}$.




Plume detection	σ_{VEG50} (ppm)	Number of plumes	MB		SD		RMSD		Mean of est. uncertainty	
			Mt yr ⁻¹	%	Mt yr ⁻¹	%	Mt yr ⁻¹	%	Mt yr ⁻¹	%
CO ₂ -based	0.5	14	-4.8	-24	6.7	34	5.2	26	3.3	17
	0.7	10	-6.5	-32	7.6	38	6.9	35	4.0	20
	1.0	6	-3.1	-16	5.1	26	3.8	19	4.7	24
NO ₂ -based	0.5	39	-1.3	-6	9.2	46	1.9	10	3.8	19
	0.7	39	-1.0	-5	9.7	48	1.8	9	4.7	24
	1.0	39	-0.6	-3	10.7	53	1.8	9	6.3	32

Figure 63b and Figure 64b present the difference between estimated emissions and true emissions (average of emissions at 10 and 11 UTC) for all detected plumes and for different noise levels of the CO₂ instrument. Table 22 shows mean bias and standard deviation of the differences. These results, obtained directly from the (synthetic) observations, can be compared to those calculated in Section 5.4.1 using the perfect model tracer where instrument noise was the only source of uncertainty. The SD of the estimated emissions is about 9-11 Mt yr⁻¹, which is about three times larger than for the perfect model tracer. For the CO₂ only detection, the SD surprisingly increases when the noise level is reduced from 1.0 ppm to 0.7 ppm. With a lower noise instrument more plumes can be detected which, however, have a low signal-to-noise ratio and correspondingly large uncertainties. For the same reasons, a larger negative bias between estimated and true emissions is deduced for the two instruments with lower noise (up to -33%, Table 22). Biases are substantially reduced when using an NO₂ instrument for plume detection consistent with the analysis of biases in XCO₂ backgrounds presented in Figure 60.

The mean of the estimated uncertainty is about half of the SD, because not all error sources are considered. The mean emissions have a RMSD between 3.8 and 5.2 Mt yr⁻¹ when CO₂ is used for plume detection and 1.8 and 1.9 Mt yr⁻¹ when NO₂ is used instead. The better result for the NO₂ instrument is due to the smaller mean bias and the approximately three times larger number of plumes that could be detected and analyzed.

5.5 Estimating the emissions of power plants

CO₂ emissions of power plants are estimated by fitting a Gaussian plume model to the Level-2 observations. The method makes again use of the plumes detected by the plume detection algorithm but estimates the emissions in a different way as for Berlin. It is similar to the method described by Krings et al. (2013) but additionally allows the plume to follow a curved rather than a straight path.

<p>Final Report</p>	<p align="center">ESA Project SMARTCARB</p> <p align="center">Study on use of satellite measurements of auxiliary reactive trace gases for fossil fuel carbon dioxide emission estimation</p> <p align="center">contract no 4000119599/16/NL/FF/mg</p>	  
----------------------------	---	---

5.5.1 Gaussian plume model

Method

The Gaussian plume model describes the CO₂ columns (c in kg/m²) in x - and y -direction as:

$$c(x, y) = \frac{Q}{\sqrt{2\pi}\sigma(x)u} \exp\left(-\frac{(y-y_0)^2}{2\sigma^2(x)}\right) + c_{BG}(x, y) \quad (10)$$

with emission strength Q , horizontal wind speed u , CO₂ background c_{BG} , source location x_0, y_0 and

$$\sigma(x) = \sqrt{\frac{2K(x-x_0)}{u}} \quad (11)$$

where K is the eddy diffusion coefficient (in m²/s).

The x -direction is the downwind direction along the plume and described by the center line. The y -direction is the across-wind direction perpendicular to the center line. The x -coordinate is the arc-length of the center line of the plume. The center line was fitted to the pixels identified by the plume detection algorithm plus an additional boundary of one pixel. The pixels were weighted by the z -values. The location of the point source was added as an additional point with high weight to force the center line through the origin. The curve was fitted by two polynomials of degree 5 to account for a potentially meandering path.

Equation (10) calculates the CO₂ column at a point, while satellite observations are averaged over the pixel area (2×2 km²). Therefore, when the diameter of the plume is similar to or smaller than the size of the satellite pixels, it is necessary to average the Gaussian plume over each pixel. Since the calculation of the spatial average is computationally expensive, we approximately compute the average using a refined grid with 100 m resolution. The CO₂ background is estimated by applying normalized convolution using the same method as for the Berlin plume (Section 5.4.2).

Since the wind speed increases with height above ground, the plume height needs to be estimated. We use that the wind direction changes with height and match wind speed with direction of plume propagation (using the center line). If more than one plume height is found, we use the lowest height. If no plume height is found, for example, because the center line is not parallel to any wind direction, we use the mean value between stack height and 2 km.

The Gaussian plume model is fitted to the satellite observations by finding optimal values for emission strength Q and eddy diffusion coefficient K . The CO₂ background is subtracted before the fit. The optimal state vector is found as maximum likelihood (ML) optimal estimate. The uncertainties of the source strength are computed but only include the uncertainty of the CO₂ values.

Results

The method was used to estimate emissions of the power plant Jänschwalde. It was applied to synthetic Sentinel CO₂ observations using the uncertainty scenarios with σ_{VEG50} of 0.5, 0.7 and 1.0 ppm. The plume was detected either by the CO₂ instrument or the NO₂ instrument (high noise scenario; $\sigma_{\text{ref}} = 2 \times 10^{15}$ cm⁻²) using a neighborhood size of 1. The Gaussian plume

was only fitted to detected plumes with at least 10 cloud-free CO₂ pixels. Detected plumes with a large number of false detections were removed by visual inspection.

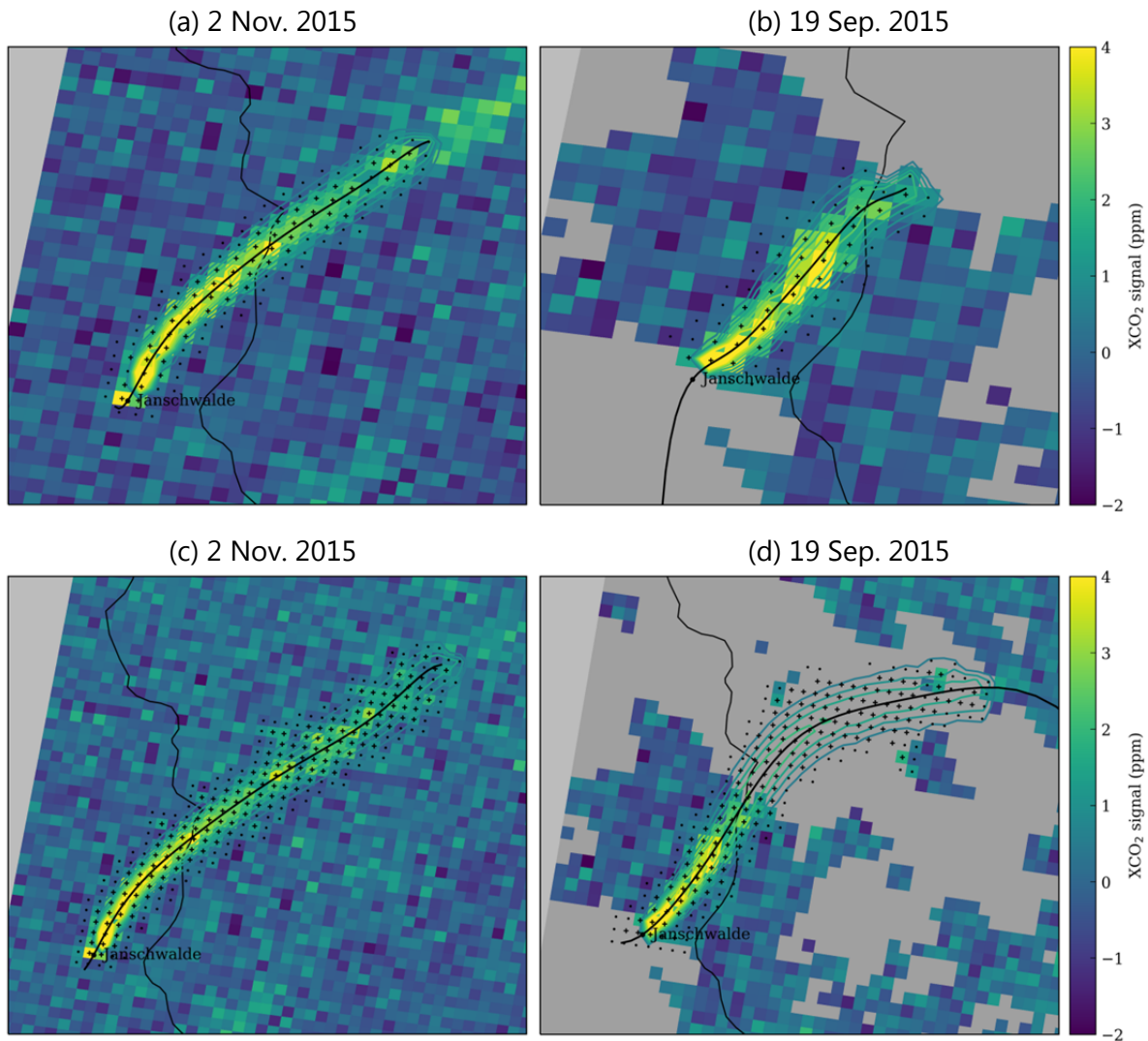


Figure 65: Examples of Gaussian plume fits to the CO₂ plumes originating from the power plant Jänschwalde on 2 November and 19 September 2015. (a, b) The plume was detected by the CO₂ instrument and (c, d) the NO₂ instrument. Plume paths were fitted with polynomials of degree 5. The detected pixels are shown as cross markers. The fitted Gaussian plume is shown by the contour lines. Note that the size of the canvas are different between the subplots.

Figure 65 presents two examples of CO₂ plumes. The plumes were detected using the CO₂ instrument (panels a and b) or the NO₂ instrument (panels c and d). The example of 2 November is an ideal case where the plume is easily detectable over a long distance by both the CO₂ and the NO₂ instrument. In the case of 19 September, thin clouds are covering both the origin of the source and the plume further downstream. In this case, the NO₂ instrument allows tracing the plume back to its origin and following the path of the plume over a longer distance, both enabling a better plume fit.

Figure 66a and Figure 67a present the time series of estimated CO₂ emissions using a constellation of six satellites compared to the time series of true emissions (10-11 UTC average). The CO₂ instrument detects between three and six plumes per satellite with at least 10 pixels resulting in 35, 32 and 21 plumes for a constellation of six satellites with σ_{VEG50} of 0.5, 0.7 and 1.0 ppm, respectively (Figure 66a). When using the NO₂ instrument for plume detection, about seven plumes are observed per satellite resulting in 42 plumes with six satellites (Figure 67b). The number of plumes detected per satellite varies strongly due to the differences between the orbits and random variations in cloud coverage.

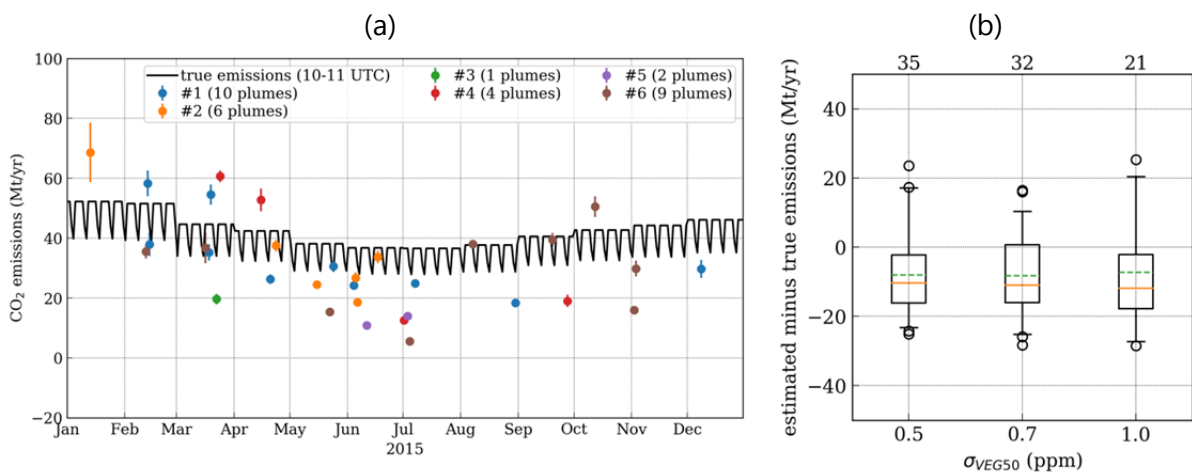


Figure 66: (a) Time series of estimated CO₂ emissions of Jänschwalde using six satellites with σ_{VEG50} of 0.7 ppm. The emissions were time-varying. The plumes were detected by the CO₂ instrument. Estimates from plume with less than 10 pixels and negative emissions have been removed from the time series. (b) The boxplots show the difference between estimated and true CO₂ emissions of Jänschwalde using six satellites. The boxes denote the range between 25th and 75th percentiles, orange lines are median values, the dashed lines are the mean, and whiskers are 5th and 95th percentiles.

Figure 66b and Figure 67b present the difference between estimated and true emissions (10 and 11 UTC average) as boxplots for all detected plumes and for different noise levels of the CO₂ instrument. Table 23 summarizes the mean bias and standard deviation of the differences. The emissions estimated from plumes detected by the CO₂ instrument have a large negative bias about -20% which is likely caused by an overestimation of the CO₂ background as already observed for Berlin (Section 5.4.2). Detecting the plumes with a NO₂ instrument significantly reduces the biases, again similar to the results obtained for Berlin.

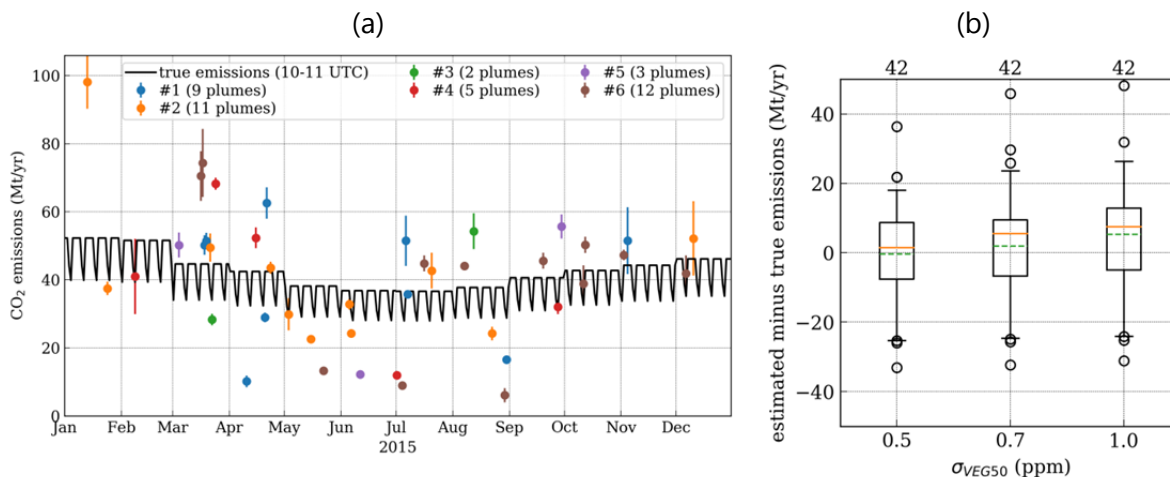





Figure 67: (a) Time series of estimated CO₂ emissions of Jänschwalde using six satellites with σ_{VEG50} of 0.7 ppm. The emissions were time-varying. The plumes were detected by the NO₂ instrument (high noise). Estimates from plume with less than 10 pixels and negative emissions have been removed from the time series. (b) The boxplots show the difference between estimated and true CO₂ emissions of Jänschwalde using six satellites. The box shows 25th, 50th and 75th percentile and the whiskers are 5th and 95th percentile.

Table 23: Mean bias, standard deviation and root mean square deviation of the differences between estimated and true CO₂ emissions (10-11 UTC) as well as mean of estimated uncertainties of Jänschwalde based on observations with six satellites and using all plumes with at least 10 pixels. Relative uncertainties refer to the mean of 10 UTC and 11 UTC emissions used in the simulations (~40 Mt/yr).

Plume detection	σ_{VEG50} (ppm)	Number of plumes	MB		SD		RMSD		Mean of est. uncertainty	
			Mt yr ⁻¹	%	Mt yr ⁻¹	%	Mt yr ⁻¹	%	Mt yr ⁻¹	%
CO ₂ -based	0.5	35	-8.0	-20	12.6	31	8.3	21	1.7	4.3
	0.7	32	-8.3	-21	12.2	30	8.6	21	2.3	5.6
	1.0	21	-7.3	-18	16.0	39	8.1	20	2.5	6.3
NO ₂ -based	0.5	42	-0.4	-1	14.7	38	2.3	6	2.5	6.4
	0.7	42	1.9	5	16.1	41	3.1	8	3.5	9.1
	1.0	42	5.3	14	18.9	49	6.1	16	5.2	13.4

The SD of the estimated emissions is 30-39% and 38-49% for plumes detected with either a CO₂ or a NO₂ instrument, respectively. The uncertainty of the mean emissions is 20-21% for plumes detected with the CO₂ instrument and 6-16% for plumes detected with the NO₂ instrument. The estimated uncertainty is much smaller than the SD, because it only includes the uncertainty of the CO₂ measurements.

The two major error sources that are not included are biases in the estimated XCO₂ background and uncertainties in the location of the plume, i.e. computation of the center line. Additional smaller uncertainties are expected through the assumption of constant wind speed and constant emissions.

<p>Final Report</p>	<p>ESA Project SMARTCARB</p> <p>Study on use of satellite measurements of auxiliary reactive trace gases for fossil fuel carbon dioxide emission estimation</p> <p>contract no 4000119599/16/NL/FF/mg</p>	  
----------------------------	--	---

6. Summary and recommendations




6.1 Summary

A detailed analysis was conducted to investigate the capability of a constellation of CO₂ satellites, i.e. the proposed Sentinel CO₂ mission, for quantifying the emissions of a large city (Berlin) and a power plant (Jänschwalde) with or without an additional NO₂ instrument. The results are based on unique, one year period (1 Jan. – 25 Dec. 2015) very high resolution (1 km x 1 km) atmospheric CO₂ simulations. These were generated with the model COSMO-GHG accounting for anthropogenic and biospheric fluxes as realistically as possible. Synthetic satellite observations (2 km x 2 km pixels, 250 km wide swath) were generated by sampling the XCO₂ model fields along the tracks of constellations of up to six satellites equally spaced in a common orbit and adding parameterized noise of three different magnitudes ($\sigma_{\text{VEG50}} = 0.5 \text{ ppm}$, 0.7 ppm and 1.0 ppm) corresponding to a low noise, medium noise and high noise instrument. Synthetic NO₂ data were generated in the same way for two noise levels ($\sigma_{\text{ref}} = 1 \times 10^{15} \text{ cm}^{-2}$ and $2 \times 10^{15} \text{ cm}^{-2}$) and additionally for a Sentinel-5 instrument with lower spatial resolution (8 km x 8 km pixels) but much wider swath and flying in an early morning orbit.

The CO₂ emissions of the city of Berlin and the power plant Jänschwalde were quantified by three different methods to assess the range of uncertainties associated with different assumptions. Emissions from Berlin were quantified (i) by scaling the simulated XCO₂ tracer representing only emissions from Berlin to match the synthetic XCO₂ observations minus simulated background, and (ii) by applying an image processing algorithm determining the extent of Berlin's emission plume directly from the noisy synthetic observations and estimating the flux of CO₂ through vertical control surfaces perpendicular to the direction of propagation of the plume. The first method assumes perfect knowledge of atmospheric transport and background XCO₂ levels. In this case, the uncertainty of the emission estimates is entirely driven by the ratio of instrument noise to the XCO₂ enhancements within the plume, which varies from case to case due to varying winds and cloud cover. The second method is a simple mass balance approach requiring minimal a priori knowledge. It only requires an estimate of the mean wind speed within the plume, which would typically be obtained from a numerical weather prediction model. Emissions from Jänschwalde, were quantified by matching a Gaussian plume model to the individual plumes detected by the image processing algorithm. Again, this required no prior knowledge except for an estimate of mean wind speed. The individual results as well as some limitations of the methods are summarized in the following.

6.1.1 Plume detection algorithm

The detection of Berlin's CO₂ plume was difficult in many cases. Cloud coverage only permitted the detection of the plume on one out of 5 to 6 satellite overpasses and even under cloud free conditions the plumes were often too weak to be easily detected by the CO₂ instrument. Plumes with more than 100 detectable pixels could only be seen in about 10% of cloud-free cases with a high-noise instrument ($\sigma_{\text{VEG50}} = 1.0 \text{ ppm}$) and about 26% with a low-noise instrument ($\sigma_{\text{VEG50}} = 0.5 \text{ ppm}$). With a perfect instrument, roughly 10 Berlin plumes

<p>Final Report</p>	<p>ESA Project SMARTCARB</p> <p>Study on use of satellite measurements of auxiliary reactive trace gases for fossil fuel carbon dioxide emission estimation</p> <p>contract no 4000119599/16/NL/FF/mg</p>	  
----------------------------	--	---

could be observed by a single satellite during one year. This number is consistent with the 14 cloud-free overpasses per year estimated in the LOGOFLUX study and the 13 (52 cloud-free overpasses with 4 satellites) reported in the Copernicus CO₂ Monitoring MRD (2018) since very small plumes with less than 100 pixels were excluded in our case.




The success rate of 26% for an imperfect but still precise instrument ($\sigma_{\text{VEG50}} = 0.5 \text{ ppm}$) would only allow for 2 to 3 favorable plume observations from Berlin per year and satellite. These numbers illustrate the challenge and call for a larger constellation or a wider swath to increase the opportunities for plume detection and emission quantification, and for a CO₂ instrument with as low noise as possible.

Adding an NO₂ instrument greatly enhanced the capability for detecting the CO₂ plumes (67%-71% of cloud-free cases), since the NO₂ plumes largely overlap with the CO₂ plumes and the signal-to-noise ratio is better for the NO₂ instrument compared to the CO₂ instrument. Therefore, the CO₂ plume can be better identified even in situations with variability in the background of CO₂ and the NO₂ measurements are less sensitive to cloud coverage. With an NO₂ instrument the number of detectable plumes per satellite was estimated to be 6 to 7 plumes from Berlin per year and satellite.

The Sentinel-5 NO₂ instrument is well suited to detect the NO₂ plume of Berlin. However, the different overpass times of the Sentinel CO₂ mission (11:30 local time) and Sentinel-5 (9:30 local time) frequently resulted in a significant spatial mismatch between the plumes which reduced the number of matching plumes to 39% of the cloud-free cases, thus only about half the rate of an NO₂ instrument on the Sentinel CO₂ satellite.

The detection of plumes from strong point sources like the power plant Jänschwalde was easier than the detection of city plumes, because point sources tend to have stronger and more confined CO₂ plumes for the same amount of emitted CO₂. In addition, the number of pixels required to map out such a plume was smaller, with only 10 detectable pixels being potentially sufficient for emission estimation. With a constellation of six satellites, about 30-40 plumes from Jänschwalde (23.6 Mt/yr emissions) with more than 10 detectable pixels could be observed per year even with a high-noise CO₂ instrument. This is two to three times more plumes than could be detected for Berlin (16.9 Mt yr⁻¹) with the best instrument. The number of detectable plumes from Jänschwalde further increased by about 50% with the addition of a NO₂ instrument (~55 plumes). Smaller point sources with emissions of about 10 Mt yr⁻¹ (e.g. Lippendorf, Schwarze Pumpe and Turow) were only detectable with a low-noise CO₂ instrument, but could also be detected with an NO₂ instrument.

The plume detection algorithm presented here worked well even with weak signals well below the single sounding precision, but tended to fail when the CO₂/NO₂ field was complex, for example when several plumes from adjacent sources overlapped or when the background had a spatial gradient. These cases can be easily identified by a trained human as done in this study, but will have to be automatized for application at the global scale, for example by applying machine learning methods that have been out of scope for the present study. The detection algorithm assumed knowledge of the mean and variance of the background which should be replaced with an estimate obtained directly from the satellite observations in a future study. Further development and improvement of the algorithm presented here has the

Final Report	ESA Project SMARTCARB Study on use of satellite measurements of auxiliary reactive trace gases for fossil fuel carbon dioxide emission estimation contract no 4000119599/16/NL/FF/mg	  Max Planck Institute for Biogeochemistry 
---------------------	---	---

potential for increasing the number of detectable plumes per satellite with the CO₂ and NO₂ instrument as well as the number of CO₂ pixels per plume. Consequently, the number of plumes useful for estimating CO₂ emissions (e.g. plumes with more than 100 pixels) would also increase.

6.1.2 Emissions from Berlin




The results of the individual emission estimates are summarized in Table 24 in the form of mean systematic uncertainties (mean bias) and random uncertainties (standard deviation) as well as the number of plumes that could be detected with a constellation of 6 satellites and an estimate of the uncertainty of the mean (root mean square deviation). Values are presented for the three different CO₂ instrument noise scenarios as well as for the cases, where the plumes were first detected by an NO₂ instrument before the CO₂ emissions were estimated. The systematic uncertainties are independent of the number of plumes, whereas the random uncertainty reduces by a factor \sqrt{n} for the mean of n detected plumes.

Table 24: Summary of results for estimating (time-varying) CO₂ emission of Berlin for a constellation of six satellites. The root mean square deviation (RMSD) is the uncertainty of the mean over all plumes computed as $RMSD = \sqrt{MB^2 + SD^2/n}$, with MB the mean bias, SD the standard deviation, and n the number of plumes. Relative uncertainties refer to the mean of 10 UTC and 11 UTC emissions of Berlin used in the simulations (~ 20.0 Mt yr⁻¹).

σ_{VEG50} (ppm)	Mean bias		Standard deviation		Root mean square deviation of mean		Number of plumes
	Mt yr ⁻¹	%	Mt yr ⁻¹	%	Mt yr ⁻¹	%	
Analytical inversion using tracer information provided by the model, time-varying emissions							
0.5	0.1	0.6	3.3	17	0.4	2.1	69
0.7	0.0	0.1	3.2	16	0.4	2.1	62
1.0	0.2	0.9	4.1	20	0.6	2.9	55
Mass balance approach using CO₂ for plume detection with $n_s = 37$ and $q = 0.99$							
0.5	-4.8	-24	6.7	34	5.2	26	14
0.7	-6.5	-32	7.6	38	6.9	35	10
1.0	-3.1	-16	5.1	26	3.8	19	6
Mass balance approach using NO₂ for plume detection with $n_s = 37$ and $q = 0.99$							
0.5	-1.3	-6	9.2	46	1.9	10	39
0.7	-1.0	-5	9.7	48	1.9	9	39
1.0	-0.6	-3	10.7	53	1.8	9	39

Emissions estimated from perfect model tracer

Emissions were estimated both for the case of constant and time-varying emissions from Berlin. For constant emissions, the estimates were essentially bias-free. With a total of about 60 plumes observed by a constellation of 6 satellites, the uncertainty (RMSD) of the mean emission estimate was of the order of 0.3 Mt yr⁻¹ for the low-noise ($\sigma_{VEG50} = 0.5$ ppm) and 0.7 Mt yr⁻¹ for the high-noise ($\sigma_{VEG50} = 1.0$ ppm) CO₂ instrument. This corresponds to a relative uncertainty of only 2.0% and 3.9% of the emissions of Berlin of 16.9 Mt yr⁻¹. For time-varying emissions, the standard deviations were similarly small but a small seasonal bias appeared,

<p>Final Report</p>	<p align="center">ESA Project SMARTCARB</p> <p align="center">Study on use of satellite measurements of auxiliary reactive trace gases for fossil fuel carbon dioxide emission estimation contract no 4000119599/16/NL/FF/mg</p>	  
----------------------------	---	---

because the sensitivity to emissions, which was deduced from the constant emissions tracer, did not perfectly represent the sensitivity of the XCO₂ signal at satellite overpass time to time-varying emissions. Our analysis did not estimate annual emissions in the case of time-varying emissions, because this would require incorporating information on the diurnal and day-to-day variation of the emissions.




Results obtained with the perfect model tracer can be compared to those of the CarbonSat support study LOGOFLUX-1 (RD-2), which estimated an annual mean uncertainty between 5 and 10 Mt CO₂ yr⁻¹ for the cities of Berlin and Paris for a single satellite with 1.0 ppm of noise. Our results indicate a similar but slightly smaller random uncertainty of 4.1 Mt yr⁻¹ for single overpasses for an instrument comparable to CarbonSat.

Emissions estimated from plume images by mass balance

The uncertainties in the individual emission estimates were much larger when the emissions were estimated directly from the plume images by analyzing the fluxes through control surfaces perpendicular to the main axis of the plume. The number of plumes useful for estimating CO₂ emissions in this way (i.e. with more than 100 detectable pixels) was reduced from about 53 to 6 and 14 per year for six satellites with an instrument with high ($\sigma_{\text{VEG50}} = 1$ ppm) and low noise ($\sigma_{\text{VEG50}} = 0.5$ ppm), respectively. This number could be significantly increased to 39 plumes per year with an additional NO₂ instrument for the detection of the location of the CO₂ plume. The uncertainties of estimated emissions for a single overpass were about 5 to 10 Mt yr⁻¹ (30%-60%). These absolute uncertainties are comparable to those obtained in the LOGOFLUX study for a perfect model tracer, but the relative uncertainties are much larger because the total emissions of Berlin assumed here were more than two times smaller than those assumed in LOGOFLUX.

The NO₂ instrument did not only enhance the potential for plume detection but also greatly helped to quantify the XCO₂ background. The reason for this is that the CO₂ instrument could only detect a reduced fraction of the real plume, so that the background, estimated from the values surrounding the plume, actually contained significant amounts of XCO₂ emitted from Berlin and falsely attributed this to the background. This resulted in an overestimation of background XCO₂ within the plume and a corresponding underestimation of Berlin's emissions by about 15-25%. The NO₂ instrument detected a much larger portion of the plume and therefore enabled an almost unbiased estimation of the background and of the emissions of the city (MB < 10%). Since the number of pixels detected by the NO₂ instrument is large, the level of noise of the CO₂ instrument had only a minor influence on the uncertainty of the estimated emissions when the NO₂ instrument was used for plume detection.

The Report for Mission Selection for CarbonSat (RD-7) formulated a requirement of 7 Mt yr⁻¹ uncertainty for single overpasses over a city. Our results indicate that this level of accuracy is within reach using a mass balance approach as presented here, but clearly requires an additional NO₂ instrument to enhance the plume detection capability and to limit the systematic biases in the emission estimates. Even with more sophisticated data assimilation methods using atmospheric transport models, NO₂ measurements with their favorable

Final Report	ESA Project SMARTCARB Study on use of satellite measurements of auxiliary reactive trace gases for fossil fuel carbon dioxide emission estimation contract no 4000119599/16/NL/FF/mg	  Max Planck Institute for Biogeochemistry 
---------------------	---	--

signal:noise ratios will be critical to assess the quality of the transport simulations and to guide the assimilation process.

Besides measurement uncertainty, the major sources of uncertainty of the mass balance method were the estimation of the background XCO₂ field and uncertainties in the mean wind speed and direction of propagation of the plume. To take full advantage of the detected plumes, algorithms need to be developed that either improve the mass balance calculation for these plumes or flag failed inversions based on objective and independent criteria.




6.1.3 Emissions from power plants

Emissions from power plants were estimated using a mass balance method based on fitting a Gaussian plume model to those detected with the plume detection algorithm. The path of each plume was fitted with a 2D polynomial function. Estimates of the emission rate and of the horizontal dispersion were then obtained from the fit of the Gaussian plume to the observed plume. A mean wind speed within the plume had to be estimated which was deduced from the COSMO model by comparing the wind directions at different altitudes to the direction of plume propagation at the location of the power plant. About 30-40 plumes could be observed per year with 6 satellites for the power plant Jänschwalde (23.6 Mt yr⁻¹). The NO₂ instrument increased this number to about 55 plumes. Not all of these plumes could be used for emission estimation due to overlaps with plumes from neighboring power plants.

Table 25: Summary of results for estimating CO₂ emission of the power plant Jänschwalde for a constellation of six satellites. The root mean square deviation (RMSD) is the uncertainty of the mean over all plumes computed as $RMSD = \sqrt{MB^2 + SD^2/n}$, with *MB* the mean bias, *SD* the standard deviation, and *n* the number of plumes. Relative uncertainties refer to the mean of 10 UTC and 11 UTC emissions used in the simulations (~40 Mt yr⁻¹).

σ_{VEG50} (ppm)	Mean bias		Standard deviation		Root mean square deviation of mean		Number of plumes
	Mt yr ⁻¹	%	Mt yr ⁻¹	%	Mt yr ⁻¹	%	
CO₂ -based plume detection							
0.5	-8.0	-20	12.6	31	8.3	21	35
0.7	-8.3	-21	12.2	30	8.6	21	32
1.0	-7.3	-18	16.0	39	8.1	20	21
NO₂-based plume detection							
0.5	-0.4	-1	14.7	38	2.3	6	42
0.7	1.9	5	16.1	41	3.1	8	42
1.0	5.3	14	18.9	49	6.1	16	42

The uncertainties of the emissions estimated from single overpasses were rather large, about 10-20 Mt yr⁻¹ (30-50%) for Jänschwalde. This number is significantly larger than the requirement of 4 Mt yr⁻¹ formulated in the CarbonSat Report for Mission Selection (RD-7). The poor performance appears to be related to the problem of fitting a Gaussian plume to real plumes that often did not have a Gaussian shape. Further attempts using the same

<p>Final Report</p>	<p>ESA Project SMARTCARB</p> <p>Study on use of satellite measurements of auxiliary reactive trace gases for fossil fuel carbon dioxide emission estimation</p> <p>contract no 4000119599/16/NL/FF/mg</p>	  
----------------------------	--	---

methodology as for Berlin should be made to better constrain the uncertainties. Similar to the results for Berlin, the NO₂ instrument allowed to greatly reduce the systematic biases by allowing a better estimation of XCO₂ background levels within the plumes.

6.2 Recommendations

6.2.1 Recommendations on the usage of NO₂ and CO observations

Based on the results described in this report, we draw the following conclusions regarding the utility of an additional NO₂ and CO instrument:

- **An additional NO₂ instrument on the same platform as the CO₂ instrument is highly recommended**

The NO₂ instrument will be able to image the plumes of cities and power plants with a higher signal-to-noise ratio (SNR) as compared to the CO₂ instrument. Furthermore, NO₂ plumes stand out more clearly from the background due to the short lifetime of NO₂ and the correspondingly low background levels. An NO₂ instrument would therefore significantly increase the number of detectable CO₂ plumes and thus the number of cases available for source estimation. Since the NO₂ instrument will detect a larger proportion of the CO₂ plume, the NO₂ instrument will also enable a more accurate, unbiased estimation of the CO₂ background surrounding the plume. This is critical since systematic biases in the background directly translate into systematic biases in the emission estimates. The NO₂ instrument scenario with high noise ($\sigma_{\text{ref}} = 2 \times 10^{15}$ molecules cm⁻²) and a pixel size of 2×2 km² was found sufficient for these applications.




Because the shape and extent of the plume can be imaged more accurately, the NO₂ instrument could also be useful to assess the quality of atmospheric transport simulations and eventually improve these simulations through data assimilation.

- **The benefit of an additional CO instrument of the performance assumed in this study would be small**

For the city and power plant plumes studied in SMARTCARB, the SNR of the assumed CO instrument was significantly smaller than the SNR of the NO₂ instrument and even smaller than that of the CO₂ instrument. Furthermore, variations in background CO are larger and thus more problematic as in the case of NO₂ due to the longer lifetime of CO. Such a CO instrument would add little useful information to the detection of individual plumes. This doesn't preclude its suitability to characterize local enhancements averaged over long time periods, but this was not analysed as part of this study. Furthermore, a CO instrument could potentially be beneficial in less developed countries where CO:CO₂ emission ratios tend to be higher due to less well-controlled combustion processes.

- **An NO₂ instrument on the upcoming Sentinel-5 would not have the same benefits as an NO₂ instrument on Sentinel-7**

The assumed difference of 2 hours between the overpass times of Sentinel-5 (9:30

<p>Final Report</p>	<p>ESA Project SMARTCARB</p> <p>Study on use of satellite measurements of auxiliary reactive trace gases for fossil fuel carbon dioxide emission estimation</p> <p>contract no 4000119599/16/NL/FF/mg</p>	  
----------------------------	--	---

local time) and the Sentinel CO₂ satellites (11:30 local time) often resulted in a significant spatial mismatch of the plumes. Furthermore, the coarser resolution of Sentinel-5 will make it more difficult to detect the boundaries of a plume and will lead to larger overlaps between plumes of neighbouring sources.

- A CO instrument on the upcoming Sentinel-5 could add valuable information**

Because of the comparatively high noise of the CO instrument, operating a high-resolution imaging CO instrument on the Sentinel CO₂ satellite will have little benefits. Averaging CO measurements over longer periods, however, could provide very useful information, on the type of source and efficiency of the combustion (different CO:CO₂ and NO₂:CO₂ ratios). Such information could be readily obtained from Sentinel-5 with its better global coverage.




6.2.2 Recommendations on instrument precision and coverage

The Report for Mission Selection for CarbonSat (RD-7) formulated a requirement of 7 Mt yr⁻¹ uncertainty for single overpasses over a city with more than 35 Mt CO₂ yr⁻¹, and a requirement of 4 Mt yr⁻¹ uncertainty for a point source with more than 20 Mt CO₂ yr⁻¹. Since even large cities such as Berlin emit much less than 35 Mt and since only a small fraction of power plants worldwide emit more than 20 Mt, we propose to revise these requirements to be relevant for sources of a smaller magnitude, i.e., for cities with more than 15 Mt CO₂ yr⁻¹ and for power plants with more than 10 Mt CO₂ yr⁻¹.

Annual mean emissions of Berlin are about 16.9 Mt yr⁻¹. Since emissions are higher during daytime than during nighttime, the emissions at satellite overpass time (11:30 local time) are somewhat higher, about 20 Mt yr⁻¹. For this magnitude of emissions the requirement of an uncertainty of 7 Mt yr⁻¹ for single overpasses was met under the assumption of a perfect model (3.3 to 4.1 Mt yr⁻¹). When using a mass balance approach applied to plumes detected with the NO₂ instrument, the requirement was almost met (~10 Mt yr⁻¹), irrespective of the uncertainty scenario used for the CO₂ instrument (σ_{VEG50} of 0.5, 0.7 and 1.0 ppm). Since the number of pixels was high when plumes were detected with the NO₂ instrument, the emission estimate did not depend strongly on the precision of the CO₂ instrument. Besides instrument noise, the major sources of uncertainty of the mass balance method were the estimation of the background XCO₂ field and uncertainties in the mean speed and direction of propagation of the plume.

For the power plant Jänschwalde, the uncertainties of the estimated emissions were rather high (10–20 Mt yr⁻¹), because the meandering plumes could often not be described well by a Gaussian plume. A mass-balance approach similar to the one applied to the city plumes might have yielded better results, but was not explored in the framework of this study. Since the number of pixels in power plant plumes is smaller compared to city plumes, the uncertainty was found to depend more strongly on the instrument precision.

An important goal of the satellite mission will be to quantify emissions at the annual time scale and to trace the evolution over multiple years, notably over the 5 year intervals of the Global Stocktake under the Paris Agreement. The uncertainty of an annual average will not only depend on the uncertainties of the individual plume estimates but also on the number

<p>Final Report</p>	<p>ESA Project SMARTCARB</p> <p>Study on use of satellite measurements of auxiliary reactive trace gases for fossil fuel carbon dioxide emission estimation</p> <p>contract no 4000119599/16/NL/FF/mg</p>	  
----------------------------	--	---




of successfully observed plumes per year. For a single satellite with a 250 km swath and medium noise ($\sigma_{\text{VEG50}} = 0.7$ ppm), the number of useful plumes per year was 10.3 (range: 5-17) when the location of the plume was assumed to be perfectly known, 1.6 (range: 0-3) when the plume was detected by a CO₂ instrument (medium noise scenario) and 6.5 (range: 2-11) when the plume was detected with an auxiliary NO₂ instrument (high noise scenario). In this study, power plant plumes could be detected even with an NO₂ instrument with high noise. The power plants were equipped with wet scrubber technology for reducing SO₂ and NO_x emissions but not with the latest available technology. Future updates using selective catalytic or non-catalytic reduction have the potential to further reduce NO_x emissions by up to a factor 2, which would place higher requirements on the NO₂ instrument and would make the low noise scenario more beneficial.

In the optimal case of no temporal variability of the emissions, these plumes would result in relative uncertainties of 7% of the annual mean emissions of Berlin of 16.9 Mt yr⁻¹ under the assumption of a perfect model and 47% and 23% with the mass-balance approach using CO₂ or NO₂ for plume detection, respectively. To reduce this uncertainty to a value below 10% (formulated as a requirement for CarbonSat for cities with >35 Mt yr⁻¹), a single satellite would be sufficient only under the assumption of a perfect model. With an NO₂ instrument for plume detection and the mass-balance approach, which does not rely on the highly optimistic assumption of perfect knowledge of transport, at least two satellites with single overpass uncertainties of 7 Mt yr⁻¹ (requirement for CarbonSat) would be needed to reduce the uncertainty below 10%. Without an NO₂ instrument for plume detection, not even six satellites would be sufficient

The annual estimate additionally depends on how well the temporal variability of the source at the diurnal, day-to-day (including weekends versus weekdays) and seasonal time scale is sampled, or on how well this information can be obtained by other means. Satellites with a fixed overpass time cannot resolve the diurnal variability as they are primarily sensitive to the emissions of a few hours prior to the overpass. However, the satellite observations have the potential to sample the day-to-day and seasonal variability. A single satellite will on average only observe 1.3 plumes (range: 0-3) in winter (December to February), which is insufficient to reliably characterize the seasonal cycle, and it will only sample 2.2 weekend days (range: 0-6) during the year, which is again insufficient to characterize the contrasts between weekday and weekend emissions.

To sample the day-to-day variability and the seasonal cycle, the temporal coverage needs to be increased either with a constellation of three or more satellites or by increasing the swath width of the individual satellites. A wider swath could be obtained at the price of a poorer single sounding precision.

Our study suggests that CO₂ emission estimates depend less on the precision of the CO₂ instrument for large plumes, e.g. a city plume, when an NO₂ instrument is used for detecting the location of the plume and estimating the CO₂ background. For these cases, a wider swath and somewhat worse CO₂ single sounding precision might be a reasonable trade-off. For smaller plumes e.g. from power plants, a high precision of the CO₂ instrument is more relevant because of the small number of pixels contained in the

<p>Final Report</p>	<p>ESA Project SMARTCARB</p> <p>Study on use of satellite measurements of auxiliary reactive trace gases for fossil fuel carbon dioxide emission estimation</p> <p>contract no 4000119599/16/NL/FF/mg</p>	  
----------------------------	--	---

plume. Also in terms of NO₂ a high precision instrument is preferred considering that the next generation removal technology will likely further reduce NO_x emissions from power plants.

6.2.3 Recommendations for follow-up studies

The SMARTCARB study created a large dataset of high-resolution simulations and synthetic satellite observations that can be used in follow-up studies to address topics that were outside the scope of our study.

Recommendations for follow-up studies building on SMARTCARB:

- **Monte Carlo experiments to better constrain the number of observable plumes with different constellations**




The number of observable plumes per satellite depends strongly on the equator starting longitude of the first orbit, as this determines whether a source is visited only once or twice during an 11-day repeat cycle of the satellite and whether the source is located near the centre or the edge of the swath. To compute robust statistics of the probability of plume observations with a given satellite constellation, a Monte Carlo experiment with variable starting longitudes of the first satellite of the constellation would be needed.

- **Development of more advanced and robust plume detection algorithms**

The plume detection algorithm developed for SMARTCARB worked well even with weak signals below the single sounding precision, but tended to fail when the CO₂ (or NO₂) field was complex. These cases can be easily identified by a trained human as done in this study, but will have to be automatized for application at the global scale, for example by applying machine learning. The algorithm also assumed accurate knowledge of the mean and variance of the background, which in a more realistic setup would have to be estimated directly from the satellite observations. Further improvements of the algorithm have the potential to increase the number of detectable plumes per satellite as well as the number of detected pixels per plume.

- **Analysis of the potential of estimating CO₂ emissions from NO₂ observations**

In SMARTCARB, NO₂ observations were used only in a qualitative way to better describe the extent of the emission plumes. They could also be used in a quantitative way by first quantifying NO_x:CO₂ emission ratios and then estimating CO₂ emissions directly from the NO₂ observations. Representative NO₂:CO₂ emission ratios could be established for plumes observed under favourable conditions and then applied to situations where CO₂ observations are not sufficiently accurate e.g. due to clouds. The established NO₂:CO₂ ratios could also be used to estimate CO₂ emissions from other platforms measuring NO₂ but not CO₂ such as Sentinel-4 and Sentinel-5, which have the advantage of providing almost daily coverage and hence could better sample the temporal variability of the emissions. Model simulations with a full chemistry scheme would be useful to investigate

<p>Final Report</p>	<p>ESA Project SMARTCARB</p> <p>Study on use of satellite measurements of auxiliary reactive trace gases for fossil fuel carbon dioxide emission estimation</p> <p>contract no 4000119599/16/NL/FF/mg</p>	  
----------------------------	--	---

how NO₂:CO₂ ratios evolve within the plume and how variable these ratios are depending on weather conditions.

- **Further improvements of the mass-balance method for CO₂ emission estimation**

Besides measurement uncertainty, the major sources of uncertainty of the mass balance method applied in SMARTCARB were the estimation of the background XCO₂ field and uncertainties in the mean wind speed and direction of propagation of the plume. Rather simple assumptions were made and the range of associated uncertainties could not be sufficiently explored. Further improvements of the method could be targeted at better quantifying uncertainties and finding objective and independent criteria for flagging of failed inversions.

- **Estimating annual mean emissions and their uncertainties from single overpass estimates**

The uncertainty of an annual mean estimate derived from satellite observations does not only depend on the number of individual plume estimates but also on the magnitude and correlation structure of the temporal variability of the emissions. We therefore propose to study how different satellite constellations are able to constrain this variability assuming realistic temporal correlations. Such an analysis should be combined with the Monte Carlo sampling of orbits proposed earlier to obtain robust statistics.


Recommendations for follow-up studies beyond SMARTCARB:

- **Analysis of the sensitivity of the representation of city plumes to different transport models and model settings**

A matter of concern is the fact that little is known about the realism of the plumes simulated in the SMARTCARB project. Other settings of the transport model may have led to more or less rapidly dispersing plumes with potentially significant effects on plume structure and detectability. It would therefore be desirable to compare the simulations with other transport models and to study the sensitivity to different model settings (e.g. advection scheme, magnitude of horizontal diffusion). The uncertainty in the representation of a given plume could be investigated by means of ensemble simulations, where each member is driven by a different member of a larger-scale ensemble system (e.g. as developed in EU project CHE), and/or by different settings of selected model parameters. Direct comparisons with airborne CO₂ observations e.g. during the C-MAPExp or COMET campaigns or with NO₂ plumes detected by the recently launched Sentinel-5P satellite could provide further valuable insights.

- **Application of methods to a city in a developing country**

SMARTCARB focused on a European city with specific conditions in terms of meteorology and NO₂/CO₂ and CO/CO₂ emission ratios. It would be useful to extend the study to a megacity in a developing country with a different combination of sources and likely a

<p>Final Report</p>	<p>ESA Project SMARTCARB Study on use of satellite measurements of auxiliary reactive trace gases for fossil fuel carbon dioxide emission estimation contract no 4000119599/16/NL/FF/mg</p>	
----------------------------	--	---




much higher CO/CO₂ emission ratios. Such a study could also investigate the added benefit of CO observations from Sentinel-5.

- **Inversions in a more realistic setup without assuming a perfect transport model**

In order to account for the uncertainties existing in current transport models, OSSEs should be designed, where the models used for the inversion are different from the model used for the production of the synthetic observations. Different methods for dealing with these uncertainties should be tested including ensemble approaches or pragmatic methods such as the one proposed by Ye et al. (2018) where the simulated fields are simply rotated and stretched to better match the "observed" ones. The results could further be compared with mass balance approaches not requiring any transport model.




- **Development of an advanced data assimilation system**

Assimilating observations of emission plumes poses great challenges for traditional inverse modeling systems, since accurately simulating the structure and orientation of the plumes is very challenging for any mesoscale atmospheric transport model. Spatial mismatches between real and simulated plume, however, may lead to large errors in the emission estimates. One way forward could be to develop an advanced data assimilation system able to extract wind information directly from the plume observation as demonstrated e.g. by Allen et al. (2013) for a 4D-Var ozone assimilation system. Such a system would have the potential to use the satellite CO₂ (or NO₂) observations to simultaneously optimize the emissions and the meteorology.

<p>Final Report</p>	<p>ESA Project SMARTCARB</p> <p>Study on use of satellite measurements of auxiliary reactive trace gases for fossil fuel carbon dioxide emission estimation</p> <p>contract no 4000119599/16/NL/FF/mg</p>	  
----------------------------	--	---

7. References

- Copernicus CO₂ Monitoring Mission Requirements Document, Ref-EOP-SM/3088/YM-ym, European Space Agency, 2018.
- Allen, D. R., Hoppel, K. W., Nedoluha, G. E., Kuhl, D. D., Baker, N. L., Xu, L., and Rosmond, T. E.: Limitations of wind extraction from 4D-Var assimilation of ozone, *Atmos. Chem. Phys.*, 13, 3501-3515, doi: 10.5194/acp-13-3501-2013, 2013.
- Ban, N., Schmidli, J., and Schär, C.: Evaluation of the convection-resolving regional climate modeling approach in decade-long simulations, *Journal of Geophysical Research: Atmospheres*, 119, 7889-7907, doi: 10.1002/2014JD021478, 2014.
- Boersma, K. F., Eskes, H. J., and Brinksma, E. J.: Error analysis for tropospheric NO₂ retrieval from space, *Journal of Geophysical Research*, 109, D04311, doi, 2004.
- Bovensmann, H., Buchwitz, M., Burrows, J. P., Reuter, M., Krings, T., Gerilowski, K., Schneising, O., Heymann, J., Tretner, A., and Erzinger, J.: A remote sensing technique for global monitoring of power plant CO₂ emissions from space and related applications, *Atmos. Meas. Tech.*, 3, 781-811, doi: 10.5194/amt-3-781-2010, 2010.
- Briggs, G. A.: Plume rise predictions. In: *Lectures on air pollution and environmental impact analyses*, Springer, 1982.
- Buchwitz, M., Reuter, M., Bovensmann, H., Pillai, D., Heymann, J., Schneising, O., Rozanov, V., Krings, T., Burrows, J. P., Boesch, H., Gerbig, C., Meijer, Y., and Löscher, A.: Carbon Monitoring Satellite (CarbonSat): assessment of atmospheric CO₂ and CH₄ retrieval errors by error parameterization, *Atmos. Meas. Tech.*, 6, 3477-3500, doi: 10.5194/amt-6-3477-2013, 2013.
- Builtjes, P., van Loon, M., Schaap, M., Teeuwisse, S., Visschedijk, A., and Bloos, J.: Project on the modelling and verification of ozone reduction strategies: contribution of TNO-MEP, TNO-report, MEP-R2003/166, Apeldoorn, The Netherlands, 2003.
- Busch, D., Harte, R., Krätzig, W. B., and Montag, U.: New natural draft cooling tower of 200 m of height, *Engineering Structures*, 24, 1509-1521, doi: 10.1016/S0141-0296(02)00082-2, 2002.
- Ciais, P., Crisp, D., Gon, H. v. d., Engelen, R., Heimann, M., Janssens-Maenhout, G., Rayner, P., and Scholze, M.: Towards a European Operational Observing System to Monitor Fossil CO₂ emissions - Final Report from the expert group. European Commission, Copernicus Climate Change Service, http://www.copernicus.eu/sites/default/files/library/CO2_Report_22Oct2015.pdf, 2015.
- Düring, I., Bächlin, W., Ketzler, M., Baum, A., Friedrich, U., and Wurzler, S.: A new simplified NO/NO₂ conversion model under consideration of direct NO₂-emissions, *Meteorologische Zeitschrift*, 20, 67-73, doi: 10.1127/0941-2948/2011/0491, 2011.
- ESA: Report for mission selection: CarbonSat, ESA SP-1330/1 (2 volume series), European Space Agency, Noordwijk, The Netherlands, 2015.
- Flemming, J. and Inness, A.: Volcanic sulfur dioxide plume forecasts based on UV satellite retrievals for the 2011 Grímsvötn and the 2010 Eyjafjallajökull eruption, *Journal of Geophysical Research: Atmospheres*, 118, 10,172-110,189, doi: 10.1002/jgrd.50753, 2013.
- Fuhrer, O., Osuna, C., Lapillonne, X., Gysi, T., Cumming, B., Bianco, M., Arteaga, A., and Schulthess, T.: Towards a performance portable, architecture agnostic implementation strategy for weather and climate models, *Supercomput. Front. Innov.: Int. J.*, 1, 45-62, doi: 10.14529/jsfi140103, 2014.

<p>Final Report</p>	<p>ESA Project SMARTCARB Study on use of satellite measurements of auxiliary reactive trace gases for fossil fuel carbon dioxide emission estimation contract no 4000119599/16/NL/FF/mg</p>	  
----------------------------	--	---

Guevara, M., Soret, A., Arévalo, G., Martínez, F., and Baldasano, J. M.: Implementation of plume rise and its impacts on emissions and air quality modelling, *Atmospheric Environment*, 99, 618-629, doi: 10.1016/j.atmosenv.2014.10.029, 2014.

Jung, M., Henkel, K., Herold, M., and Churkina, G.: Exploiting synergies of global land cover products for carbon cycle modeling, *Remote Sensing of Environment*, 101, 534-553, doi: 10.1016/j.rse.2006.01.020, 2006.

Krings, T., Gerilowski, K., Buchwitz, M., Hartmann, J., Sachs, T., Erzinger, J., Burrows, J. P., and Bovensmann, H.: Quantification of methane emission rates from coal mine ventilation shafts using airborne remote sensing data, *Atmos. Meas. Tech.*, 6, 151-166, doi: 10.5194/amt-6-151-2013, 2013.

Kuenen, J. J. P., Visschedijk, A. J. H., Jozwicka, M., and Denier van der Gon, H. A. C.: TNO-MACC_II emission inventory; a multi-year (2003-2009) consistent high-resolution European emission inventory for air quality modelling, *Atmos. Chem. Phys.*, 14, 10963-10976, doi: 10.5194/acp-14-10963-2014, 2014.

Liu, Y., Gruber, N., and Brunner, D.: Spatiotemporal patterns of the fossil-fuel CO₂ signal in central Europe: Results from a high-resolution atmospheric transport model, *Atmos. Chem. Phys.*, 2017, 14145-14169, doi: 10.5194/acp-17-14145-2017, 2017.

Mahadevan, P., Wofsy, S. C., Matross, D. M., Xiao, X., Dunn, A. L., Lin, J. C., Gerbig, C., Munger, J. W., Chow, V. Y., and Gottlieb, E. W.: A satellite-based biosphere parameterization for net ecosystem CO₂ exchange: Vegetation Photosynthesis and Respiration Model (VPRM), *Global Biogeochemical Cycles*, 22, doi: 10.1029/2006GB002735, 2008.

Pillai, D., Buchwitz, M., Gerbig, C., Koch, T., Reuter, M., Bovensmann, H., Marshall, J., and Burrows, J. P.: Tracking city CO₂ emissions from space using a high-resolution inverse modelling approach: a case study for Berlin, Germany, *Atmos. Chem. Phys.*, 16, 9591-9610, doi: 10.5194/acp-16-9591-2016, 2016.

Pinty, B., Janssens-Maenhout, G., Dowell, M., Zunker, H., Brunhe, T., Ciais, P., Dee, D., Gon, H. D. v. d., Dolman, H., Drinkwater, M., Engelen, R., Heimann, M., a, K. H., Husband, R., Kentarchos, A., Meijer, Y., Palmer, P., and Scholz, M., doi: 10.2760/39384, 2018.

Pregger, T. and Friedrich, R.: Effective pollutant emission heights for atmospheric transport modelling based on real-world information, *Environmental Pollution*, 157, 552-560, doi: 10.1016/j.envpol.2008.09.027, 2009.




Roches, A. and Fuhrer, O.: Tracer module in the COSMO model, COSMO Technical Report, available online at <http://cosmo-model.org>, 2012.

Rood, R. B.: Numerical advection algorithms and their role in atmospheric transport and chemistry models, *Reviews of Geophysics*, 25, 71-100, doi: 10.1029/RG025i001p00071, 1987.

Schatzmann, M. and Policastro, A. J.: An advanced integral model for cooling tower plume dispersion, *Atmospheric Environment* (1967), 18, 663-674, doi, 1984.

Senatsverwaltung für Stadtentwicklung und Umwelt: Emissionskataster Berlin, Erstellung der Berliner Emissionskataster Industrie, Gebäudeheizung, sonstiger Verkehr, Kleingewerbe, sonstige Quellen, Baustellen, Leipziger Institut für Energie (AVISO) im Auftrag der Senatsverwaltung für Stadtentwicklung und Umwelt, Schlussbericht. Juni 2016.

Sharp, E., Dodds, P., Barrett, M., and Spataru, C.: Evaluating the accuracy of CFSR reanalysis hourly wind speed forecasts for the UK, using in situ measurements and geographical information, *Renewable Energy*, 77, 527-538, doi: 10.1016/j.renene.2014.12.025, 2015.

<p>Final Report</p>	<p>ESA Project SMARTCARB Study on use of satellite measurements of auxiliary reactive trace gases for fossil fuel carbon dioxide emission estimation contract no 4000119599/16/NL/FF/mg</p>	  
----------------------------	--	---

Taylor, T. E., O'Dell, C. W., Frankenberg, C., Partain, P. T., Cronk, H. Q., Savtchenko, A., Nelson, R. R., Rosenthal, E. J., Chang, A. Y., Fisher, B., Osterman, G. B., Pollock, R. H., Crisp, D., Eldering, A., and Gunson, M. R.: Orbiting Carbon Observatory-2 (OCO-2) cloud screening algorithms: validation against collocated MODIS and CALIOP data, *Atmos. Meas. Tech.*, 9, 973-989, doi: 10.5194/amt-9-973-2016, 2016.

VDI: Dispersion of Air Pollutants in the Atmosphere, Determination of Plume Rise , VDI Guideline 3782(3). Verein Deutscher Ingenieure (VDI), Düsseldorf, 1985.

VDI: Environmental Meteorology, Dispersion Modelling for the Discharge of Flue Gas via Cooling Towers, VDI Guideline 3784(2). Verein Deutscher Ingenieure (VDI), Düsseldorf, 1990.

Velazco, V. A., Buchwitz, M., Bovensmann, H., Reuter, M., Schneising, O., Heymann, J., Krings, T., Gerilowski, K., and Burrows, J. P.: Towards space based verification of CO₂ emissions from strong localized sources: fossil fuel power plant emissions as seen by a CarbonSat constellation, *Atmos. Meas. Tech.*, 4, 2809-2822, doi: 10.5194/amt-4-2809-2011, 2011.

Wenig, M. O., Cede, A. M., Bucsela, E. J., Celarier, E. A., Boersma, K. F., Veefkind, J. P., Brinksma, E. J., Gleason, J. F., and Herman, J. R.: Validation of OMI tropospheric NO₂ column densities using direct-Sun mode Brewer measurements at NASA Goddard Space Flight Center, *Journal of Geophysical Research*, 113, D16S45, doi, 2008.